

# **NUMERICAL SIMULATION FOR PREDICTION OF TORSIONAL STRENGTHS OF HELICAL HOLLOW STRAND TUBE PRODUCTS**

by

**Dilipkumar Umeshbhai Devpalli**

**A Thesis**

*Submitted to the Faculty of Purdue University*

*In Partial Fulfillment of the Requirements for the degree of*

**Master of Science in Engineering**



Department of Civil and Mechanical Engineering

Fort Wayne, Indiana

May 2019

**THE PURDUE UNIVERSITY GRADUATE SCHOOL  
STATEMENT OF COMMITTEE APPROVAL**

Dr. Zhuming Bi, Chair

Department of Civil and Mechanical Engineering

Dr. Hosni Abu Mulaweh

Department of Civil and Mechanical Engineering

Dr. Nashwan Younis

Department of Civil and Mechanical Engineering

**Approved by:**

Dr. Carol Sternberger

Head of the Graduate Program

## **ACKNOWLEDGMENTS**

I would like to thank, first and foremost, Dr. Zhuming Bi for guiding me down the proper design path, and for dedicating so much time to me. Dr. Hosni Abu-Mulaweh is also thanked for support while pursuing this degree. The entire faculty of Civil and Mechanical Engineering department is thanked for preparing me to this point in the curriculum.

Thank you to my family for the encouragement and inspiration. While it may have sometimes seemed more like a freight train behind me in a tunnel rather than a light at the end, your advice and actions are one of my greatest motivations.

And thank you to my friends who have gotten me out of the work pressure when I needed a break, made me get out and try new things, and helped me grow into a better person or at least a more entertaining one.

Last, but not least, I would like to thank Mr. Rob Mitchell, Austin Cisna and his team of Fort Wayne Metals for providing such a well-defined thesis project and their support in the all required information for completion the task.

## TABLE OF CONTENTS

LIST OF TABLES .....	7
LIST OF FIGURES .....	8
ABSTRACT .....	10
1. INTRODUCTION .....	12
1.1 Wires in Instrumentation of Medical Devices .....	12
1.2 Characterization of Cables .....	13
1.3 Helical Hollow Strand Tubes .....	13
1.4 Characterization of Wires or Cables and Limitations .....	16
1.5 Process Characteristics of Wire Drawing .....	16
1.6 Limitations and Problem Statements .....	18
1.7 Scope of Research .....	19
1.8 Organization of Thesis .....	22
2. LITERATURE REVIEW ON ANALYTICAL MODELLING .....	23
2.1 Development of Wire Ropes .....	23
2.2 Wire Rope Theories and Models .....	24
2.2.1 Analytical Model by Hruska et al .....	25
2.2.2 Analytical Model by Costello et al .....	27
2.2.3 Analytical Models by Machida, Huang, Knapp et al .....	31
2.3 Summary of Existing Analytic Modelling Methods .....	33
3. PREDICTION BY NUMERICAL SIMULATION .....	34
3.1 Finite Element Methodology .....	34
3.1.1 Discretization and Representation of Elements .....	36
3.1.2 General Formulation of Solid Elements .....	38
3.1.3 Representation of Field Variables .....	39
3.1.4 Meshing Techniques .....	41
3.1.5 Explicit Integration .....	41
3.1.6 Numerical Implementation .....	42
3.1.7 Incremental Stability .....	43
3.2 Commercial Software Tool - Abaqus .....	44

3.3	Modelling Procedure.....	45
3.3.1	Boundary Conditions .....	47
3.3.2	Fracture Analysis .....	48
3.4	Case Study .....	49
3.5	Summary of Numerical Simulation .....	52
4.	PARAMETRIC STUDY FOR SIMULATION AND PRODUCTS .....	54
4.1	Parametric Study .....	54
4.2	Procedure of a Parametric Study.....	60
4.2.1	Automation of Parametric Generation:.....	62
4.3	Parametric Study on Simulation Model.....	65
4.3.1	Mesh Sensitivity Study .....	65
4.3.2	Friction Co-Efficient.....	68
4.3.3	Boundary Condition.....	70
4.4	Parametric Study on Product Variations.....	70
4.5	Summary of Parametric Design Capabilities .....	71
5.	VERIFICATION AND VALIDATION.....	73
5.1	Verification and Validation (V & V).....	73
5.2	Verification of Simulation Model.....	78
5.2.1	Analytical Model .....	78
5.2.2	Numerical Model .....	78
5.2.3	Verification of Analytical and Numerical Results.....	80
5.3	Validation of Simulation or Numerical Model .....	81
5.3.1	Experimental Setup.....	81
5.3.2	Validation by Experiments .....	82
5.4	Difficulties and Challenges V & V .....	86
5.5	Summary of V & V .....	86
6.	CONCLUSION AND FUTURE WORKS .....	88
6.1	Summary of Thesis Work .....	88
6.2	Conclusion .....	89
6.3	Future Works .....	91
	REFERENCES .....	93

APPENDIX A. ANALYTICAL CALCULATION.....	100
APPENDIX B. LETTER OF SUPPORT.....	101

## LIST OF TABLES

Table 1.1 HHS Tube Models Geometrical configuration.....	20
Table 3.1 Common Commercial FEA Software Used by Industries.....	35
Table 3.2 True Stress and True Strain Formulas ((NPL) National Physical Laboratory Manual) .....	40
Table 4.1 Mesh Sensitivity Result .....	66
Table 4.2 Friction Results .....	69
Table 4.3 HHS Tube Geometrical Dimension Variable Values .....	70
Table 4.4 HHS Tube Parametric Study Results.....	71
Table 5.1 Overview of Verification and Validation. (Sargent, 2011) .....	76
Table 5.2 Geometrical Data of HHS Tubes and Type of Analysis.....	76
Table 5.3 HHS Tube Models Analytical Results @ 180 <sup>0</sup> Rotation.....	78
Table 5.4 HHS Tube Models with Total Number of Elements and Nodes .....	79
Table 5.5 HHS Tube Models Numerical Results @ 180 <sup>0</sup> Rotation.....	80
Table 5.6 Comparison of Numerical and Analytical Results with Relative Discrepancy Percentage .....	80
Table 5.7 Experimental Results of HHS Tube @ 180 <sup>0</sup> Rotation.....	82
Table 5.8 Comparison Results Overall of Numerical and Experimental with Relative Discrepancy Percentage. ....	86
Table 5.9 Overall HHS tube model torque results at 180 <sup>0</sup> .....	87

## LIST OF FIGURES

Figure 1.1 Wire Rope Build Up (Costello 1990).....	14
Figure 1.2 HHS® Tube Isometric View (Fort Wayne Metals 2018) .....	14
Figure 1.3 HS® Tube with Multiple Layers Front View (Fort Wayne Metals 2018) .....	14
Figure 1.4 Geometrical Representation of Helical Lay Angle for Spiral Wire .....	15
Figure 1.5 Regular and Lang’s Lay Wire Rope (Costello 1990).....	16
Figure 1.6 HHS tube models Front View .....	20
Figure 1.7 HHS Tubes Models single filars and isometric view. ....	21
Figure 1.8 HHS Tubes Models Mesh models.....	21
Figure 2.1 (a) Cylindrical Helix and (b) Its Development.....	29
Figure 3.1 Fem Approximation Methods (Gokhale Et Al 2008).....	35
Figure 3.2 Element Types and Their Degrees of Freedom (Norton 2006).....	36
Figure 3.3 Element Types with Various Node Configurations (Abaqus 6.12 User Manual).....	37
Figure 3.4 The H-Refinement and P-Refinement Approaches (Sheshu 2003).....	38
Figure 3.5 FEM Procedure to Perform Simulation by CAE Software .....	46
Figure 3.6 Load and Boundary Condition of HHS Tube.....	48
Figure 3.7 HHS Tube Classification.....	50
Figure 3.8 1x12x0.005 HHS Tube Clockwise Angular Rotation Vs Torque at 180 <sup>0</sup> .....	51
Figure 3.9 Damage Of 12 Filar Strand Due to Fracture Strain.....	52
Figure 4.1 Various Geometric Shapes of The Filars (Lee 1989).....	55
Figure 4.2 Classification of HHS Tube.....	56
Figure 4.3 Various Types of Single Layer HHS Tubes .....	57
Figure 4.4 Typical Wire Rope Lays Comparison (Costello ,1990) .....	58
Figure 4.5 Classification & Boundary Condition of HHS Tube.....	59
Figure 4.6 Inner and Outer Radii of HHS Tube.....	59
Figure 4.7 Flowchart of Automation Possibilities with Python.....	62
Figure 4.8 Parametric Study Performing with Python Script example (Abaqus Manual).....	64
Figure 4.9 Parametric Study Output Reports after Running Script example (Abaqus Manual)..	64



Figure 4.10 Variant Mesh size FE Models .....	67
Figure 4.11 Mesh Comparison Graph of Torque Vs Angular Displacement @ $180^0$ .....	67
Figure 4.12 Friction Co-Efficient Comparison Graph of Torque Vs Angular Displacement @ $180^0$ .....	69
Figure 4.13 Torque Vs Angular Displacement @ $180^0$ Clockwise Direction .....	71
Figure 5.1 Activities and Process for Modeling, Simulation, Verification and Validation (Thacker Et Al 2004) .....	74
Figure 5.2 Model Development, Verification and Validation Process (Thacker Et Al 2004).....	75
Figure 5.3 Geometrical Dimensions and Material Data of HHS Tube 1x12x0.005;0.028.....	77
Figure 5.4 Load and Boundary Condition of HHS Tube.....	77
Figure 5.5 Hexa-Penta Mesh with C3d8I and C3d6 Element on Spiral Strand.....	79
Figure 5.6 HHS Tube_CW_1x6x0.0075;0.050_ Torque Comparison Results of Numerical and Experimental @ $180^0$ .....	83
Figure 5.7 HHS Tube_CW_1x8x0.010;0.055_ Angle Comparison Results of Numerical and Experimental @ $180^0$ .....	83
Figure 5.8 HHS Tube_CW_1x12x0.005;0.028_ Torque Comparison Results of Numerical and Experimental @ $180^0$ .....	84
Figure 5.9 HHS Tube_CW_1x16x0.005;0.045_ Torque Comparison Results of Numerical and Experimental @ $180^0$ .....	84
Figure 5.10 HHS Tube_CW_1x18x0.005; 0.045_ Torque Comparison Results of Numerical and Analytical @ $180^0$ .....	85

## ABSTRACT

Author: Devpalli, Dilipkumar, U. MSE

Institution: Purdue University

Degree Received: May 2019

Title: Numerical Simulation for Prediction of Torsional Strengths of Helical Hollow Strand Tube Products

Committee Chair: Zhuming Bi

Due to reduced pain, shortened hospital stay and recovery, minimally invasive surgery (MIS) is becoming more and more popular in healthcare systems. MIS requires some devices for the motion and force transformation from outside to the inside of the body of a patient, and the strangled cables play a significant role in developing the instrumentations to serve for such purposes. However, current design and selection of a strangled cable is mostly intuitive that depend greatly on designers' experiences and availability of experimental data, which leads to non-optimized designs and longer design cycles. In this thesis, both of analytical modelling and numerical simulation are proposed to build the relation of applied torque and deflection of part, so that a strangled cable with a given configuration can be characterized in term of its load-deflection relation. The defined relation has its great significance and application potential in the design optimization and precise controls of medical devices for MISs.

Besides the various patterns of strangled cables, a Helical hollow strand (HHS®) tube is a special type of strangled cables with single- or multiple- layer configurations., In each layer, each of the helical wires touches its two neighboring helical wires, and it has a coreless hollow at the center. Its primary application is to carry a torsional load in a twisting mode. As an extreme, there is a possibility that all helical wires touch each other, and this forms a statically indeterminate contact obstacle in design analysis. Numerical simulation would predict that contacts occur simultaneously at all possible contacting points under the circumference that the strand is fixed at one end against rotation. In addition, the friction at contacts will affect the torsional deformation; therefore, these contacts must be taken into consideration in the development of analytical and numerical simulation models.

This thesis reports the results of the investigation on the characteristics of Helical hollow strand tube (HHS®), more specifically, the relation of torsional deflection and the applied torque

over a tube in the clockwise (CW) direction. The numerical simulation approach to predict the torsional deflection of HHS with various design parameters and configurations is emphasized.

**Keywords:** HHS tube, cable characterization, torsional loads, correlation, deflection, steel alloys, and numerical simulation.

# 1. INTRODUCTION

In this chapter, a small introduction is presented about the background of this thesis study; the emphasis is on the type of products the proposed method applies for. Based on the limitation of existing works, the thesis problem is formulated, the research questions to be investigated are discussed, and the scope of the thesis is outlined.

## 1.1 Wires in Instrumentation of Medical Devices

Many medical devices need to transfer motion/force from one place to another in distance in a confined path, such as within a human body. Wires and cables have their flexibilities in moving along complicated pass-ways, therefore, they are widely used as essential components in medical devices. *Strangled cables* have been used as critical parts for *actuators*, *catheter*, *endovascular devices*, and *minimally invasive surgery* (MIS) systems (Rosen et al. 1999).

The MIS and vascular treatment signify the treatment of vascular disease from the inside of the blood vessel. Such therapy uses a minimally invasive, catheter-based procedure using specialized equipment and techniques (Korean et al. 2011). These methods expect only a tiny incision, through which a thin catheter is inserted. Using the advanced imaging technology and with the help of cables, the catheter is managed through a blood vessel to eliminate blockages and open narrowed regions. The human veins are considerably slimmer and soft; therefore, excellent flexibility and stiffness becomes the highest priority to accomplish the function accurately (James et al. 2014). In such devices, the unifilar coil, multi-filar coil, and the strand with a hollow working in center tubes are utilized (Newman 1881). It incorporates a broad range of areas within medical device and equipment such as *cameras*, *scanning tools*, *surgical tools*, *probe tools* and *sampling tools* (Calmont Wire and cable 2018). In almost any of equipment, the variant types of wires are used. Generally, wires and cables are needed to develop medical devices for catheters, probes, stimulators, neural prosthesis, implants and cardiac surgeries. Therefore, how to characterize wires or cables is critical but this has turned into a big challenge to wires or cables suppliers. Since the requirements for a cable or wire product depend on the specified requirements of a given application. In other words, design parameters and configurations of cable products must be tailored to meet specified requirements. Most of the

wires and cables used in medical applications are customized to specific applications; therefore, the wires and cables even from one supplier are highly diversified (Calmont Wire and cable 2018).

## 1.2 Characterization of Cables

The products in the medical industry directly relate to the well-being of people. Therefore, medical products need to meet a strictly high standard of functionalities and quality. This applies to all of the products as well as components and parts such as wires and cables in medical devices (Emergo group 2018, Medical Device Regulatory Compliance and Recall 2009). In contrast to the cables and wires used in other sectors, typical cables and wires in medical devices are considerably small in geometry (e.g., the diameter of a wire ranges from 10 microns to 2.5 mm). Other than the features of small sizes, wires in medical applications generally have the great flexibility under axial, bending and torsional loads which is essential characteristic to their applications (Benini 2010), (Tobushi et al. 1998). Such wires are functioned to transmit the torque with the required flexibility and effectual strength. For meeting the demand of flexibility and strength, design parameters to be analyzed include *material properties*, *wire diameters*, and *cable configurations*. Parametric design of such wires depends on the characteristics of wires, i.e., the deflection of a wire relating to the given constraints and loading conditions such as tension, compression and torsion.

## 1.3 Helical Hollow Strand Tubes

In a helical hollow strand (HHS®) Tube cable, a number of metallic filars or wires are twisted along a circular line to be shaped into a coreless hollow configuration (Miyata et al. 2005). The hollow in a HHS cable is particularly useful; it allows to incorporate medical guide wires inside the HHS® tube. In the HHS cable, a uniform contact pressure is sustained between two adjacent metallic filars to form seamless contacts (Miyata et al. 2005).

The HHS tubes can be configured differently with varying *number of filars*, *helical pitches*, and *the number of wire layers*. Figure 1.1 gives an example of a wire rope strand with different components (Costello G.A. 1990) and Figure 1.2 shows an example of the two-layer HHS® tube in its isometric view (Fort Wayne Metals 2018).

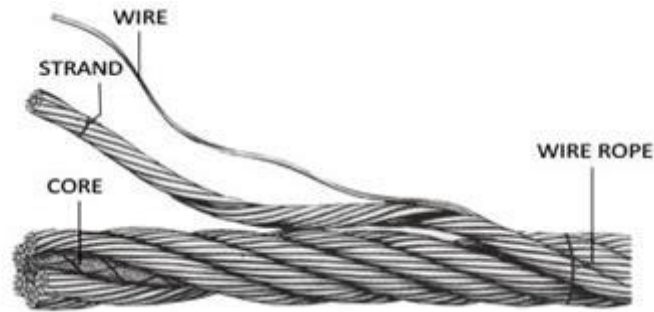


Figure 1.1 Wire Rope Build Up (Costello 1990)

One can determine by a comparison of Figure 1.2 and Figure 1.3 that a HHS® tube is hollow from the center, which is considerably different from a general wire rope strand commonly used in other sectors such as construction (Fort Wayne Metals 2018).



Figure 1.2 HHS® Tube Isometric View (Fort Wayne Metals 2018)

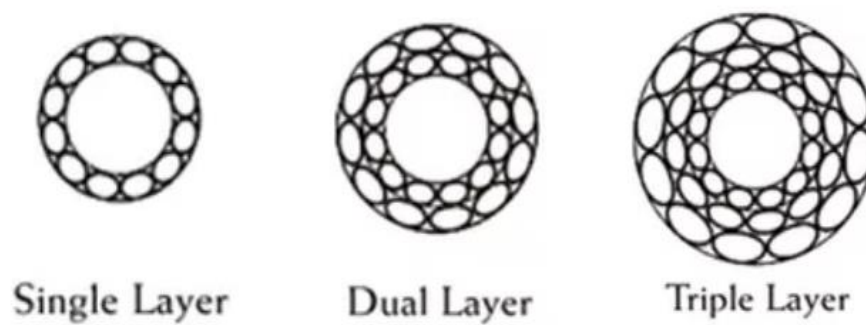


Figure 1.3 HS® Tube with Multiple Layers Front View (Fort Wayne Metals 2018)

In a configuration of a stranded cable, a *helical angle* refers to the helical strands' angle with the vertical axis of the strand (refer Figure 1.4) and this angle is constant along its length for single helical wire strand.

The helical angle's direction is either *clockwise* (CW) or *counterclockwise* (CCW). A normal twist rope has a reverse direction for wire and strand helical angles. Moreover, Lang's lay rope also has a comparable direction for the wire and strand angle as seen in Figure 1.5.

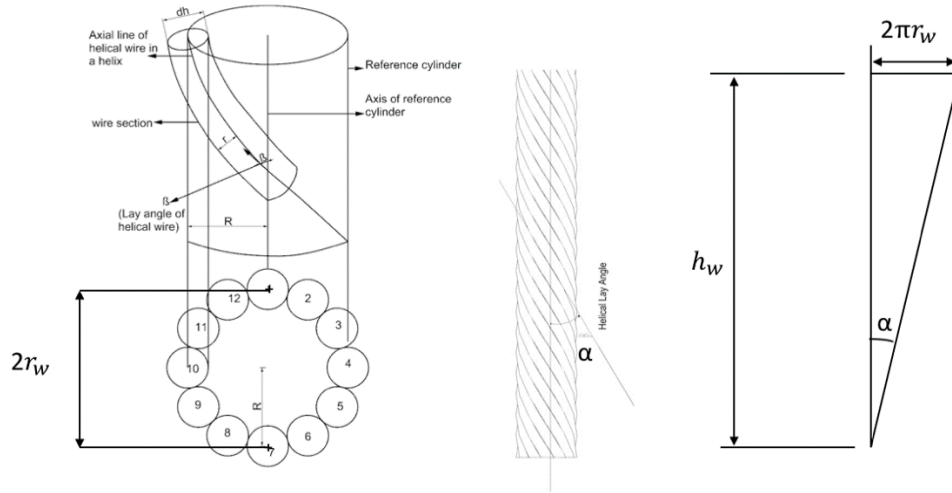


Figure 1.4 Geometrical Representation of Helical Lay Angle for Spiral Wire

HHS Tubes are extensively applied in the medicinal arena. For example, they have been used in *guide channels*, *endoscopic shafts* and also in *catheters* (Fort Wayne Metals 2018). They have been also used in medical devices such as orthopedic drills and laparoscopic instruments for keyhole surgery (Cisna and Wehrle 2018).

HHS Tube are essentially utilized in the medical industry. Moreover, in the post-operations processes, the HHS tubes are adaptable enough to meet the needs of various non-medical applications (Cisna and Wehrle 2018).

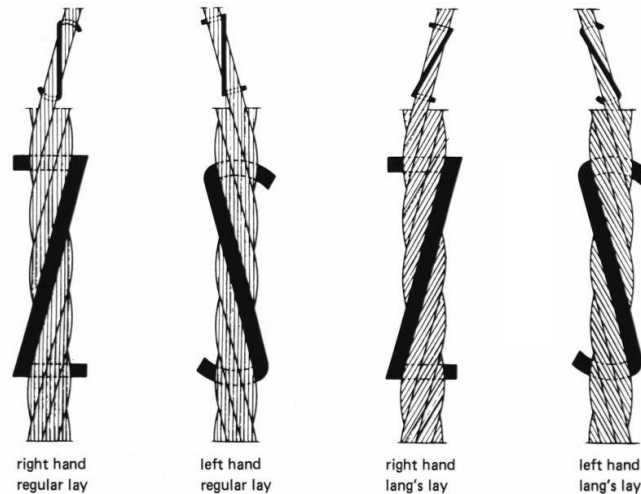


Figure 1.5 Regular and Lang's Lay Wire Rope (Costello 1990)

#### 1.4 Characterization of Wires or Cables and Limitations

The characterization of a wire or cable is crucial to its applications. Due to the complexity of a cable configuration and contact conditions of wires in cable, the characterization of HHS cable relies intensively on experiments heavily in current practice. To gain the understanding of the cable performance in its applications, both of the torque testing and tensile testing are needed to obtain the relations of external loads and deflections (Lee 1989).

Two major experimental methods for the characterization of cables are (1) *torque testing* and (2) *tensile testing*. With available testing machine setup, the development time for each experiment would take 3-5 minutes. Fort Wayne Metals have conducted 10 number of specimen samples for each type of strand and an average result has been considered for the comparison.

The cost would be higher as for experiments since the testing machines are specialized machine tools; moreover, for each time, multiple specimens have to be tested to get accurate material physical data. The limitation to support parametric design is very restricted as each variant of wire with a different configuration has its own characteristic properties.

#### 1.5 Process Characteristics of Wire Drawing

Wires in HHS product are usually from extrusion. In the extruding process, wire drawing technique is pulling a metal wire through a die. In wire drawing, mechanical pulling



causes stretching of the material with a reduction in its cross-sectional area. The magnitude of the dragging force must be defined, and it relates to the material properties; the stress by the pulling force must be below the yield strength of materials, so that no fracture will occur to the object due to an exceeded load. The dragging force required for the wire in the die is known based on reduction size in the area of cross-sectional. The greater a reduction rate is, the greater is the force required to pull over the die. As a summary, the maximum possible decline in diameter is restrained by the strength of the wire (Avitzur 1983).

The yield strengths of materials depend on the composition of material. Generally, it is a common practice that the reduction of area over a die should be between 20 and 40%. If there is a requirement for higher reduction, the net reduction rate has to be decomposed into a number of steps, so that each step can be an acceptable reduction rate. This is carried out by drawing the wire and the deformation on cables in plastic deformation, this tends to increase hardness and reduce ductility when the materials pass through a die. This makes it tougher to decrease the area of cross-section. To perform an annealing process between successive draws is important, so that materials can accommodate a high-level of strain without a fracture. On the other hand, the increased tensile strength that results from drawing is seen as an attractive property (Adam and Sanchez 1999).

Wire drawing is normally performed subjected to a room temperature; there are some cases where the metal is drawn at an elevated temperature to improve the ductility for large deformation. To reduce friction and pulling force, the die should be lubricated in a cold drawing for getting a smooth finish of the surface and increase the durability of tooling. One significant advantage of drawing is that it is a type of net-shaping process with little material waste. However, it involves in the high cost of tooling and it brings the need of carrying out an annealing process to suppress the impact of work hardening (Castro et al. 1996).

The plastic deformation of wire in wire drawing processing can be measured in the following approaches:

Draft – the reduction of the wire diameter before and after wire drawing, i.e.,

$$\text{Draft} = D_o - D_f \quad \text{eq. (1.1)}$$

where  $D_o$  and  $D_f$  are the diameter of wire before and after the drawing, respectively.

Reduction in area – the reduction of cross-section area before and after wire drawing, i.e.,

$$\text{Reduction in area} = \frac{A_o - A_f}{A_f} \times 100 = \frac{D_o^2 - D_f^2}{D_f^2} \times 100 \quad \text{eq. (1.2)}$$

where  $A_o$  and  $A_f$  are original and final cross-sectional areas, respectively.

Elongation – the displacement changes over a unit length, i.e.,

$$\text{Elongation} = \frac{L_f - L_o}{L_o} \quad \text{eq. (1.3)}$$

where  $L_o$  and  $L_f$  are the original and final lengths of wire, respectively.

For single stage cold drawing, the allowable area reduction depends upon many factors such as the type of material, wire size, initial metallurgical condition, desirable mechanical properties, die design, and lubrication efficiency; generally, the percent of the area reduction should be less than 50% (Dieter 1986).

Assume the friction is ignore, the force required to pull the stock through the die can be computed as follows.

$$F = Y_{avg} \cdot A_f \cdot \ln\left(\frac{A_o}{A_f}\right) \quad \text{eq. (1.4)}$$

where  $F$  is the pulling force;  $Y_{avg}$  is average true stress of the material of wire, and  $A_o$ ,  $A_f$  are original and final areas of the cross-section of wire.

## 1.6 Limitations and Problem Statements

- 1)
- 2) The modelling method and procedure of finite element analysis (FEA) is presented to build a relation of angular displacement and applied torque.
- 3) The proposed numerical method is verified and validated by a comparative study between the simulation result and those obtained from experiments results models.

A number of case studies will be developed to illustrate how the proposed numerical simulation method can be used to characterize the stranded cables with specified configuration

and the given design parameters of wires. The case studies will be solved in the Abaqus solver for HHS tubes to know the response of cables under a varying load and the maximum torque for a fracture failure.

## 1.7 Scope of Research

Many scientists and mathematicians (Hruske 1951, Costello 1990, Machida 1973, Durelli 1973, Laura 1973, Casarella 1974, Chi 1971 and Leissa 1959) have worked on the basic principles of helical strands with a core under axial, torsional, bending load conditions with a number of mathematic models for the relations of deflections and loads. However, it is our knowledge that no work has been found on the characterization of HHS tubes due to their unique features. HHS tubes have their special features which are fundamentally different from the cables with similar geometries and shapes in other applications. Design parameters to be investigated are different significantly from existing studies.

To make this thesis's research manageable, the following design variables are selected to define the scope of the thesis:

- 1) The influence of cable configurations and wire geometries on torsional capabilities are concentrated. Without losing the generality, the variation of material properties are not expanded; the 300 Series Stainless Steel alloy wire strands with a hollow in the center are taken as exemplifying materials throughout the thesis.
- 2) The method and procedure of FEA simulation can be applicable to any HHS tubes. However, for the purpose of verification and validation, the experiments have to be conducted to obtain comparable data. In this thesis, the case studies are developed for the cable configurations for five variants, i.e., 1x6x0.0075;0.050, 1x8x0.010;0.050, 1x12x0.005;0.028, 1x16x0.005;0.045 and 1x18x0.005;0.045 4inch length with a number of fixed pitches and helical angles as described in below table 1.1 and figure 1.6, 1.7 and 1.8.

Table 1.1 HHS Tube Models Geometrical configuration.

Sr.No	HHS tube Configuration	Number of Filars	Filar diameter (inch)	Inner diameter of the Tube (inch)	Mean Diameter of the Tube (inch)	Outer Diameter of the Tube (inch)	Pitch (inch)	Helical angle (Degree)
1	1x6x0.0075;0.050	6	0.0075	0.035	0.0425	0.05	0.0486	69.99
2	1x8x0.010;0.055	8	0.01	0.035	0.045	0.055	0.0986	55.1
3	1x12x0.005;0.28	12	0.005	0.018	0.023	0.028	0.107	34.03
4	1x16x0.005;0.045	16	0.005	0.035	0.04	0.045	0.1053	50.03
5	1x18x0.005;0.045	18	0.005	0.035	0.04	0.045	0.1309	43.82

The below figures are shown as per the above table 1.1, HHS tube model number respectively.

(1) 6 filar HHS tube (2) 8 filar HHS tube (3) 12 filar HHS tube (4) 16 filar HHS tube and (5) 18 filar HHS tube.

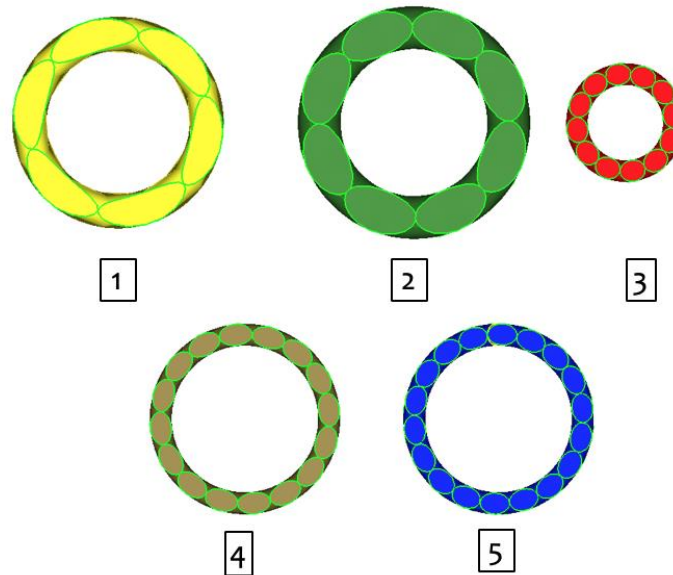


Figure 1.6 HHS tube models Front View

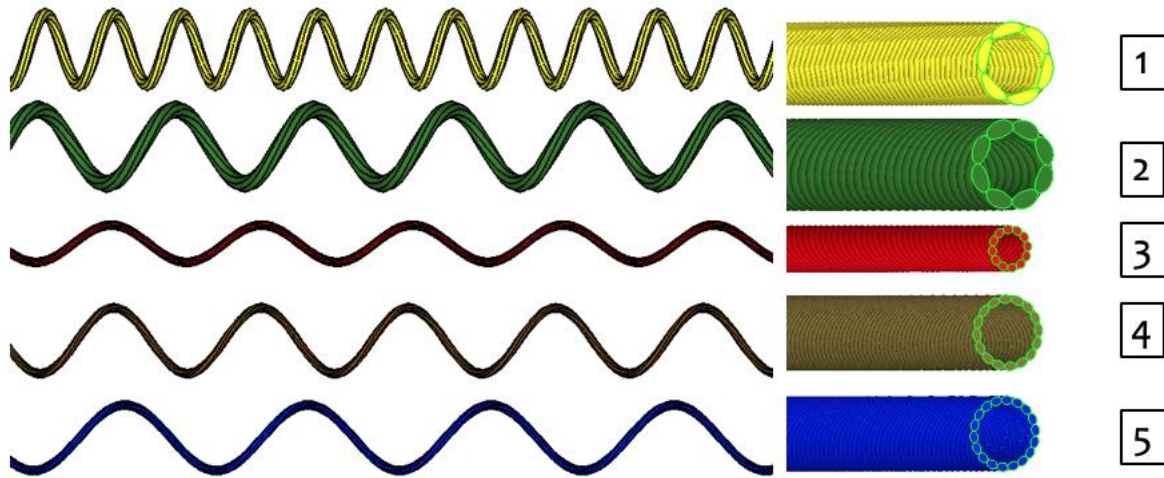


Figure 1.7 HHS Tubes Models single filars and isometric view.

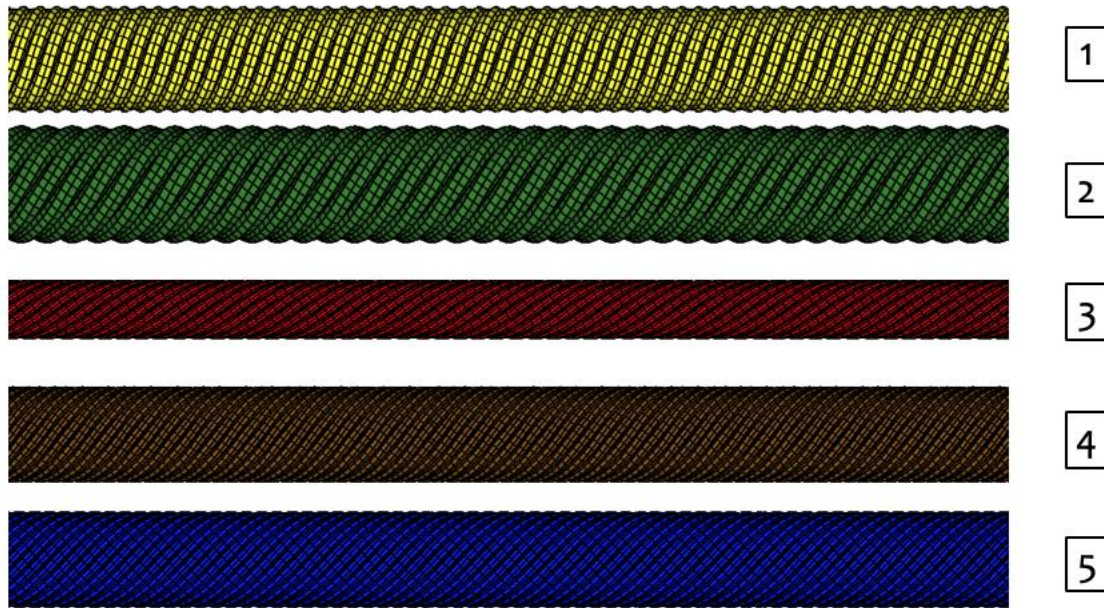


Figure 1.8 HHS Tubes Models Mesh models.

- 3) For the variety of boundary conditions, the current setup of experiments at the client company Fort Wayne Metal is taken as reference. The cable is fixed on the testing machine and torque is applied at the other end, and the angular displacement is continuously measured with respect to the changing torque applied. The load on the

300 Series Stainless Steel alloy wire rope is defined with a torsional load. This serves for the need of characterization of cables for the partner company. For the failure analysis, the torsional force applied on an HHS tube keep increasing until the HHS cable completely fracture occurs.

## **1.8 Organization of Thesis**

This thesis is organized in the following way:

Chapter 1 provides an outline of research backgrounds, existing works in the field and limitation of existing methods to predict the torsional deflection of a HHS tube under given torque.

Chapter 2 provides comprehensive discussions and summary of relevant works in the study of strangled cables.

Chapter 3 develops the method and the procedure of using finite element analysis (FEA) method to predict the relationship between angular displacement vs applied torque.

Chapter 4 introduces the Design of experiments to characterize the HHS tubes.

Chapter 5 discuss the verification and validation of the proposed numerical simulation approach.

Chapter 6 gives a summary of the presented work, new contributions via this thesis study and the recommendations of future research in this field of research.

## 2. LITERATURE REVIEW ON ANALYTICAL MODELLING

In this chapter, an overview of most relevant literatures related to analytical modelling of wire ropes is given. The study through literature survey helps to understand the behaviors of cable strands subjected to various loading conditions.

**Keywords** – Literature review, wire ropes, cable strands, HHS tubes, wire rope theory.

### 2.1 Development of Wire Ropes

Some structural components such as ropes, yarns, cables, cords, and the strands share their commonality of superior capabilities in withstanding a relatively large axial load in comparison with their weakness in resisting bending and torsional loads. According to Costello (1990), ropes, due to their special characteristics, became one of the oldest tools that humans used to lead a better life for themselves. Clark (1930) indicated that the use and manufacturing of wires was tracked back to 3000 B.C. As the matter of fact, a copper cable found in the ruins of Nemeveh near Babylon proved that wire ropes were used as construction materials in about 700 B. C. Sayega (1980) summarized the history of the industrial development of wire ropes in the United States. It was found that the industry for steel wire rope manufacturing was firstly inspired by the direct needs from coal-mining industries and the civil construction where wire ropes were badly needed to build suspension bridges. The United States (US) engineers in those professions tried to learn knowledge and experience from the European to use wire ropes for bridge building. Many US engineers travelled to Britain, Germany and France to study bridge design, in particular, how to use wire ropes in haulage and ropeways. At that time, no American university was able to offer engineering degrees related to designing and applying wire ropes in construction or coal-mining.

In the United States, the development of wire ropes was initialized due to a new law. In 1832, the Congress passed the law stating that in existing paddle-wheel riverboats with thread cordage, the tiller ropes must be replaced by “metallic” ropes to achieve the required safety standards. This law stimulated Americans to design “metallic” wire ropes (Sayega 1980). As a result, Isaac McCord patented the first American wire rope in 1839. His design was to have a rope from three small selva cables which were twisted together like a cordage. Sequentially,

various standardized wire ropes were developed in the United States; for examples, John Roebling design “three side” wire-ropes also called as Warrington wire ropes in 1886, Ferdinand Roebling patented the “alternative lay” in 1875, and Jame Stone patented filler wire ropes in 1889.

Nowadays, the application of wire ropes are employing in almost all domains such as, automotive, marine applications, medical devices, orthodontic arc wires, actuators, guidewires, surgical instruments, mandrels, springs, needles, aerospace components, jet engine stator vanes and resistance heating elements for industrial devices such as water heaters, flat irons, soldering irons, plastic molding dies and many more. The material family will change as per its application and the specific requirement. In contrast to straight rod, wires give their distinctive features for more multiple variations of design which are widely needed in every industry (Ulbrich Inc. 2018).

## **2.2 Wire Rope Theories and Models**

The manufacturing industry of steel wires ropes began to grow in the 1950s when engineers became concern possible failures of wire ropes; those products experienced the stresses and strains beyond their static or fatigue strengths. Throughout the years, numerous reviews were published of modeling of wire ropes and cables. For examples, Triantafyllou (1987) reviewed the horizontal elastic cable dynamics, which cover most of important works in two historical periods, i.e., from 1600s to 1800s and 1940s to 1980s, respectively. He made a special remark on the work of Irvine and Caughey in 1974; since they thoroughly investigated the outcome of elasticity on the dynamics of horizontal cables, and this work was followed by many other researchers in the field, including the most notable scholar, F. H. Hruska, in the wire rope theory. The most important contribution by Hruska (1951) was a simple mathematical model on the strength of material for single layer strand, which was adopted and extended by many researchers. The details of this simplified model will be discussed and utilized in details in the following section. In regards to existing analytical models of wire rope products, the literatures can be categorized based on who proposed original methods, i.e., existing analytical models were rooted and expanded based an original model by Hruska et al (1951), Machida et al (1973), and Costello et al (1990), respectively.



### 2.2.1 Analytical Model by Hruska et al

H. M. Hall and F. H. Hruska are considered as the pioneers in modeling ropes; in their works, the theory for the strength of materials was applied to calculate the tensile stresses for ropes with core wires or helical wires at different layers of strand. Hall (1951) indicated that when the external tensile load was given, the tensile stress was greater at the outermost layer while that stress at the inner layer was less within a strand. However, the extended work by Hruska (1953) proved that the above statement was wrong; Hruska provided the evidences with his analytical studies on the mechanical response of wires within strands and ropes. The design variables are included in mathematic model, which includes *the tensile stress ratio* between core and helical wires, *the tangential force* acting on helical wire, and *the torque* provoked at the rope termination, *the radial force* among the wires at contacts, and *the cross-section shape* of a helical wire on a transverse section. In his method, he summarized the sectional geometry of helical wire and reaction forces at the contact position. He showed that the cross-sectional shape of the helical wire was considered as an ellipse. A similar analytical approach for prediction of the radial force and wire sectional geometry for a 6/1 strand shown in a article called "Geometrie im Drahteil" were found by Costello and Phillips (1973).

However, Hruska's work was limited in sense that (1) the friction factor was not taken into consideration and (2) all helical wires within a rope were over simplified as single bonded helical wire. In his model, he assumed that a rope provided no resisting moment (i.e., unwinding moment) to create a body diagram of entire helix geometry for condition of moment equilibrium. The proposed model was not applicable to a helical wire, which has multiple helical filar wires, since the rope geometry is deformed when the applied load changes. In addition, only the tensile component was considered in wires.

The Hruska's method was simplified and limited to the strands made up of single helical wires subjected to tensile loads. Such a model met the challenge when the configuration and geometries of wire became complicated or the stress components other than tensile or compression had to be considered (for examples, *bending*, *twisting* and *shear components*). Hruska's concept, idea, and Machida and Durelli (1973) and Costello et al (1985) in the later studies improved the approach by considering stress and strain on a core wire and single helical wire, force and moment equilibrium, displacement, helix geometry and friction.

Based on the Hertzian contact theory, Hruska's work provided three principal compressive stress equations subjected to a tensile load with single helix geometry and elastic properties of the material. This contact geometry was studied with equal diameter filars with a core strand. Analysis of contact stress of a wire rope of 6 x 7 was published in an article by Leissa (1959) and it was alike the work of Cress (1955). In response to Leissa's (1959) paper, Starkey and Cress (1959) analyzed the critical stresses and failure mode of a wire rope. It was a minor improvement to the earlier work of Cress (1955) and it offered further analytical results on the Hertzian contact theory. The geometry of wires at the contact points was idealized by the geometry of parallel and cross cylinders. In their study, they pointed out that the critical stresses occurring between wires were at the crossover points between adjacent strands. Bert and Stein (1962) further investigated complicated rope structure of 6 x 37 for the analysis of contact force and introduced the curvature geometry effect at the contact position following the work of Cress and Leissa. They proved that the calculated contact stress value was five times the yield stress of the wire material. Torque characteristics (unwinding moment) of wire ropes were studied by Gibson et al (1970). In their research, Hruska's approach for strands and ropes were pursued. They pointed out that the unwinding torque generated is linear with respect to tensile load for six stranded ordinary lay rope, Lang's lay rope and fiber core ropes. Reensnyder et al. (1972) summarized Hruska's analytical approach towards the study of the mechanical behavior of strands and ropes.

Hruska's strength of material approach was utilized to solve the wire rope problem (straight strand) and is assumed to be the original and an approximate method to evaluate forces and torque components that act on the helical wires and helical strands. However, this approach had a number of limitations since it ignored the following geometrical and mechanical influences on the strand and rope under external loading:

- 1) The geometrical relationships between core and helical wire, i.e., spatial configuration of strand and  $R/r$  ratio,
- 2) The mechanical interactions among adjacent wires and strands relating to friction, secondary bending and twisting,
- 3) The change of the helical geometry resulting from the incremental change in external applied load, i.e., the change in curvature, torsion and helix angle,

- 4) Mechanical components other than tension, i.e., shear force, bending and twisting moment on a single helical wire, and
- 5) Geometry of double helical wires in the rope.

The procedure by Hruska was implemented in the same decade to deal with the problem of contact in the 6/1 strand and 6 x 7 wire rope by Cress, Leissa, Starkey, Bert and Stein. However, the parallel cylinder, cross cylinder and the improved curvature method did not consider the three-dimensional interaction between wires at the contact locations, which greatly depended upon the strand and rope geometry and other design factors as follows:

- 1) The three-dimensional slippage, friction, wear and thermal effects,
- 2) The influence of galvanized coating,
- 3) The influence of mechanical interactions other than radial force,
- 4) The geometry at the contact locations, i.e., the double helix angle and curvature,
- 5) The influence of lubricants, and
- 6) The spatial relationship between the core wire radius, helical wire radius, helix angle and number of helical wires per layer.

### **2.2.2 Analytical Model by Costello et al**

In early 1970, S. Machida and A.J. Durelli (1973) presented detailed mathematical and analytical equations based on the Hruska's model. This will be further covered in Chapter 3; that model was for both of tensile and torsional loads, and the boundary conditions could be either of restricted or unrestricted ends. Their analytical models were well documented for the level of details. Many US engineers took advantage of their works for the further investigation on helical strands. One of them was Costello (1974). He worked with his fellow students at the University of Illinois, Urbana Champaign on the static and dynamic response of simplified bending theory of 6/1 strand wire and 6 x 19 construction of the Seale rope along with an *independent wire rope construction* (IWRC). Its approach was on a basic model response of helical wire within a strand. These strands, modeled as thin curved rods, were subjected to a combination of internal tensions, twisting moments, bending moments, shear forces and radial forces. The non-linear displacements and axial strains of wire strands were obtained from the “developed triangle” (refer Figure 2.1 (b)) in a deformed helix. Then, the non-linear

displacement equations were linearized by dropping the second and higher order differential terms. The relationships between helical wire and strand deformations are shown in Figure 2.1, and the first expressions required to solve the extension of a helical wire regarding tensile strain, contractions and rotation are given by:

$$\varepsilon_s = \frac{\Delta P_L}{P_L} \quad \text{eq. (2.1)}$$

$$\Delta\theta^* = \frac{\Delta\theta}{2\pi} \quad \text{eq. (2.2)}$$

where

$\varepsilon_s$  = strand strain

$\Delta P_L$  = Change in strand's lay length

$P_L$  = Strand's lay length

$\Delta\theta$  = Strand rotation per lay length

$\Delta\theta^*$  = Strand rotation per lay length (Defined parameter)

The radial contraction of helical radius is given by

$$\frac{\Delta R}{R} = \frac{\nu(a_c \varepsilon_s + a_h \varepsilon_w)}{R} = \Delta R^* \quad \text{eq. (2.3)}$$

where

$R$  = Initial helical radius

$\Delta R^*$  = Change in helical radius

$a_c$  = Core wire radius

$a_h$  = Helical wire radius

$\varepsilon_w$  = Helical strain

$\nu$  = Poisons ration of wire

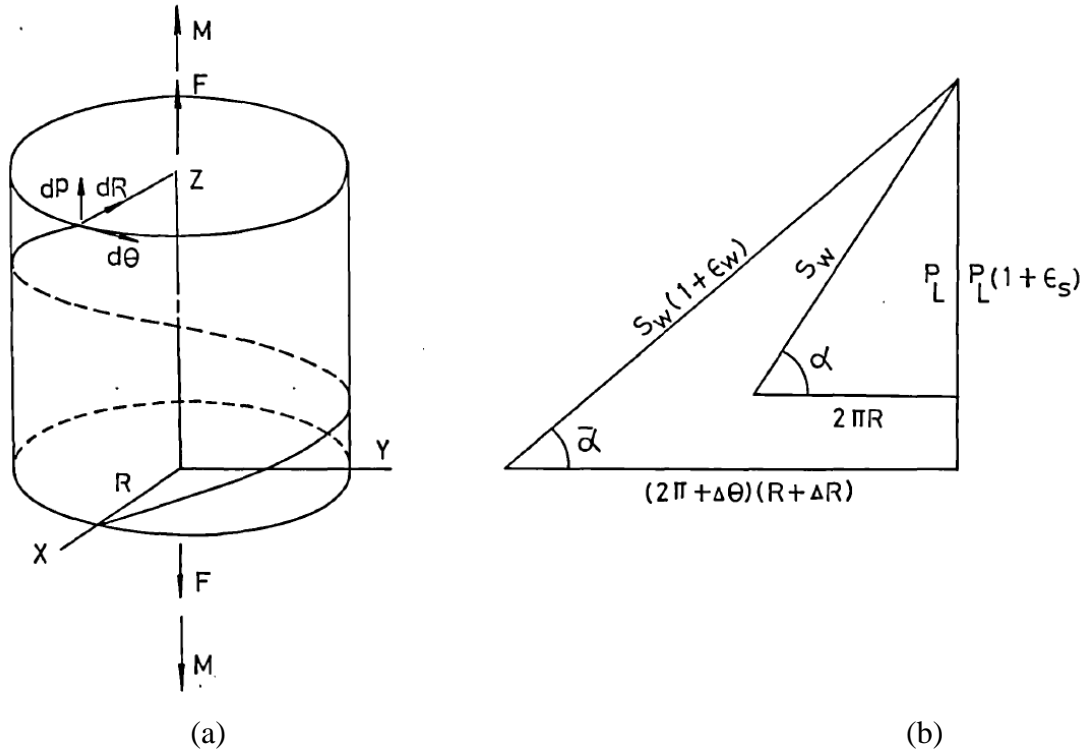


Figure 2.1 (a) Cylindrical Helix and (b) Its Development.

From the triangle of the developed helix, as shown in Figure 2.1(b), the obtained relationship is given by

$$\begin{aligned} S_w^2 &= (1 + \epsilon_w)^2 \\ &= P_L^2 (1 + \epsilon_s)^2 + (2\pi + \Delta\theta)^2 (R + \Delta R)^2 \end{aligned} \quad \text{eq. (2.4)}$$

where

$S_w$  = the length of Helical wire

Finally, a linearized model was developed to evaluate static response of helical wires within a strand. Frictional effects were not considered until the early 1980s when Buston (1981), one of the Costello's PhD students, introduced the frictional effects into the static and dynamic models for the responses of a 6/1 strand. Costello published the *Theory of Wire Rope* (1990), which promoted the understanding of helical geometries in detail about multiple filars with different configurations. Such models, where the geometry was a big contribution, the bending stiffness of cable was calculated as sum of the individual bending stiffness of wires and filars

interaction were assumed to have zero friction. Costello (1983) examined behavior of a under axial of a multilayered cable, loading conditions such as bending and torsional and concluded that the center wire suffered the highest stress in the axial. Similarly, Velinsky (1989) developed a methodology for multilayered wire strands; but the expectation was that a strand can retain its helical shape before and after its deformation. Kumar (1997) studied contact stresses under torsion and tension and found that the contact stresses are influenced by helix angle.

Velinsky (1981) worked on a higher complex rope construction. He was able to describe the bending and torsional effects; he modeled single wires of cables as lean rods (1985) and continued his model for various geometries core. The thin rod models were summed up with the forces on a section of wire to provide six moment equations, four of which were insignificant. Torsion and curvature were combined with the properties of cable and with the usage of a stiffness matrix in association with the equations of the moments to provide the cable response. During the investigation, the appreciation was given for the consideration of radial force along wires in contact and the ratio of helical wire radius to helical wire strand as functions of the number of helical wires per layer and helix angle.

The consideration was appreciated despite the comparable study published by Hruska (1951) in "Geometrie im Drahtseil". The similarity of their works are shown as below:

According to Costello's Publication, (1974)

$$\frac{r_1}{R} = \left\{ 1 + \frac{\tan^2 \left( \left( \frac{\pi}{2} \right) - \left( \frac{\pi}{n} \right) \right)}{\sin^2 \alpha'} \right\}^{1/2} \quad \text{eq. (2.6)}$$

where,

$r_1$ : Radius of individual helical wire

$R$ : Helical radius of individual helical wire

$\alpha'$ : Helix angle of wire

According to Hruska's Publication, (1958)

$$\frac{D'}{d} = \left\{ 1 + \frac{\cot^2 \left( \frac{180}{n} \right)}{\cos^2 \alpha} \right\}^{1/2} \quad \text{eq. (2.7)}$$

where,

$D'$ : Diameter of single helical strand

$d$ : Diameter of a single helical wire (filar)

$\alpha$ : Helix angle of wire

Above two equations are similar when  $\alpha'$  is equal to  $(90-\alpha)$ .

The Kirchhoff's naturally curved rod theory solved the static mechanical response of single helical wires within a strand. It was not a new concept as a similar assumption was proposed by Hansom (1949) in a Ph.D. thesis titled "The Mechanics of Locked Coil Ropes" at the University of Birmingham. Hansom didn't utilize the rod theory to analyze his rope problem, but Costello and his fellow workers used the rod theory to study the static response of strands and ropes. Apart from the methods of Hruska and Costello, other scientists showed their interest in the single layer helical strand and took control of equations on the static response of cables under tensile and torsional loads. Their work review will be discussed in the next section.

### **2.2.3 Analytical Models by Machida, Huang, Knapp et al.**

The Machida and Durelli's (1973) paper explained in a precise mathematical model for single layer 6/1 strand response under the tensile and torsional loading conditions. The procedure used was similar to the Hruska's strength of material method but with the consideration of the change of helix geometry as the result of loading. The acting forces and moments on each of the filars was combined toward the applied loads. Four major boundary conditions were *fixed ends*, *free ends*, *twisting and combined loads* (both tension and torsional); and the corresponding equations were developed based on the analysis.

Knapp (1978) worked on the mechanical behavior of helically armored cable. He proposed the linearized and non-linear analytical cable models that were subjected to a pulling (tension) load. The Knapp's approach towards analytical equation was very comparable to the Machida's work. However, the improvements were made to especially deal with the problems of cable especially. He proposed that the analytical models to dealt with the bending of cable over sheaves under frictionless and high friction conditions. There was a comparison of the analytical results with the experimental results and a good agreement was proven.

Huang (1978) used the rod theory in his work to study the static response of a 6/1 strand, which was similar to Costello. He considered friction between adjacent filars and did not notice any significant effect in the contrast with and without friction in the spatial configuration of the strand. Huang concluded that when core and filars were made of the same materials, the extension of the wire rope would cause a separation between them.

Beginning with the wire geometry, Chiang (1996) implemented the finite element approach to find six significant parts that influenced cable stiffness and stress with the parameters of the core wire radius, helical (layer) wires radius, strand length, helical angle, boundary condition and the contact conditions among the core wire and helical wires. His work was unique during the publication time since he looked at the interactions between various parameters of cable. The results were comparably favorable with particular models of thin rod.

Utting and Jones (1987), Velinsky (1985), Caughey and Irvine (1974) modelled the helical wire strands with cores initially as tension of strings. This involved an insignificant stiffness of bending and torsion. But the stiffness value for bending and torsion were not insignificant for cables when they were utilized in medical devices. Modelling wire rope efforts were put by using beam formulations. As discussed earlier, the stiffness of bending and torsion of individual wires of a thin rods wire rope was first incorporated by Costello. In contradiction to the model of thin rod, Raoof and Hobbs (1988) and Jolicoeur and Cardou (1996) created semi-continuous models. In their models, a layer of wires was modelled as an orthotropic cylinder with qualities that matched layer of the rope. Strand stiffness and interwire effects were considered. Analytical modeling schemes worked as a progressive incorporation of different mechanical contributions on the coupled axial and the torsional response of helical structures. In early modeling developments, the axial stiffness of the helix cross-section had only one mechanism taken into accounts for the record of the helix response (Hruska 1951). Machida and Durelli (1971) incorporated the outcome of the torsional stiffness of the helix cross-section which was further elaborated by McConnell (1982). Lastly, Sathikh et al (1996) presented the thin beam theory model, which provided a symmetric axial torsional strain stiffness matrix. Yuen (1979) and Karamchetty (1979) analyzed the contact problem in a wire rope and the contact stresses induced at contact points resulting due to deformation under loading. Several finite element (FE) models of wire rope under tension were available, which incorporated the non-linear behavior of wire rope. There were limited number of models that included bending and torsional Helical strand. A wire-stranded medical hollow tube construction and manufacturing patent was invented and registered by Asahi Intec Co., Ltd. US Patent No- 6881194 B2 April-2005. They described the construction and manufacturing process but never disclosed the characteristic performance calculations. The term HHS® tube was developed and registered by



Fort Wayne Metals, Fort Wayne, Indiana. It is a medical equipment manufacturer and is one of the major manufacturers and supplier of HHS® tubes in the medical application industries.

### **2.3 Summary of Existing Analytic Modelling Methods**

The majority of existing methods were developed a few of decades ago, and the applicable wire and rope products were mainly in structures and constructions. The main features of those products were (1) the main load types are tensional loads, (2) the dimension along the wire or rope profile is significantly larger than other directions over its cross-section, (3) the impact of wire designs such as the number of wires, pitch angles, and configurations on the capacities of wires or ropes are not main concerns since the resistance of tensile or compression mainly depended on the area of cross-section. The existing analytical models have their limitations to take into consideration of the complexity, and all of the main design variables involved in HHS tubes are the relational model of angular displacement and torsional torques.

### 3. PREDICTION BY NUMERICAL SIMULATION

This chapter reports the prediction of torsional torque subjected to a given angular displacement using numerical simulation. The FEA methodology is introduced, and the Abaqus software is utilised to create and run FEA model for HHS tubes. The experiment setup is replicated to develop FEA models in simulation; input material data such as yielding stresses and strains was taken from experiments data. The Hypermesh software was used as a pre-processing tool to mesh the models, and Abaqus CAE 6.14 version was used as the tool for solving and post processing. Numerical analysis in Abaqus is performed by following the Explicit integration method with the combination of Hexahedron and pentahedron (C3D8I- 8 node brick element) meshing.

**Keywords** – Abaqus, Hypermesh, Explicit integration method.

#### 3.1 Finite Element Methodology

A finite element method (FEM) technique is used to obtain a similar solution to engineering problems governing by partial differential equations. An engineering problem is a group of partial differential equations with defined boundary conditions; therefore, they are referred as *boundary value problems*. The discretization in an FEM converts partial differential equations into algebraic equations that are easy to solve. Because of its capability to handle complex problems and its flexibility for a variety of engineering problems, FEM has gained a prominent role in engineering analysis and design.

FEM is an approximated approach which requires the models from different perspectives. As shown Figure 3.1, a real system with a mathematical model and the continual model is assumed in discretized as FEM model with nodes and elements. The solution from an FEM approach appropriately representates a real physical system into a mathematical model and can provide a similar solution to a mathematical model; the approximation of obtained solution is ensured by the convergence. FEM has become a default design tool in engineering practice.

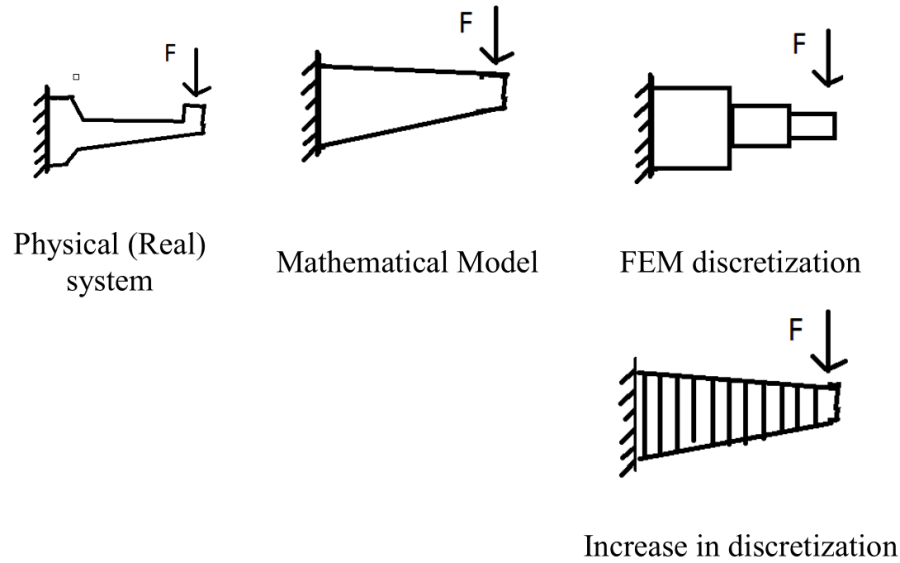


Figure 3.1 Fem Approximation Methods (Gokhale Et Al 2008)

Numerous software tools are available for finite element analysis, and Table 3.1 shows some common packages which are specialized in fulfilling some tasks related to FEM.

Table 3.1 Common Commercial FEA Software Used by Industries

Generally used FEA commercial software's in Industries		
Pre-processing	Solver	Post-Processing
Hypermesh, SimLab	Optistruct, Radioss	HyperView
Abaqus CAE	Abaqus	Abaqus Post
Ansa, Primer	LS Dyna	LS Pre-post
MSC. Patran Preprocessor	MSC. Nastran	MSC Patron Post processor
ANSYS Preprocessor	ANSYS	ANSYS Post processor

### 3.1.1 Discretization and Representation of Elements

In FEM, a solid object is partitioned into small pieces and they are hence called as *elements*. Fig. 3.2 shows some types of elements and their degrees of freedom. Exemplifying the *brick elements*, which are used for the modeling HHS tube.

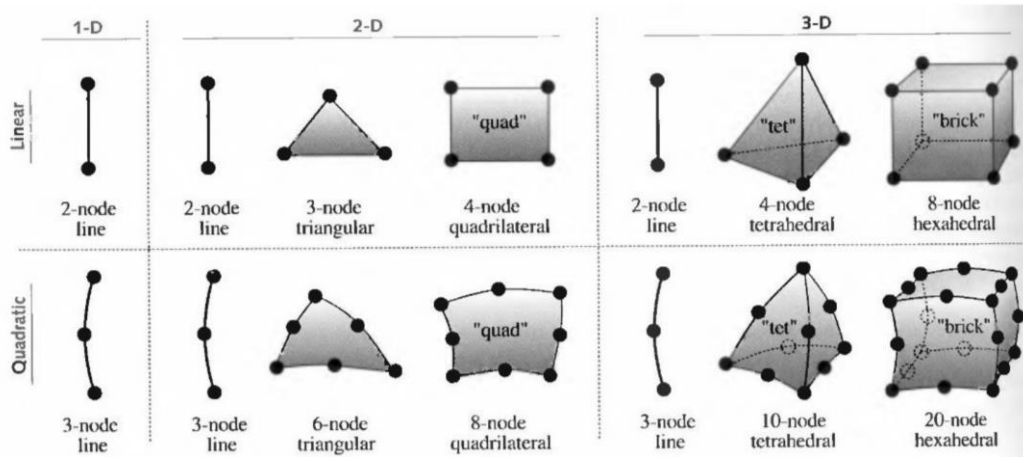


Figure 3.2 Element Types and Their Degrees of Freedom (Norton 2006)

**Tetrahedral and Hexahedral Elements** are three-dimensional and generic solid elements used for complex thick parts. Brick elements are widely used to predict the distribution of field variables which vary cross the thickness of part. By their definitions, a solid element does not have rotational degrees of freedom; however, since a solid element has more nodes and thus a high number of total degrees of freedom; it takes longer to solve the model. Such types of elements are commonly used for a part with bulk volume and complex geometry.

Element types can also differ with each other based on the order of shape functions an element uses. A *shape function* could be *quadratic*, *cubic* or *linear* and so on up to the  $n^{th}$  order of polynomial functions.

Each of these element topologies has its own advantages and disadvantages. For example, tetrahedral elements are easier to create on complex geometries but have slower convergence compared hexahedral elements, while brick elements are very much desired in computational expensive simulations such as damage modelling due to better convergence and accuracy but cannot be created easily. Figure 4.3 shows some examples of element types in Abaqus. An element's number of nodes determines the interpolation of freedom of nodal degrees (Displacements and Rotations) over domain of element. In this thesis, Hexahedral elements

(C4D8I 8-node brick element incompatible mode) are adopted for complex spiral geometry. These elements can fit better for complex geometry with distortion controls. The incompatible mode 8-node element is an improved version of C3D8-brick element.

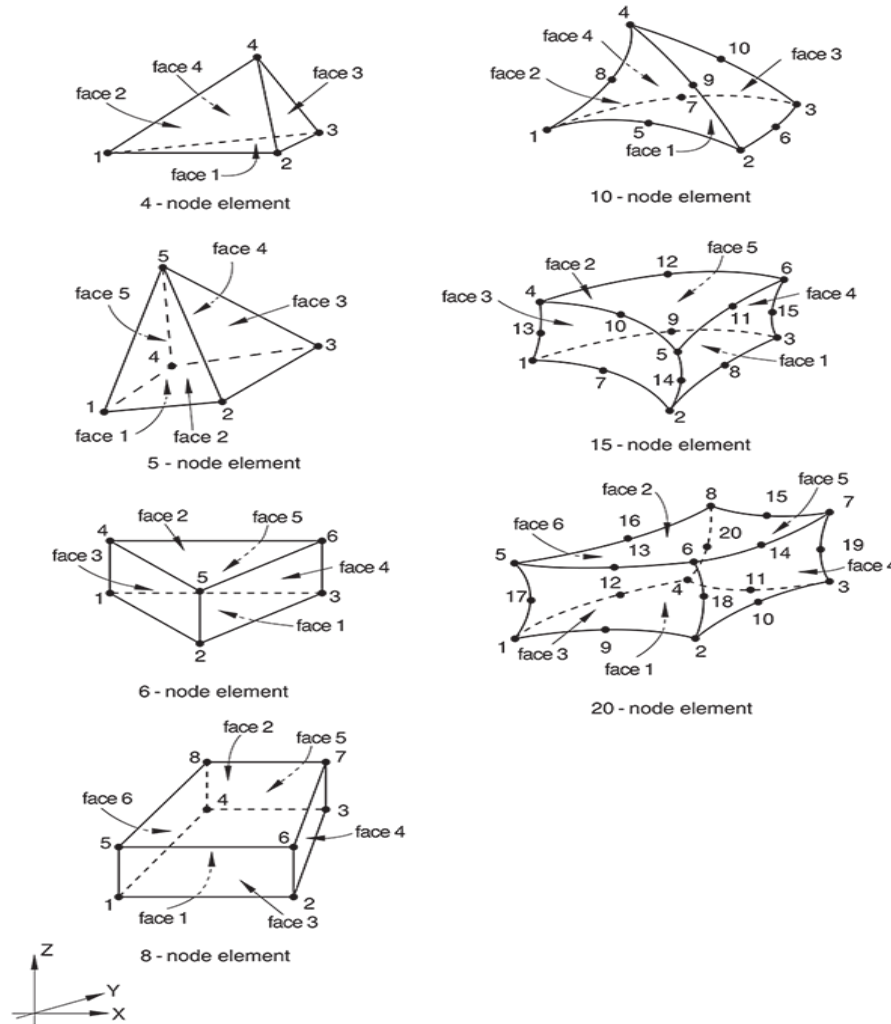


Figure 3.3 Element Types with Various Node Configurations (Abaqus 6.12 User Manual)

In an analysis of finite element, the model mesh may be required to refine for a converged result. The refinement of a mesh can be performed in either of the *h-refinement* or *p-refinement* approach. Figure 3.4 shows the ideas of the two approaches.

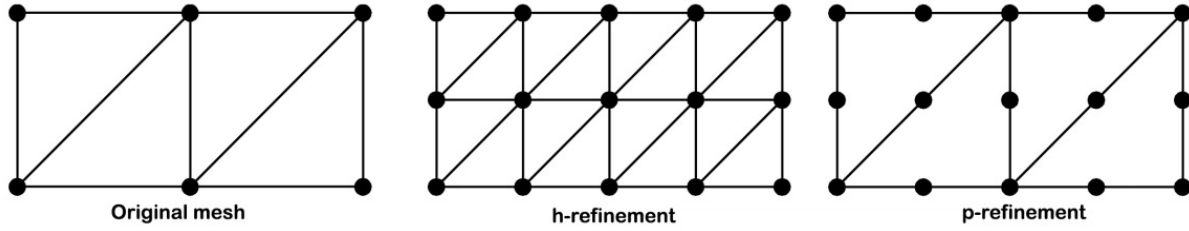


Figure 3.4 The H-Refinement and P-Refinement Approaches (Sheshu 2003)

The most common elements used by FEM codes are the h-refinement approach. In h-refinement approach, the order of an element is not changed, but the mesh is refined by the size increase and number of elements at the regions of high stress gradient. In a p-refinement approach, the number of elements are not changed, but the order of elements are increased which allow higher order shape functions to represent the behaviors of elements better. This type of refinement is also gaining its popularity in many commercial FEM codes.

### 3.1.2 General Formulation of Solid Elements

In this research, solid elements are primarily used for FEM analysis. Hence, the representation and the model solution of solid elements are discussed. In a solid model, the interpolation of displacement field using the shape function  $N_i$  is (Bathe, 1996),

$$u = \sum_{i=1}^N (N_i u_i) \quad v = \sum_{i=1}^N (N_i v_i) \quad w = \sum_{i=1}^N (N_i w_i) \quad \text{eq. (3.1)}$$

Where,  $u_i$ ,  $v_i$  and  $w_i$  are the displacement nodal values of the element and  $N$  represents the quantity of nodes on the element. Eq. 4.1 can be written into a matrix form as,

$$\begin{pmatrix} u \\ v \\ w \end{pmatrix} = \begin{pmatrix} N_1 & 0 & 0 & N_2 & 0 & 0 & \dots \\ 0 & N_1 & 0 & 0 & N_2 & 0 & \dots \\ 0 & 0 & N_1 & 0 & 0 & N_2 & \dots \end{pmatrix} \times \begin{pmatrix} u_1 \\ v_1 \\ w_1 \\ u_2 \\ v_2 \\ w_2 \\ \dots \end{pmatrix} \quad \text{eq. (3.2)}$$

Or

$$\mathbf{u} = \mathbf{N} \mathbf{d} \quad \text{eq. (3.3)}$$

Similarly, the strain displacement relation in 3D is given by,

$$\begin{pmatrix} \varepsilon_x \\ \varepsilon_y \\ \varepsilon_z \\ \gamma_{xy} \\ \gamma_{yz} \\ \gamma_{zx} \end{pmatrix} = \begin{pmatrix} \frac{d}{dx} u \\ \frac{d}{dy} v \\ \frac{d}{dz} w \\ \frac{d}{dx} v + \frac{d}{dy} u \\ \frac{d}{dy} w + \frac{d}{dz} v \\ \frac{d}{dz} u + \frac{d}{dx} w \end{pmatrix} \quad \text{eq. (3.4)}$$

With these equations strain vector is derived by using relation given in eqs. (3.1) and (3.4)

$$\boldsymbol{\varepsilon} = \mathbf{B} \mathbf{d} \quad \text{eq. (3.5)}$$

Where,  $\mathbf{B}$  matrix relates the nodal displacement vector  $\mathbf{d}$  to the strain vector  $\boldsymbol{\varepsilon}$ .

The stored strain energy in an element, is given by

$$U = \frac{1}{2} \int_V \boldsymbol{\sigma}^T \boldsymbol{\varepsilon} dV \quad \text{eq. (3.6)}$$

Finally, general formulation is obtained for stiffness matrix of element, which is

$$\mathbf{k} = \int_V \mathbf{B}^T \mathbf{E} \mathbf{B} dV \quad \text{eq. (3.7)}$$

The above equation is written in matrix form by calculating by finite element method.

### 3.1.3 Representation of Field Variables

For structural analysis, the elemental behaviours are represented by some field variables such as *stresses*, *strains*, and *strain rates*. To define plastic deformation, *true stress* and *true strain* is used to interpret the data correctly for calculating parameters of elastic-plastic model. Note that the material test data is supplied from standardized tensile test using nominal stress and strain values for *engineering stress* and *engineering strain* where varying cross section with increase in load is not taken into account. To avoid those situations plastic material data is converted from nominal to true stress-strain values by following formulas from Table 3.2 (NPL).

Table 3.2 True Stress and True Strain Formulas ((NPL) National Physical Laboratory Manual)

True Stress	$\sigma_T = \frac{\sigma'_T}{(1 - \nu' \varepsilon'_T)^2}$
True Strain	$\varepsilon_T = \ln(1 + \varepsilon'_T)$
True Transverse Strain	$\varepsilon_t = \ln(1 + \varepsilon'_t)$
Nominals Poison's Ratio	$\nu' = -\frac{\varepsilon'_t}{\varepsilon'_T}$
Young's Modulus	$E = \frac{\sigma_T}{\varepsilon_T^e}$
True poison's ratio	$\nu = -\frac{\varepsilon_t}{\varepsilon_T}$
True plastic strain	$\varepsilon_T^P = \varepsilon_T - \ln(1 + \frac{\sigma_T}{E})$
True Transverse Plastic Strain	$\varepsilon_t^P = \varepsilon_t - \ln(1 - \nu' \frac{\sigma_T}{E})$
True Plastic Poisson's Ratio	$\nu^P = -\frac{\varepsilon_t^P}{\varepsilon_T^P}$

$\sigma'_T, \varepsilon'_T, \varepsilon'_t$  denote nominal values of tensile stress, axial strain and transverse strain respectively, which is calculated by using original specimen dimensions.

$\sigma_T, \varepsilon_T, \varepsilon_t$  denote actual values of tensile stress, axial strain and transverse strain respectively, they consider the instantaneous specimen dimensions.

$E, \nu'$  denote Young's modulus and nominal Poisson's ratio respectively. They are evaluated at a particular point or by reverting over a strain range. The former is calculated by dividing stress by strain. At smaller strains, true values are similar to the nominal values.

$\nu, \varepsilon_T^e$  denote true Poisson's ratio and true elastic axial strain respectively.

$\sigma_T^P, \varepsilon_T^P, \nu^P$  denote true axial plastic strain, true transverse plastic strain and true plastic poisons ratio respectively.

Abaqus estimates the smooth stress-strain behaviour of a material by connecting the given data points to a series of straight lines. The data of stress and strain curve defines the true yield stress of material as an objective of true plastic strain. While there are negligible differences between nominal and true values at small strains, it is not the case at larger strain values. At larger strain values, there are significant differences. Therefore for large strains, it is



highly advised to provide input stress-strain data in Abaqus simulation (Abaqus 6.12 User Manual).

### **3.1.4 Meshing Techniques**

It is a well-known fact in the CAE community that the efficiency and accuracy of finite element models are directly dependent on the quality of the underlying mesh of model. Abaqus/CAE provide diverse techniques to mesh various models of topologies. The various quality parameters associated with elements are element size, aspect ratio, skew angle, Jacobean, and warpage angle. Various meshing techniques provide different levels of automation and user control. Moreover, two meshing practices are available in Abaqus/CAE, they are top-down meshing and bottom-up meshing.

Top-down meshing develops a mesh by functioning down from the geometry of a part to the individual mesh nodes and the elements. The Top-down meshing meshes 1D, 2D or 3D geometry using the available type of element. The resulting mesh precisely complies to the original geometry. The rigid compliance to its geometry makes top-down meshing an automated process, but it gets complicated to produce a high-quality mesh in complex shapes regions. Producing a mesh using bottom-up meshing technique is a manual process, and the resultant mesh may differ from the original geometry. However, allowing the mesh to vary from a geometry may produce a high-quality hexahedral mesh in complex shapes regions.

The Bottom-up meshing produces a mesh by functioning up from two-dimensional entities to produce a three-dimensional mesh. The bottom-up meshing to mesh is only for solid three-dimensional geometry that uses almost all hexahedral elements.

Producing a mesh by the bottom-up meshing technique is a manual process, and the resultant mesh varies from the original geometry. However, allowing the mesh to differ from geometry allows to produce a high-quality hexahedral mesh in complex shapes regions (Abaqus 6.12 User Manual).

### **3.1.5 Explicit Integration**

A system model of numerical simulation can be solved explicitly or implicitly. To begin with, all numerical analysis for this thesis is done by using the Explicit Integration methods. It accounts for inertial effects with sectional changes that happens during dynamic simulations. An

explicit solution takes account of the finite propagation speed (at the speed of sound) of dynamic effects through the material. A good meshing technique is used to represent the spatial effects and time-steps of the similar magnitude of the transit time of sound waves from each element to its neighbors. If the time steps exceed that size, the response will usually be unstable and the analysis will fail after a few time steps. The time step size is restricted by the smallest element in model and not by the average size. It utilizes a large theory of consistent deformation, where it goes through big rotations and deformations. Additionally, it is preferred for complicated contact problems that influences results (Abaqus 6.12 User Manual).

### 3.1.6 Numerical Implementation

In general, the procedure is to implement the explicit integration rule by merging and using lumped element mass matrices diagonally. The motion equations of the body are integrated by utilizing the rule of central-difference integration (Abaqus 6.12 User Manual).

$$\dot{u}_{(i+\frac{1}{2})}^N = \dot{u}_{(i-\frac{1}{2})}^N + \frac{\Delta t_{(i+1)} + \Delta t_i}{2} \ddot{u}_i^N, \quad \text{eq. (3.8)}$$

$$u_{(i+1)}^N = u_i^N + \Delta t_{(i+1)} \dot{u}_{(i+\frac{1}{2})}^N \quad \text{eq. (3.9)}$$

$u^N$  denotes the amount of displacement element and the letter “i” denotes the increment number in a dynamics step. The operator of central-difference integration has a kinematic state, which advances by using acquired values of  $\dot{u}_{(i-1/2)}^N$  and  $\ddot{u}_i^N$  by earlier increment.

The explicit integration rule is considerably easy and on its own it does not give the efficiency linked with the method of explicit dynamics. The solution to efficiency of the explicit method is the element mass matrices diagonally utilized as beginning accelerations of the addition is computed by

$$\ddot{u}_i^N = (M^{NJ})^{-1} (P_i^J - I_i^J) \quad \text{eq. (3.10)}$$

where  $M^{NJ}$  represents mass matrix,  $P^J$  represents applied load vector, and  $I^J$  represents internal force vector. A mass matrix is utilized because its inverse is easier to compute for and also because mass inverse vector multiplication by inertial force requires “n” operations only, where “n” represents the model’s number of freedom degrees. The explicit procedure do not

require any tangent or iterations stiffness matrix.  $I^J$  represents the internal force vector formed from individual elements contributions so that there is not formation of global stiffness matrix (Abaqus 6.12 User Manual).

### 3.1.7 Incremental Stability

An estimation of limit of stability is determined by the dilatational wave's smallest transit time over any mesh other elements (Abaqus 6.12 User Manual).

$$\Delta t \approx \frac{L_{\min}}{C_d} \quad \text{eq. (3.11)}$$

$L_{\min}$  denotes the dimension of the smallest element in the mesh and  $C_d$  denotes the dilatational wave speed in  $\lambda_0$  and  $\mu_0$ , which is defined below.

The current dilatational wave speed  $C_d$  is calculated from the hypo elastic material moduli from its response. Effective Lamé's constants  $\hat{\lambda}$  and  $\hat{G} = 2\hat{\mu}$  are determined below.  $\Delta p$  defines the mean stress increment,  $\Delta S$  defines the deviatoric stress increment,  $\Delta \epsilon_{\text{vol}}$  defines volumetric strain increment, and  $\Delta e$  defines deviatoric strain increment. It is assumed as hypo elastic stress-strain rule of the form (Abaqus 6.12 User Manual).

$$\Delta p = (3\hat{\lambda} + 2\hat{\mu})\Delta \epsilon_{\text{vol}} \quad \text{eq. (3.12)}$$

$$\Delta S = 2\hat{\mu}\Delta e \quad \text{eq. (3.13)}$$

The effective moduli is then computed as

$$3\hat{K} = 3\hat{\lambda} + 2\hat{\mu} = \frac{\Delta p}{\Delta \epsilon_{\text{vol}}} \quad \text{eq. (3.14)}$$

$$2\hat{\mu} = \frac{\Delta S : \Delta e}{\Delta e : \Delta e} \quad \text{eq. (3.15)}$$

$$\hat{\lambda} + 2\hat{\mu} = \frac{1}{3}(3\hat{K} + 4\hat{\mu}) \quad \text{eq. (3.16)}$$

Shell cross-section define the shell elements that need numerical integration and the resultant section moduli is computed by adding the effective thickness of moduli at section points. They denote the stiffness and speed of current dilatational wave of the element as

$$C_d = \sqrt{\frac{\hat{\lambda} + 2\hat{\mu}}{\rho}} \quad \text{eq. (3.17)}$$

where  $\rho$  is the density of the material.

In an elastic and isotropic material, the resultant Lamé's constants are interpreted in Young's modulus,  $E$ , and Poisson's ratio,  $\nu$ , by

$$\hat{\lambda} = \lambda_o = \frac{Ev}{(1+\nu)(1-2\nu)} \quad \text{eq. (3.18)}$$

and

$$\hat{\mu} = \mu_o = \frac{E}{2(1+\nu)} \quad \text{eq. (3.19)}$$

In terms of conventional shells, beams and membranes, the dimension of cross-section of element is utilized to know the smallest element dimension. The limit of stability is established on the membrane dimensions. Transverse shear behavior also determines the stable time increment, when it is defined for shell elements.

$\Delta t$  estimates only approximately and in most cases is not a close to actual value. Generally, the increment of stable time chosen by Abaqus/Explicit is lesser than by a factor of between  $1/\sqrt{2}$  and 1 in a 2D model and it is between  $1/\sqrt{3}$  and 1 in a 3D model. The increment in time of Abaqus/Explicit accounts for stiff behavior of a model and associates with a penalty contact (Abaqus 6.12 User Manual).

### 3.2 Commercial Software Tool - Abaqus

Numerous software tools are available. In this thesis, Abaqus is adopted for numerical simulation. It is primarily used for analysis and modelling of mechanical assemblies in pre-preparation and afterwards for finite element analysis result in post-preparation visualization. Moreover, this software has various features for performing Static and dynamic analysis using both standard and advanced methods. Additionally, this software is widely used by many researchers for its good documentation, excellent user interface with option of creating animations, broad material modelling capability, and customizing ability of the program.

Moreover, Abaqus has three prominent methods that are widely used in academic and non-academic sectors and they are called as Abaqus/Standard, Implicit and Explicit methods. It is briefly explained below.

**Abaqus/Standard** is a higher efficient way of solving smooth non-linear problems; but problems of quasi static that are solved with Abaqus/Standard have problems to converge because of complexities of the material, which results in a lot of iterations. Analysis in Abaqus/Standard can be expensive because it has an iteration requiring a large quantity of linear equations solved.

**Abaqus Implicit** is comparable to the Explicit system, difference being that each increment applies Newton-Raphson algorithm to emphasize the equilibrium. Therefore, larger increments are achievable and the precision is typically higher compared to the case of Explicit. It is also numerically expensive since the system matrices are updated in the iterations of Newton-Raphson algorithm.

**Abaqus Explicit** is calculative for analyzing larger models with short response times and analyzing extremely discontinuous processes. An Explicit FEM analysis follows an incremental procedure and at the end of each increment update, the stiffness matrix bases itself on any applicable material changes. Construction of a new stiffness matrix and later displacement increments to the system are applied. This method is used for the thesis as the problem has large displacements and material non-linearity.

### 3.3 Modelling Procedure

The modelling procedure is illustrated in Figure 3.5; it consists of 10 main steps from pre-processing, processing to post-processing.

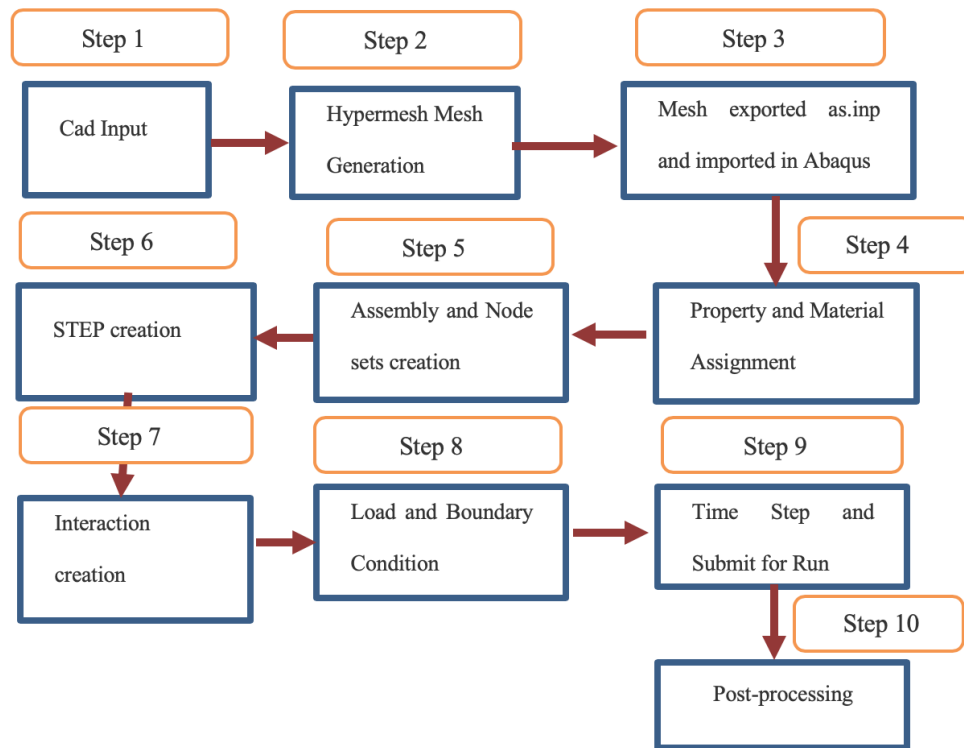


Figure 3.5 FEM Procedure to Perform Simulation by CAE Software

Figure 3.5 continued

Step	Task
1	The CAD file in .STEP format was prepared in the Altair's Hypermesh software.
2	Once the file imported in Hypermesh, the geometry is reviewed carefully through visualization to eliminate possible errors. The Hexa-Penta combined mesh is generated with given element sizes. Once the mesh is completed, all types of standard quality criteria are taken care, and the file is exported as .inp (Abaqus format).
3	The exported mesh from the Hypermesh is imported into the Abaqus software finite element analysis.
4	The experimental material data is assigned to the model as well as the data of section properties of elements.
5	The assembly is created in the default global coordinate system and the reference nodes are created on both ends, which are used to define boundary conditions.
6	The load STEP which defines the type of analysis as 'Explicit' one.
7	The contacts are defined at contacts of adjacent filars as GENERAL EXPLICIT CONTACTS and the coefficient of friction is specified.
8	Once material properties, section properties, node sets, and the contacts are defined, the loading and boundary condition are defined at both ends (refer Fig 4.6).
9	With a completed model, one can define a job, and submit, run, and solve the model.
10	A success run leads to an output file as an .odb file, it can be further post-processed to visualize results. (The executed .inp file is provided in Appendix).

### 3.3.1 Boundary Conditions

Figure 3.6 gives a parametrized representation of an HHS tube. As a case study, the total length of the strand is given as 4-inch. It is fixed at one end and angular displacement of 180 degree is applied at other end. Explicit general contact is defined between filars with the friction co-efficient of 0.5.

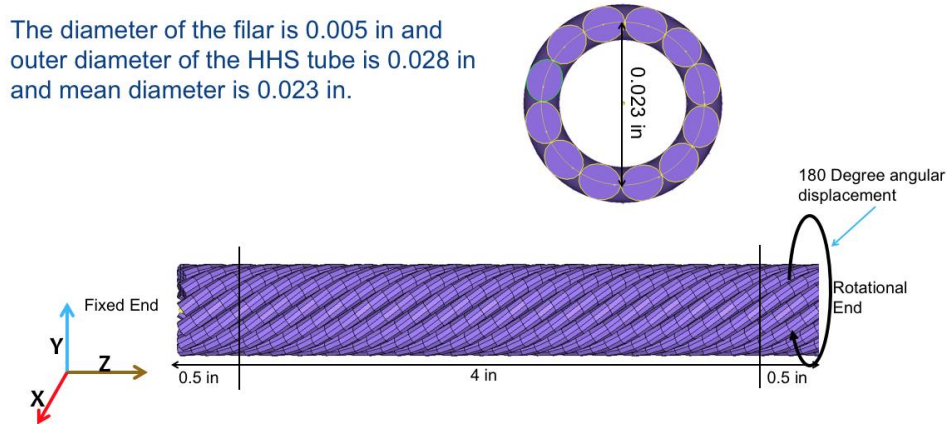


Figure 3.6 Load and Boundary Condition of HHS Tube

### 3.3.2 Fracture Analysis

To perform fracture analysis over an FEA model, the behaviour of materials in its plastic range must be defined as the inputs of simulation. Those inputs include *tri-axiality stress*, *strain rate* and *fracture strain*. The comparable plastic strain at the damage onset is a function of strain rate and stress triaxiality that can be described by following equation,

$$\text{Stress triaxiality } \eta = -p/q \quad \text{eq. (3.20)}$$

Where p: plastic strain and q: strain rate

During the deformation by a tensile test, stress is applied along axis of the specimen i.e., uni-direction in the materials. After the stress reaches the yield strength, plastic deformation occurs, and the materials begins to have necking. Necking region exhibits the stress in all of three directions, where this multi-axial stress causes a decrease of overall stress of materials. This property is called *stress triaxiality*.

Moreover, Stress triaxiality is an invariant stress, which can be defined as ratio of mean stress to the equivalent von misses stress as,

$$\frac{\sigma_h}{\sigma_{eqv}} = TF = \frac{1/3(\sigma_1 + \sigma_2 + \sigma_3)}{\frac{1}{\sqrt{2}}\sqrt{(\sigma_1 - \sigma_2)^2 + (\sigma_2 - \sigma_3)^2 + (\sigma_3 - \sigma_1)^2}} \quad \text{eq. (3.21)}$$

where  $\sigma_1$ ,  $\sigma_2$  and  $\sigma_3$  are first, second and third stresses (principal),



$$\frac{\sigma_1 + \sigma_2 + \sigma_3}{3} = \text{Hydrostatic stress, and}$$

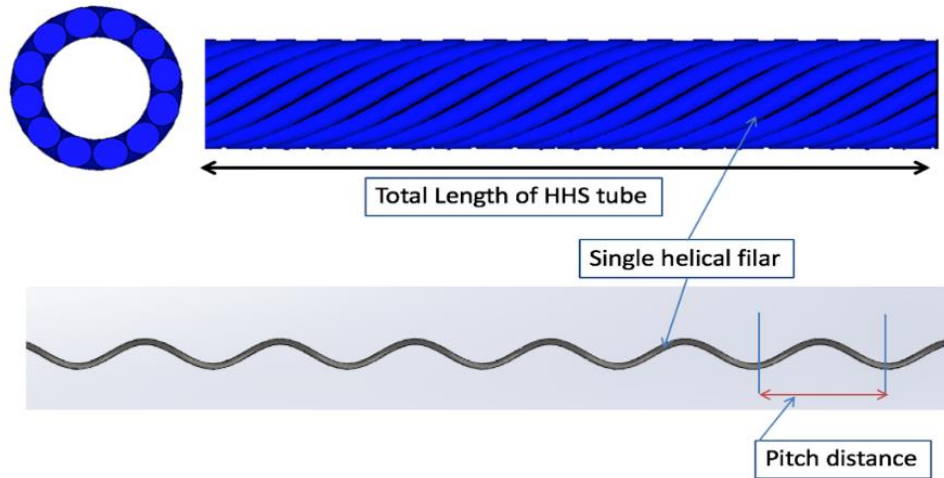
$$\frac{1}{\sqrt{2}} \sqrt{(\sigma_1 - \sigma_2)^2 + (\sigma_2 - \sigma_3)^2 + (\sigma_3 - \sigma_1)^2} = \text{Equivalent von mises stress.}$$

Hydrostatic stress and Von mises stress mentioned in above formula is obtained from Abaqus output requests. These values are used as damage parameters and later inputted into material properties where fatigue simulations are performed to determine fracture. The damage behavior strongly depends on the type of loading and it is not modeled with basic damage models on constant fracture strain based. The huge need to enhance the technologies quality, developed many tools to assist engineers with understanding the failure mechanism behavior of material such as computational mechanics.

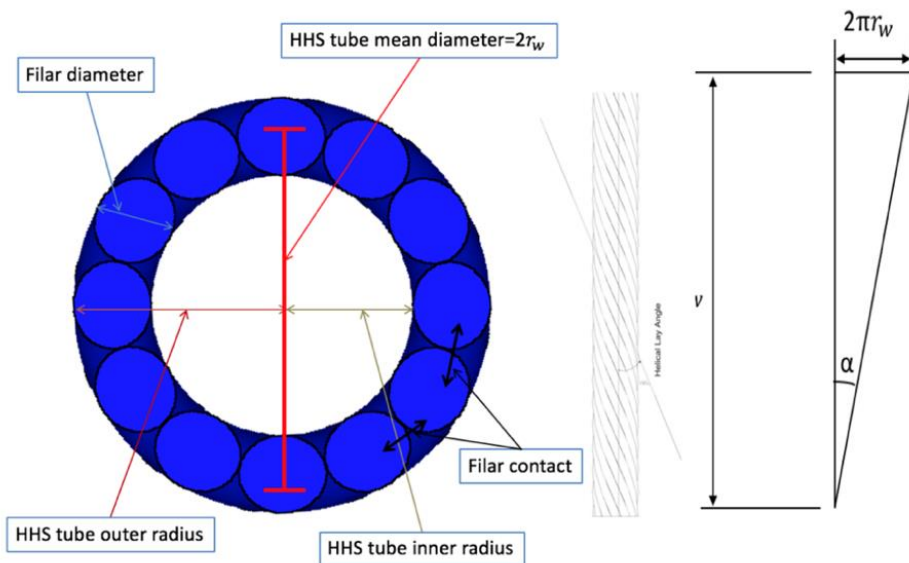
### 3.4 Case Study

As an example, this case study describes of the numerical model for 1x12x0.005, 0.028 HHS tube with loading and boundary conditions mentioned in Section 3.4.1. Abaqus Explicit is used for numerical simulation. The simulation is performed by the direction of the applied angular displacement as clock-wise (CW). The mesh is generated in the Hypermesh software with the mesh type of brick elements. The generated mesh is imported in the Abaqus CAE software 6.14 and the rest procedure is explained as figure 3.5 are defined. This study aims to understand the relationship between applied angular displacement vs. torque. secondary aim of the case study was to identify ,the design issues which influence the torque factors and as such affect leads to failure of the tube.

Figure 3.7 gives the brief about the parameter values such as pitch, radius of HHS tube, number of filars, radius of filars, total length of the HHS tube, lay type and helical angle.



(a) Pitch dimension



(b). Helical angle

Figure 3.7 HHS Tube Classification

An advantage of Abaqus Explicit is that the load is applied gradually and hence the gradually-changing response of the tube and the gradually-increasing load can be obtained in a single simulation. The relations of the torsional load and specified torsional angle in CW is obtained and illustrated in Figures 3.9. As the final outcome of result of interest is the torque vs angular displacement, only the graph is shown.

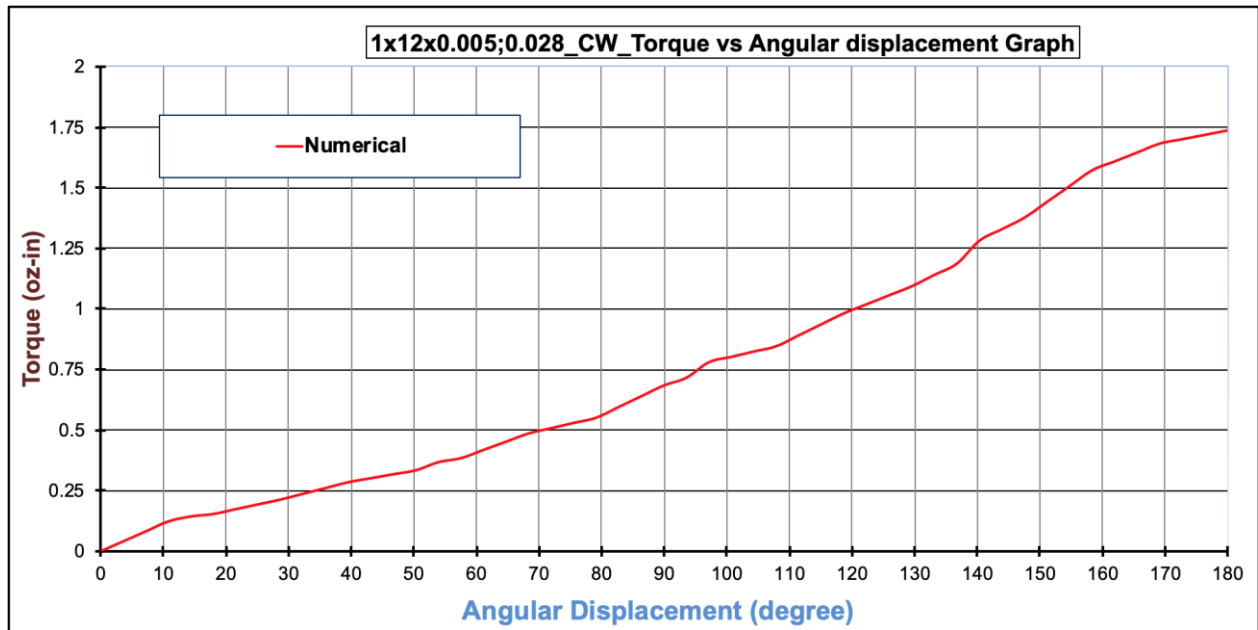


Figure 3.8 1x12x0.005 HHS Tube Clockwise Angular Rotation Vs Torque at 180°

As discussed in Section 3.5, the same model can be used for the fracture analysis. Using the equations presented in Section 3.5, the stress triaxiality can be determined, where in this case triaxiality is extracted from Abaqus output requests. The value is calculated from von mises stresses and hydrostatic stress which is found during simulation. Meanwhile, in pre-processing phase strain acquired during the fracture of the material was inputted in Abaqus along with the fracture strain rate which is obtained from axial test data. The displacement during fracture also plays vital role for damage initiation criteria in the simulation.

The stress triaxiality value obtained from the axial test simulation by ABAQUS is 1.08, where this value is inputted in torsional displacement simulation to perform breaking test, which is shown below figure 3.10.

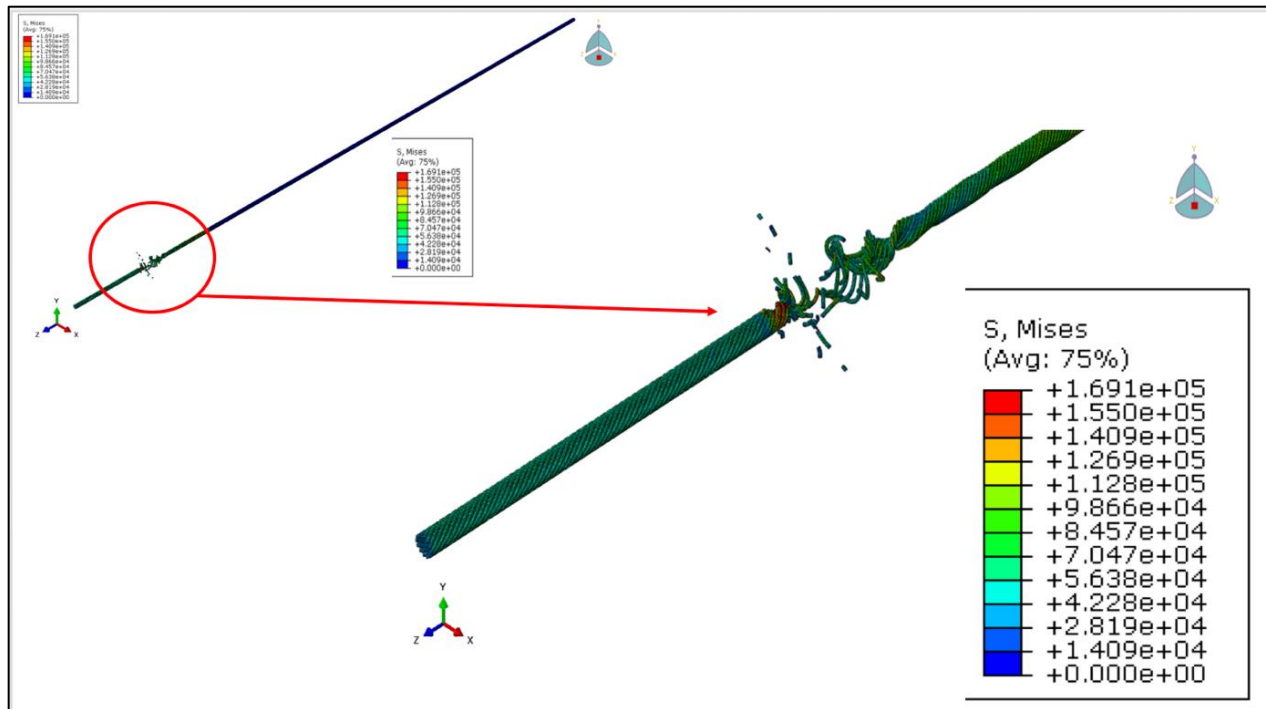


Figure 3.9 Damage Of 12 Filar Strand Due to Fracture Strain

ABAQUS can simulate and calculate the finite element analysis results. Figure 3.10 shows stress contours of damage modelling for 0.028 inch diameter wire rope. Here the wire is fractured near the torsional loading end, which is similar to experimental tests. The stresses are high near the loading end and constraint end. While stresses in the middle are limited, most stress is on steel wire rope outside. There are six strands with equal stress distribution consisting of the model of wire rope geometric symmetry. On the side of rope, a dimensional conic curvilinear staggered shaped stress is distributed on the steel surface of the helical strands. Also, there is larger stress on the steel wires contacting pare.

### 3.5 Summary of Numerical Simulation

Since the Explicit algorithm used to know the response of tube is inflicted to a gradually-increasing load, the simulation takes a lot of iterations and a significant work is required to develop and execute simulation models.

Except for the creation of a tangible CAD model, the basic of FEA modelling is discussed, and all of the steps for an FEA procedure from scratch to post-processing are

explained. It has been found that to make a simulation successful, it involves in many challenges and uncertainties in the selection of element types, the definition of contacts, the definitions of incremental conditions and terminating conditions. These issues have to be addressed by *trials and error*. Fortunately, once a successful simulation model is defined, minimal effort of changing is needed to create and run a simulation on new tube model with new design parameters. It has been found beneficial to choose the solid element type with an adjustable coefficient of frictions (CoF), as far as the presented case study is concerned, CoF is set as 0.5. The analysis type is defined as ‘explicit’ to obtain a historical response in one simulation. The appropriateness of the simulation model will be discussed in Chapter 5 for verification and validation.

## 4. PARAMETRIC STUDY FOR SIMULATION AND PRODUCTS

This chapter describes the process and effect of the parametric study which can be directly co relate with HHS tube. Parametric design is based on algorithmic analysis that enables expresses the parameters and rules that define, encode and interpret the relationship between intent and response of the design. In this chapter, the parametric studies are performed in the simulation for the evaluation of product variations. The parametric study shows the robustness of using FEA as a prediction tool; the parametric study on products gives a better understanding of the system response under varying loads or geometric dimensions. The importance of the geometric parameters and their relationship with each other are identified. The parametric study can be eventually utilized to support decision-making activities of product optimization.

**Keywords** – HHS tubes, Simulation, Parametric study, design of experiments (DoE).

### 4.1 Parametric Study

The developed simulation model and procedure is generic and should be applicable to any relevant products at the client company. In other words, there is a need to run the parametric studies to (1) approve a simulation model is robust enough to generate satisfactory results of predicted torque and (2) be applicable to a variety of products with varying configurations such as *different outside or inside diameters, pitches, wire numbers, boundary conditions, and lengths*.

After examining the available HHS tubes at the client company, the main geometric variables of a HHS tube are identified as follows: (1) *number of filars*, (2) *shape of a filar and its geometric dimensions*, (3) *inner radius of HHS tube*, (4) *outer radius of HHS tube*, (5) *the pitch*, (6) *the lay type*, and (7) *the helical angle*. The definitions of these variables were illustrated in Figure 4.1, 4.2, 4.3 and 4.4 and elaborated as follows.

**Shape of the filar** refers to the cross-section profile of a filar, which is also related to the required application and how the HHS tube is constructed. Figure 4.1 shows some common profiles a wire usually has. These common profiles include (i) *circular wire*, (ii) *trapezoidal*, (iii) *full lock*, (iv) *half lock*, (v) *triangular*, and (vi) *ribbon wire*.

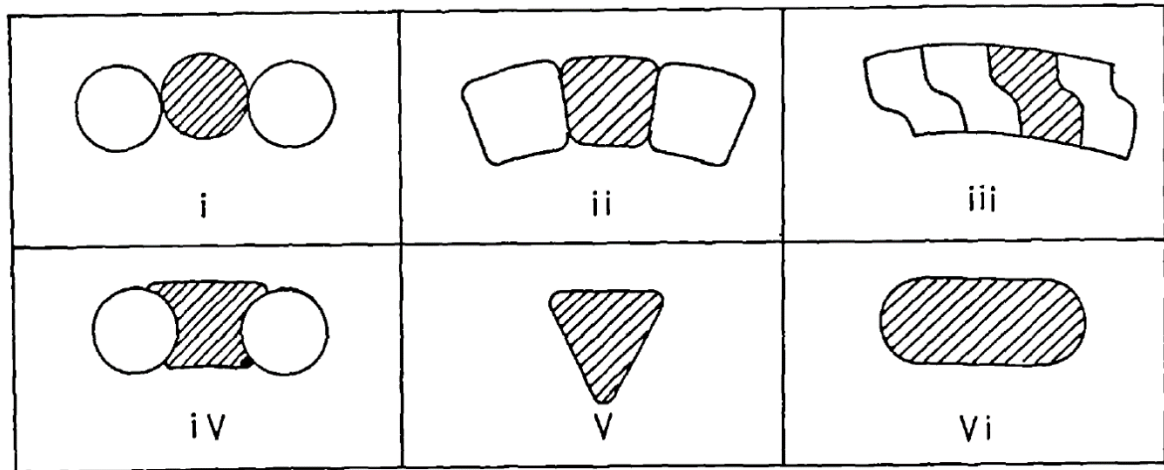


Figure 4.1 Various Geometric Shapes of The Filars (Lee 1989).

**Number of filars** is the count of filars used to form a HHS tube. A minimum of 3 filars are needed to form a HHS tube, and the actual number of filars depends on the requirements of an application; the more strength is demanded, the higher number of filars should be. Figure 4.2 shows an example of HHS tube with 12 filars.

Figure 4.2(a) depicts the complete isotropic view of HHS tube with 12 filars. Figure 4.2(b) shows the side view of HHS tube in which an individual filar and the pattern can be observed.

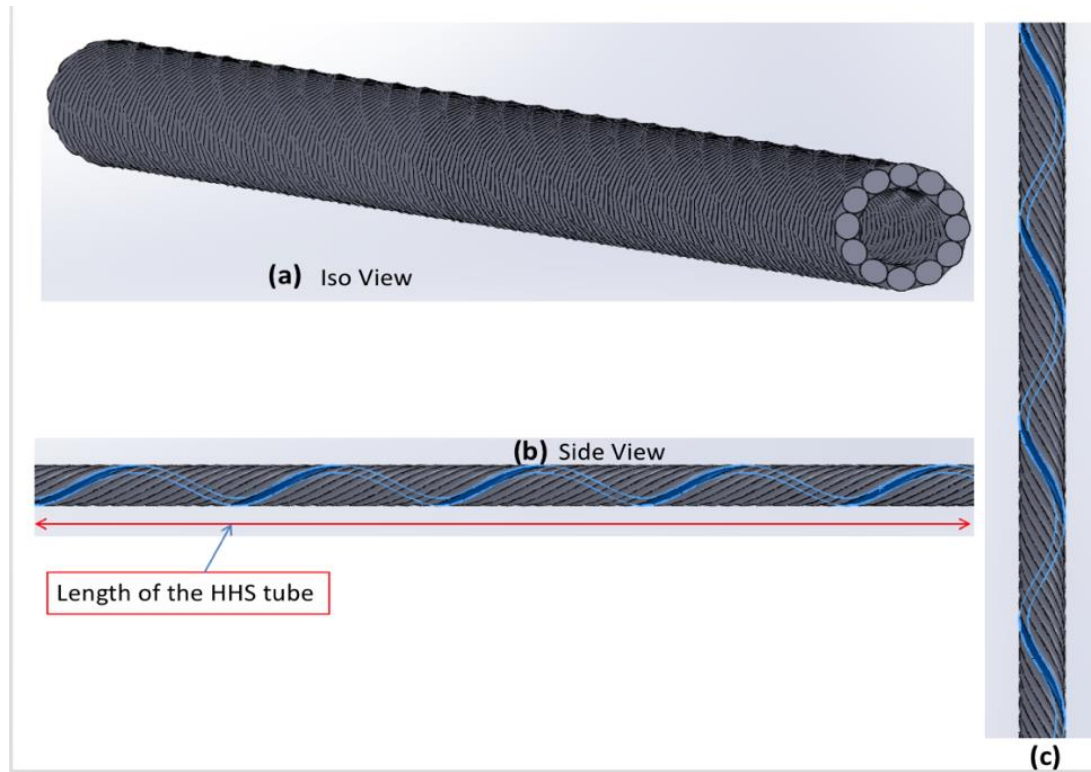


Figure 4.2 Classification of HHS Tube

Figure 4.3 gives an insightful perception of various types of single layer HHS tube. Moreover, Figure 4.3 (A), (B) and (C) are 12, 9 and 6 filar HHS tube with the variation in terms of helical angle and pitch respectively. The lower side of figure 4.3 illustrates a single filar which gives the further perception of helical pitch and angle difference individually.



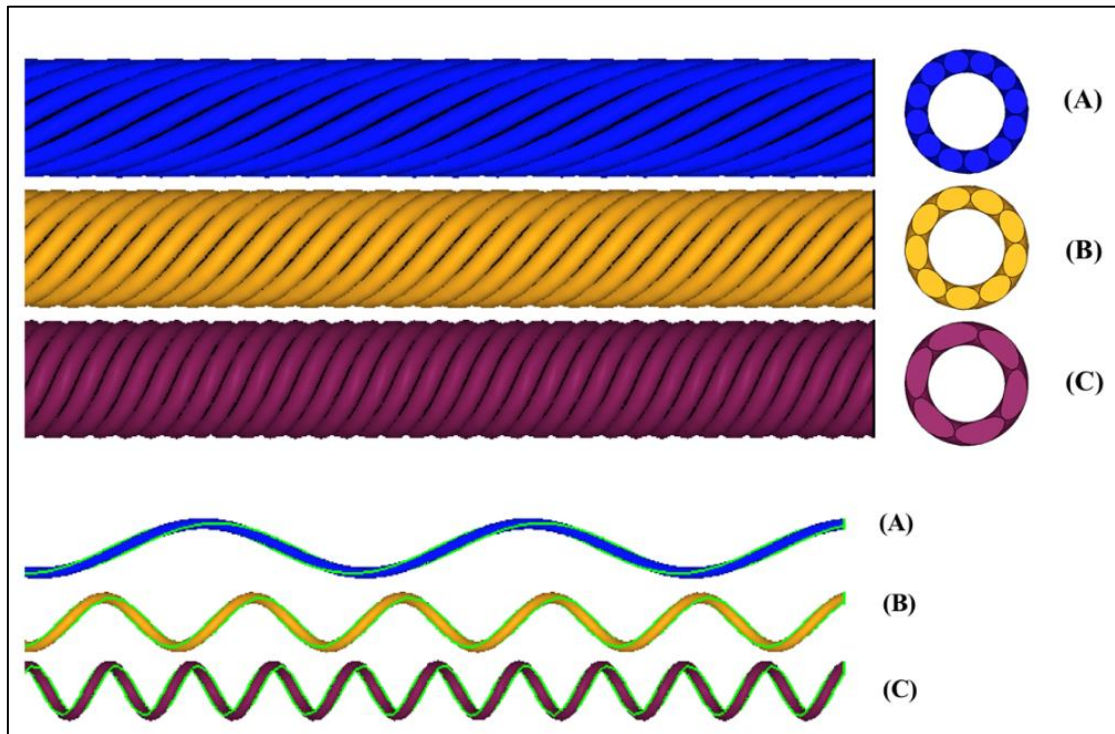


Figure 4.3 Various Types of Single Layer HHS Tubes

**Lay** can be used to describe the way filars are placed within each HHS tube. It can be a *regular or right lay* or a *Lang or left lay*. A regular lay, also known as a right lay, means the filars lay in the opposite side of strands. A Lang lay, also known as a left lay, means the filars lay on the same side of strands. Figure 4.4 (E) is alternate lay and it consists of alternating regular and lang lay strand. The lay of most of the ropes are regular right lays. Figure 4.4, (A) and (C) show strands as laid to the rope comparable to threading in right-hand twist. On the contrary, the left lay rope strands are drawn in the opposite direction as shown in Figures 4.4 (B) and (D).

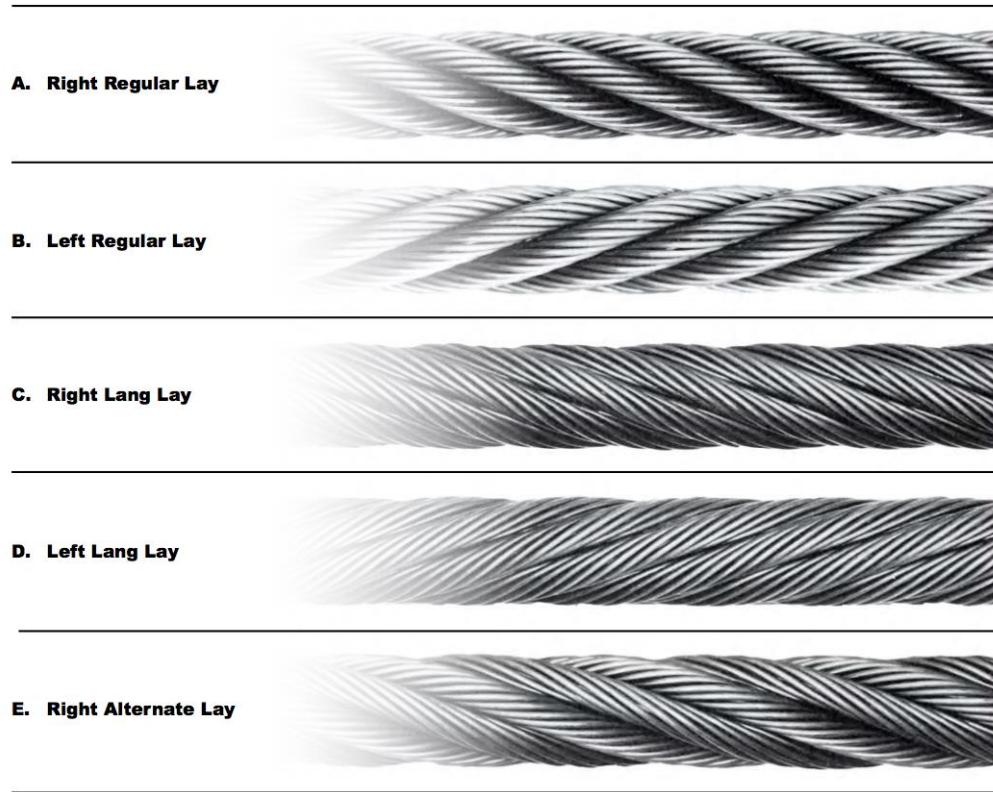


Figure 4.4 Typical Wire Rope Lays Comparison (Costello ,1990)

Figure 4.5 shows a fixed boundary condition at one end and an angular displacement applied at rotating end. This angular rotation is '*clockwise*' (CW) direction. The lower part of Figure 4.5 shows a single helical filar where the measurement of its pitch distance is illustrated.

The distance measured from one reference point to same point after one complete turn of a helical wire is known as **Pitch Size**; it is illustrated in Figure 4.5.

The radical distance measured from center of HHS tube to inner surface of the filar or tube is known as **HHS tube Inner radius**, it is illustrated in Figure 4.6.

The radical distance measured from center of HHS tube to outer surface of the filar or tube is known as **HHS tube Outer radius**, it is illustrated in Figure 4.6.

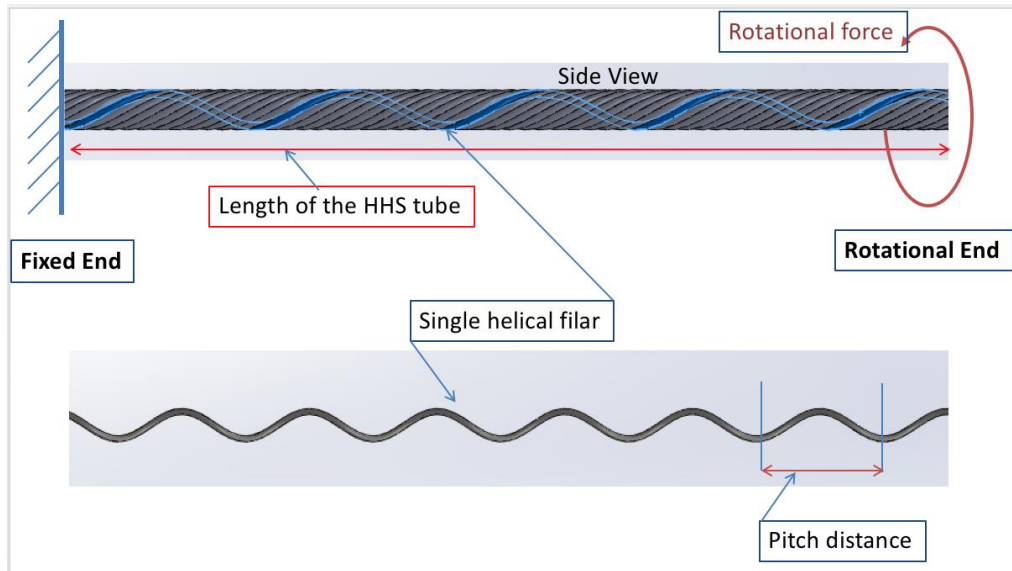


Figure 4.5 Classification & Boundary Condition of HHS Tube.

**Helical Angle** is the angle between helical filar and an axial line on its right, circular HHS tube. Figure 4.6 shows how a helical angle is defined for a HHS tube.

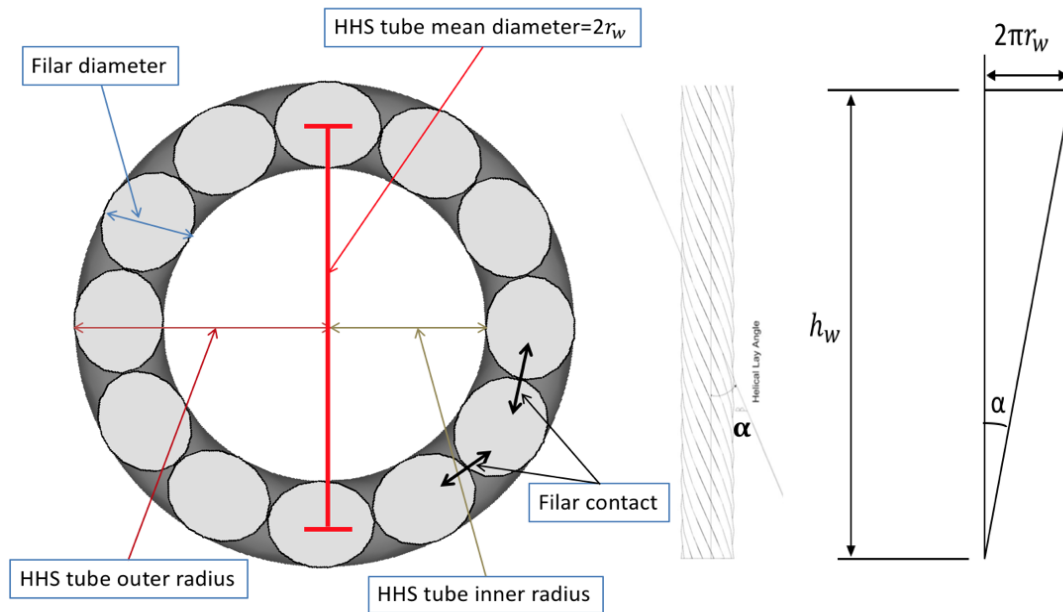


Figure 4.6 Inner and Outer Radii of HHS Tube

Figure 4.6 shows the front view of the HHS tube; it has all 12 filars with all of the defined dimensions including inner radius, outer radius, mean diameter, filar diameter and the

helical angle. Note that a helical angle  $\alpha$  is not an independent parameter, it can be calculated from below equation as

$$\tan \alpha = \frac{2\pi r_w}{h_w} \quad \text{eq. (4.1)}$$

## 4.2 Procedure of a Parametric Study

A parametric study generates, executes and gathers results of many analyses that vary only in the some of the parameters values used in input quantities. Generally, this process is helpful for the single component set of problems, whereas the geometry with varying in thickness or circular hole sizes or material E values, etc can be substituted. Abaqus uses Python extensively. Python is a powerful and object-oriented language that is widely used by many organizations in the world. Abaqus has Python embedded within its software products. Python allows direct parameterization of the variables of design that are to be optimized in finite element input file. Hence, it has an easy use of the procedure within the industrial application framework. The language is extended to comprise of a rich set of commands that are suited for the everyday works of an analyst of finite element. These extensions are also called as the Abaqus Scripting Interface (ASI).

Parametric studies in the Abaqus have a set of design parameters that define the design space. Once the benchmark simulation model is developed, only the values of the identified design parameters are to be changed in a parametric study. A new such study, if required, is built in order to investigate the outcomes for a separate set of design parameters. After selecting the considered parameters in the study, each parameter is defined then specified. Parameters are categorized in their nature as '*continuous*' and '*discrete*' and they may contain reference values. The design points in the space are created from a set of values of each parameter. The parameter samples are then incorporated to create a set of design points. Some methods are available to generate the sampling values of the parameters and to combine the available parameter values.

In a parametric study, an initial set of the samplings of each design parameters must be given before any combinations of multiple design parameters can be made. For each combination, one value from the set of the samplings for each parameter is selected, and the parametric study is flexible enough to deal with the simulation for any combination of the values within the specified ranges of design parameters. Design constraints are imposed on all the

designs and any design violating the specified constraints are eliminated. Finally, all parametric study variations are analyzed and report results across all of the parametric study designs are gathered. In summary, Abaqus' parametric study follows the below steps:

Parametric studies are conducted by:

- 1) Create a parametrized "template" input file and generate various parametric variations from it.
- 2) Prepare a script file with a .psf extension containing Python instructions and generate, execute, and gather parametric variations output for of the parametrized input file.

#### Command summary

##### **Abaqus Script**

[*=script-file*]

[**startup** = *startup file-name*]

[**noenvstartup**]

#### Command Line Options

- 1) **Script-file:** When there is a definite script file name, there is an import of parametric study module and execution of the parametric study script file's instructions. If there is an omission of a script file name from the command line, the Python interpreter imports the parametric study module.
- 2) **Startup:** It defines the name of the Python configuration commands file that is to be run at the application startup. After any configuration commands are set in the environment file, commands in this file are run.
- 3) **Noenvstartup:** It defines that all configuration commands in the environment files are not be run at the application startup. This option is utilized in combination with the **startup** command to curb all configuration commands except the ones in the **startup** file.

#### 4.2.1 Automation of Parametric Generation:

To do automated parametric modelling in Abaqus/CAE a basic scripting has to be executed initially. A greater advantage about Abaqus/CAE is that it automatically saves every action performed into a python script. This is named as abaqus.rpy (past files will be renamed at start-up to abaqus.rpy.1, .2, etc).

So we need to open Abaqus/CAE, perform exactly (and only) the steps that needs to be automated, and then close CAE. Then we need to find the abaqus.rpy file which is generated from that session, and it can be used for automation.

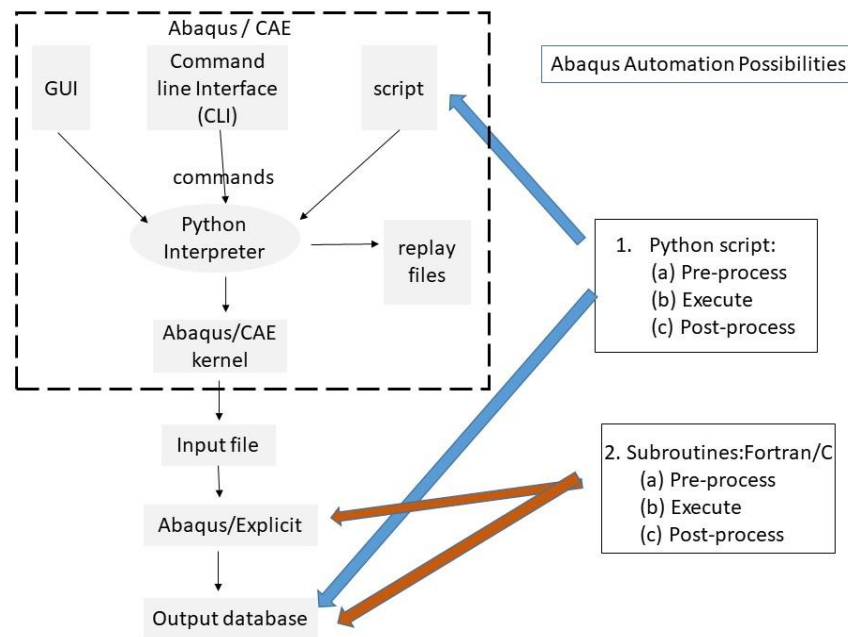


Figure 4.7 Flowchart of Automation Possibilities with Python

The Procedure steps are as follows:

- 1) Create a parametric study

```
Study=ParStudy(par=('par1', 'par2'))
```

**Study=ParStudy** scripting command to form a parametric study and select considered independent parameters for variation. *a Study* is the variable Python name assigned to the study object formed by command.

- 2) Define parameters by specifying their types (continuous or discrete valued), the varying ranges or set of possible values, and their normal values.

```
Study.define (DISCRETE, par='par1', domain=(1, 3, 5, 7, 9, 11, 13))
```

```
Study.define (CONTINUOUS, par='par2', domain=(10., 60.))
```

- 3) Define Sampling algorithms: specifying the sampling options, data and redefining domains of the parameters and reference value used

```
Study.sample (INTERVAL, par='par1', interval=1.)
```

```
Study.sample (NUMBER, par='par2', interval=10.)
```

- 4) Combine parameter samples to create sets of designs

```
Study.combine(MESH, name='dSet1')
```

```
Study.combine(CROSS, name='dSet1')
```

- 5) Constrain designs

```
aStudy.constrain ('constraint expression')
```

For example, constrain command

```
aStudy.constrain('height*width < 12.')
```

here, width and height are parameters that can be enforced if the area of cross-section of a rectangular beam is below 12.0 in each of the designs.

- 6) Generate designs and analysis job data

```
study.generate (template = 'new para')
```

- 7) Execute the analysis for chosen study designs

```
study.execute(ALL)
```


- 8) Gather key results for chosen study designs

```
study.output(step=1, file=ODB)
```

```
study.gather(results='VDISP', variable='U2', node= 232128, request=HISTORY,  
instance="part-1")
```

```
study.report(FILE, results=('VDISP'), par=('par1', 'par2'), file='filename.psr')
```

## 9) Report gathered results



```
Python 3.6.0 Shell
File Edit Shell Debug Options Window Help
Python 3.6.0 (v3.6.0:41df79263a11, Dec 23 2016, 07:18:10) [MSC v.1900 32 bit (Intel)] on win32
Type "copyright", "credits" or "license()" for more information.
>>> #create study
cstrand=ParStudy(par=('E','nu'))

#defining the parameters
cstrand.define(DISCRETE,par='E',domain=(100e9, 200e9, 300e9))
cstrand.define(CONTINUOUS,par='nu',domain=(0.15,0.35))

#sampling
cstrand.sample(INTERVAL, par='E', interval=1)
cstrand.sample(NUMBER, par='nu', interval=3)

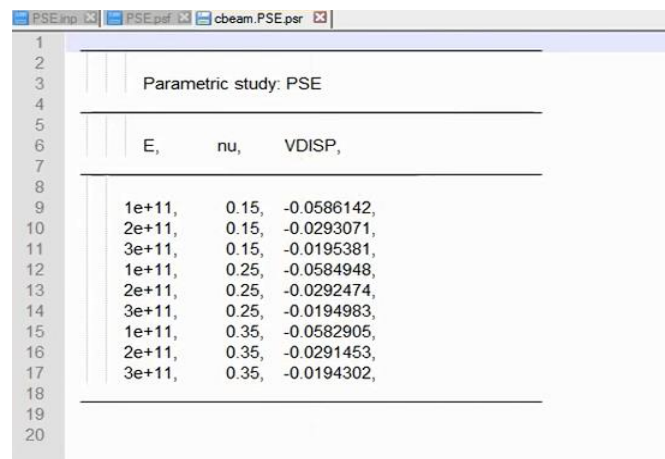
#combine the samples
cstrand.combine(MESH, name='l2_filar_strand')

#generate analysis job data
cstrand.generat(template='para_study')

#execute the jobs
cstrand.execute(ALL)

#read the results from ODB and report
cstrand.output(step=1, file=ODB)
cstrand.gather(results='VDISP', variable='U2', node=232128, request=HISTORY, instance="Part-1-1")
cstrand.report(FILE, results=('VDISP'), par=('E','nu'), file='cstrand.para_study.psr')
```

Figure 4.8 Parametric Study Performing with Python Script example (Abaqus Manual)



Parametric study: PSE			
	E,	nu,	VDISP,
1	1e+11,	0.15,	-0.0586142,
2	2e+11,	0.15,	-0.0293071,
3	3e+11,	0.15,	-0.0195381,
4	1e+11,	0.25,	-0.0584948,
5	2e+11,	0.25,	-0.0292474,
6	3e+11,	0.25,	-0.0194983,
7	1e+11,	0.35,	-0.0582905,
8	2e+11,	0.35,	-0.0291453,
9	3e+11,	0.35,	-0.0194302,

Figure 4.9 Parametric Study Output Reports after Running Script example (Abaqus Manual)



### 4.3 Parametric Study on Simulation Model

The intention of simulation model's parametric study is confirmation of the robustness of the established simulation model. The current simulation model is solved with explicit method which is much time taking procedure compared to general standard method.

For the proposed simulation model, the parametric study was performed for the design parameters mainly with varying mesh size. Note that the central interest for this thesis is to predict the torque subjected to the applied angular displacement; therefore, the analysis goal is always the Torque vs Angular displacement graphs.

#### 4.3.1 Mesh Sensitivity Study

Meshing is used by all FEA-analysis programs to divide the model into elements. Generally, a finer mesh will increase the accuracy of the results but will dramatically increase simulation time, while a coarser mesh will decrease accuracy but also decrease simulation time. If the number of elements is high, there will be a high number of equilibrium equations the program needs to solve. Getting a good balance between mesh quality and result accuracy is essential for reducing simulation time in complex analysis such as the ones carried out in this thesis.

There is a threshold point on accuracy of the results and refinement of the mesh. For example, if a model has 10 thousand elements doubling this number might get a much more accurate result while if a model has 1 Million elements to start with and this amount is doubled to 2 Million there might not be any difference in the results but it will take almost twice the time to yield almost the same results. It is common to increase the number of elements in areas of interest in the model. For examples in welds, cracks, straight corners, bolt threads and so on. Other areas of the model can consist of a coarser mesh to reduce the number of elements. This model mesh sensitivity study intends to predict the result outcome consistency at appropriate mesh size, which means the results should not have much influence over changing mesh size to further finer.

The 1x06x0.0075;0.050 HHS tube model was chosen for mesh sensitivity study as it has 6 filars which will help to control in number of elements during finer mesh. The below table the total number of elements and nodes are given with respective outcome results.

Table 4.1 Mesh Sensitivity Result

Sr.No	Mesh Size (inch)	Total Number of Elements	Total Number of Nodes	Numerical Result (oz-in)
1	0.01	105480	149533	0.237
2	0.005	218160	309163	0.132
3	0.002	534816	757759	0.13

The mesh sensitivity study graph is shown below. It can be seen that with coarse mesh size 0.01-inch the torque is predicted higher. But after the finer mesh size 0.005-inch to 0.002-inch mesh size the torque is quite in almost same range.

The coarse mesh size is not able to maximize as the helical filars need to capture appropriately. The results are quite decent, and the curve is smooth for the finer mesh but for the fine mesh it took 4 times more to solve the problem compared to coarse mesh. Choosing an appropriate mesh size is a crucial task which generally comes with multiple trials, though a functional analyst with sound experience can approximate the mesh size as per its geometric dimensions. As shown in below figure the mesh size 0.01 inch look coarse to capture the suitable geometry, whereas the 0.002-inch mesh looks more finer to capture appropriate geometry. Where the 0.005-inch mesh is a quite adequate and relevant size to obtain the required geometry to achieve the required results.

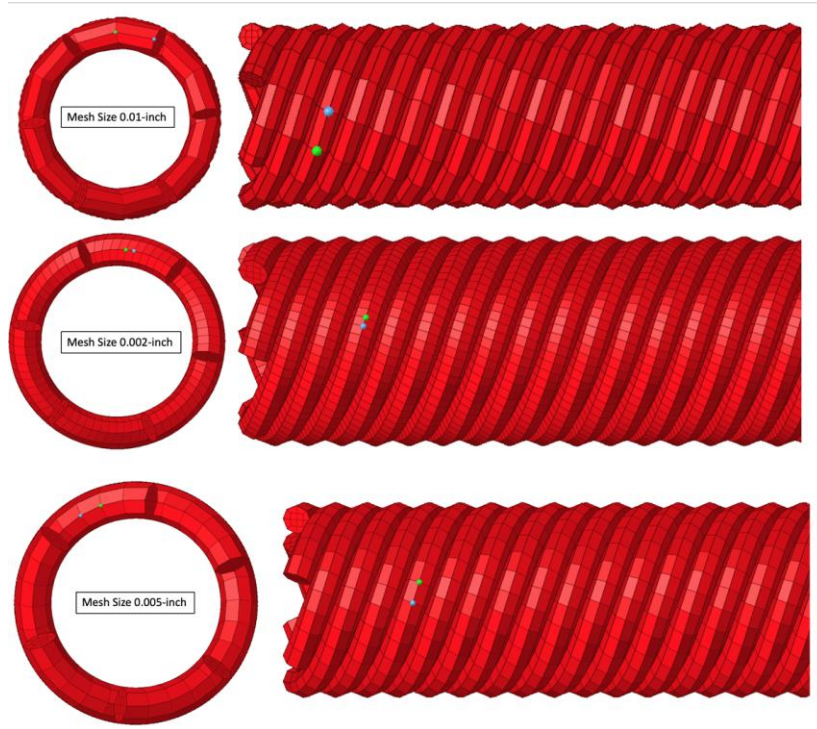


Figure 4.10 Variant Mesh size FE Models

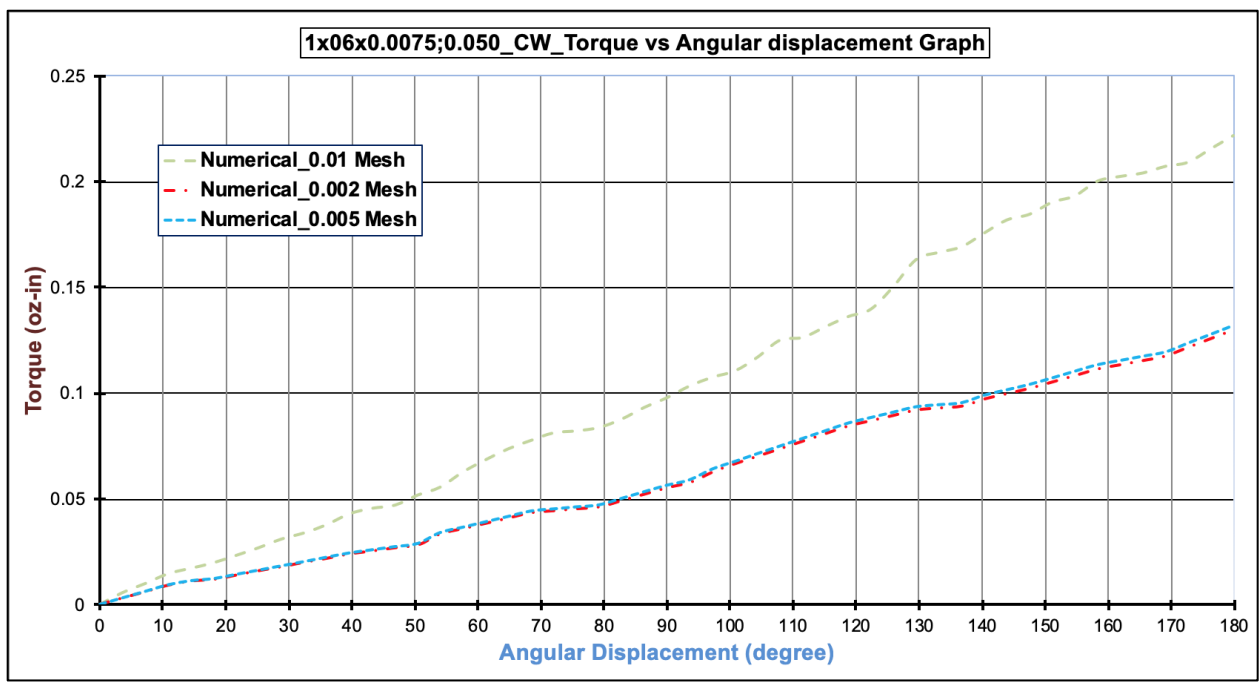


Figure 4.11 Mesh Comparison Graph of Torque Vs Angular Displacement @ 180°

From Figure 4.11 shows that with finer mesh size the results are closer but not affecting much as the difference between 0.005-inch mesh and 0.002-inch mesh result are less than 5% where fine mesh took 3 time more to solve the analysis. With this study it has been concluded to use the mesh size as 0.005 inch for the current model which gives actable results with in time frame limit. Whereas with increase in the mesh size 0.01 inch the run time is decrease as number of elements reduce but the results are not feasible.

#### **4.3.2 Friction Co-Efficient**

The coefficient of friction is a dimensionless scalar value and is the ratio of the force of friction between two bodies and the force pressing them together. such values are determined experimentally. The coefficient of friction depends on the materials used and it ranges from near 0 to greater than 1. Since in HHS tube model the all adjacent filars are in contact with each other, the response of their resistivity against applied force plays the significant role in determining the torque. If it is too large the resistivity will be higher and if it is too small the resistivity will be lower, so to identify the accurate value is essential. The purpose of this parametric study is to distinguish the valid friction coefficient value which provides a realistic behavior with the relevant result.

The 1x12x0.005;0.028 HHS tube model with inner diameter 0.018-inch, outer diameter 0.028 inch, filar diameter 0.005 inch and filar count 12 with 4-inch length of analyzed with varying in frictional co-efficient values such as 0.1, 0.5 and 1 and the outcomes are examined.

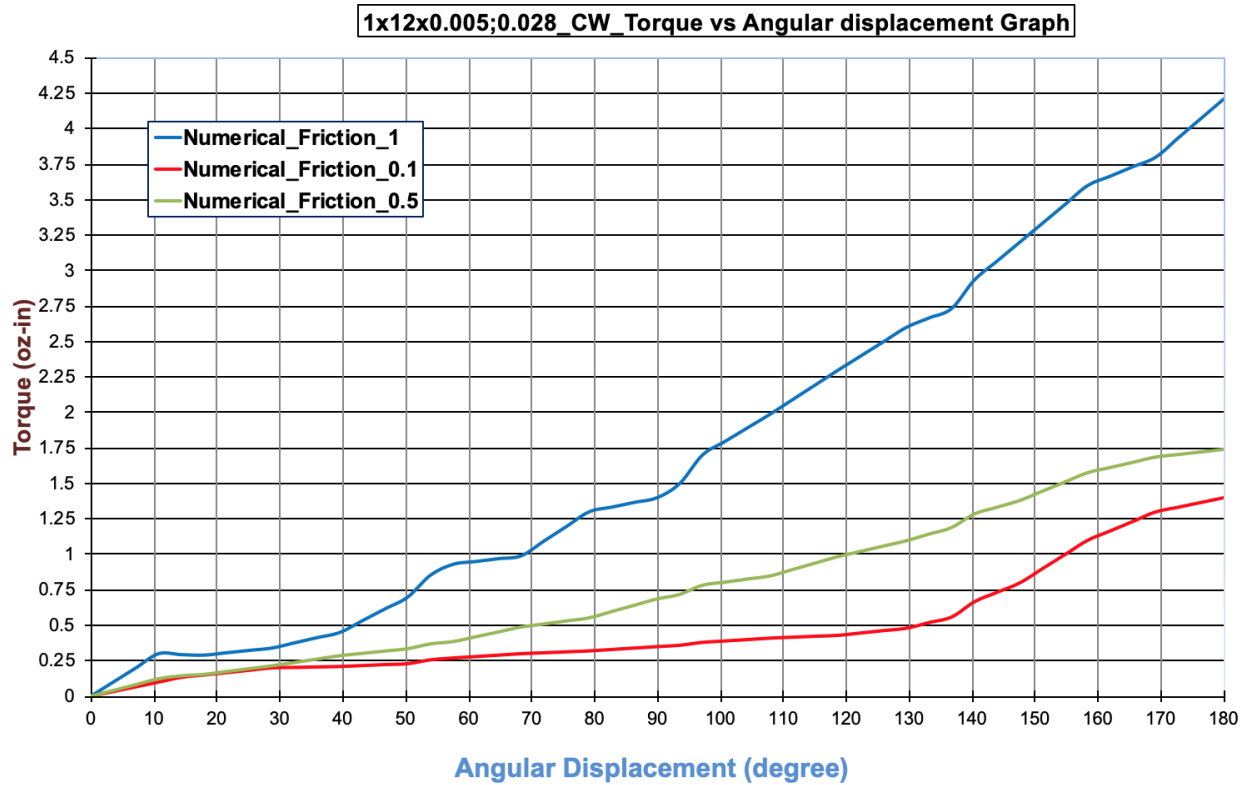


Figure 4.12 Friction Co-Efficient Comparison Graph of Torque Vs Angular Displacement @ 180°

Table 4.2 Friction Results

Sr.No	Friction Co-efficient	Numerical Result Torque (oz-in)
1	0.1	1.4
2	0.5	1.738
3	1	4.21

As in Figure 4.12, the results of simulation are as predicted when increase in friction co-efficient value the resisting torque is increasing thus for confirming the right result further steps need to follow as verification and validation which will be discussed in chapter 5.

### 4.3.3 Boundary Condition

Boundary conditions has an important role in torque determination. The BCs variations include fixed and free ends. The objective is to study the resulted torque and stresses due to difference boundary conditions. The expected results with increase in length there should not be much difference between both torque but if the length is short then the fixed end design should have higher torque than free end design.

For the Boundary conditions, the scope was not much for the current problem and due to the time consideration, it has been not conducted for this time. But it's an important aspect in a parametric study depends on the problem definition. I encourage carrying forward this step-in future if anyone would extend.

### 4.4 Parametric Study on Product Variations

Five HHS tube models with variable in parameters such as *number of filars*, *pitch distance*, and *helical angle* are chosen to perform the parametric study as each model has the variation in terms of the geometric dimensions. Such study will help to understand the influence of various features. Table 4.3 shows the all geometric dimensions values.

The geometrical dimensions as number of filars, helical angles are cannot be kept same with maintaining HHS tube inner and outer diameter constant. As these parameters will automatically vary as the number of filars change. In below, Table 4.3 can be observed that the HHS tube inner and outer diameter kept constant and the number of filar, helical angle and pitch distance has been changed according to tube.

Table 4.3 HHS Tube Geometrical Dimension Variable Values

Sr.No	HHS tube Configuration	Number of Filars	Filar diameter (inch)	Inner diameter of the Tube (inch)	Mean Diameter of the Tube (inch)	Outer Diameter of the Tube (inch)	Pitch (inch)	Helical angle (Degree)
1	1x6x0.0075;0.050	6	0.0075	0.035	0.0425	0.05	0.0486	69.99
2	1x8x0.010;0.055	8	0.01	0.035	0.045	0.055	0.0986	55.1
3	1x12x0.005;0.28	12	0.005	0.018	0.023	0.028	0.107	34.03
4	1x16x0.005;0.045	16	0.005	0.035	0.04	0.045	0.1053	50.03
5	1x18x0.005;0.045	18	0.005	0.035	0.04	0.045	0.1309	43.82

The results of the parametric study on five types of tubes with a given angular displacement in the CW direction is shown in Figures 4.13.

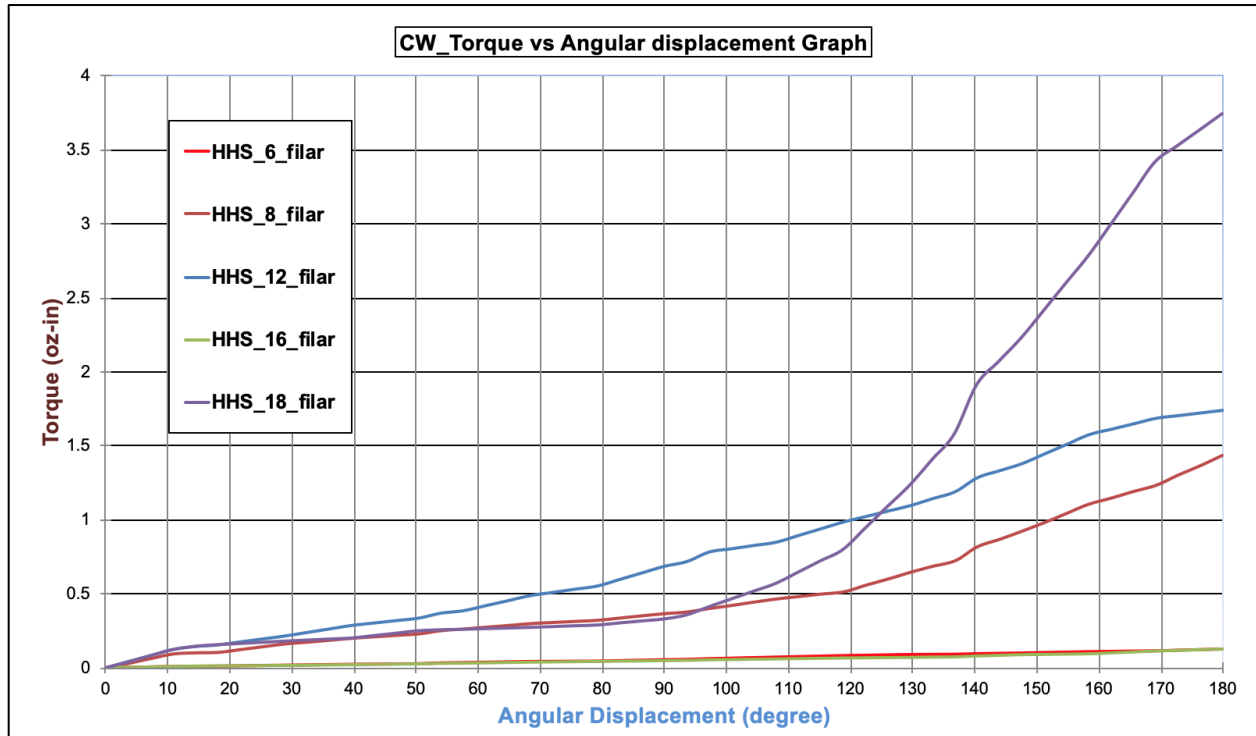


Figure 4.13 Torque Vs Angular Displacement @ 180° Clockwise Direction

Table 4.4 HHS Tube Parametric Study Results

HHS_Model	HHS_6_Filar	HHS_8_Filar	HHS_12_Filar	HHS_16_Filar	HHS_18_Filar
Torque (oz-in)	0.132	1.43	1.738	0.125	3.743

#### 4.5 Summary of Parametric Design Capabilities

The capabilities to support parametric study is very important since with changing number of filar the other associated dimensions such as helical angle and pitch are changing. In this chapter, we discussed the necessity of parametric studies to (1) verify robustness of proposed model presented in Chapter 3 and (2) verify the feasibility of defining and running parametric studies for a number of design variables by altering mesh size and the product variation etc.

For the first goal, the parametric study is run on mesh size and concluded that the with finer mesh size, the results are not significantly affected; however, it takes 3 times more computation time than the one by the coarse regular mesh. On the other hand, the mesh has its

limitation to increase the size of mesh to represent the geometry of HHS tube in appropriate way. For the second goal, the parametric study is run along with various friction coefficient values and the result outcomes shows that if the co-efficient value is increased, the torque resistance is also increased. To verify the achieved results, further steps need to be performed and these will be discussed in Chapter 5.

The other parameter study is performed with a varying number of filars, helical angle and pitch distance (see Table 4.3). Depending on the results, it is viewed that if the number of filars for an HHS tube increases, the response of the torque is also increased towards the specified angular displacement. Moreover, the helical angle and pitch distance depend on the number of fillar used in the HHS tube subjected to a given diameter of tube. Based on the requirement of torque output, the manufacturer will be able to optimize the tube design using a parametric study. The form principle follows force that is particularly suitable in structures, which transfer their loads only through in-plane or axial forces.



## 5. VERIFICATION AND VALIDATION

Modelling and simulation (M & S) play an important role in modern life increasingly. They contribute to our understanding of how things function to meet desired objectives, and they become essential, effective, and efficient tools to design, evaluate, or operate a new product or system. M & S yields the valuable information to support decision-making activities in many areas of business applications. One of the critical tasks in M & S is a physical system of verification and validation (V & V). V & V guarantees that the computer model is well developed to represent an original physical system and such a model can be simulated to yield correct and reliable results about the system's behaviours. Although significant advances in V & V have made in past years, some significant challenges remain that impede the full potential of M & S and innovative computing technologies. This chapter discusses the main challenges related to V & V in the proposed simulation; the solution alternatives to address these challenges are also presented. The V & V of the proposed FEA model and procedure is emphasized. The correlation between analytical, numerical and experimental results are described with case studies.

**Keywords** – Modeling and Simulation (M & S), Correlation, Numerical simulation, Experimental Methods, Analytical Methods, V & V.

### 5.1 Verification and Validation (V & V)

In virtual analysis, a defined system or procedure must be verified and validated. If the execution of a virtual analysis consists of a number of steps; each step in the simulation is V & V to ensure the accuracy of virtual analysis. *Society for Computer Simulation* developed Figure 5.1 in 1979 and named it as the Sargent circle. It shows a list of critical activities to model and simulate (denoted in black solid lines) and assesses activities (denoted in red dashed lines) that are in V & V.

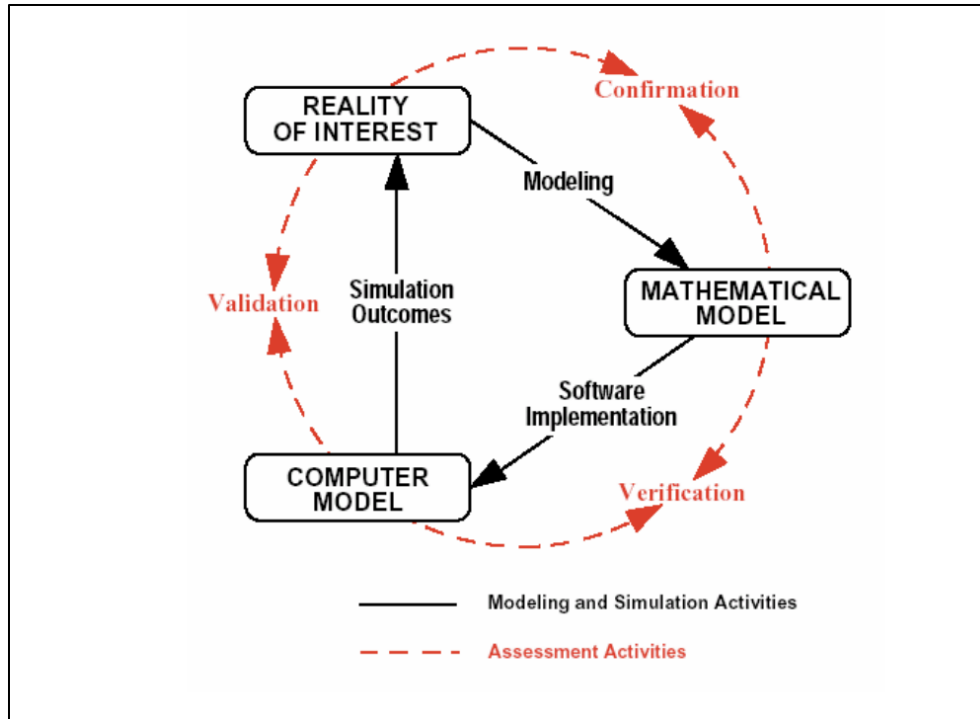


Figure 5.1 Activities and Process for Modeling, Simulation, Verification and Validation (Thacker Et Al 2004)

Figure 5.2 expands in Figure 5.1 to provide more details to address the shortcomings. In Figure 5.2, right branch shows the developing and exercising model process, and left branch shows the high quality and relevant experimental data obtaining process by physical testing. The closed boxes represent objects and data, black solid lines connectors denote modeling and experimental activities, and assessment activities are denoted by red dash lines connectors.

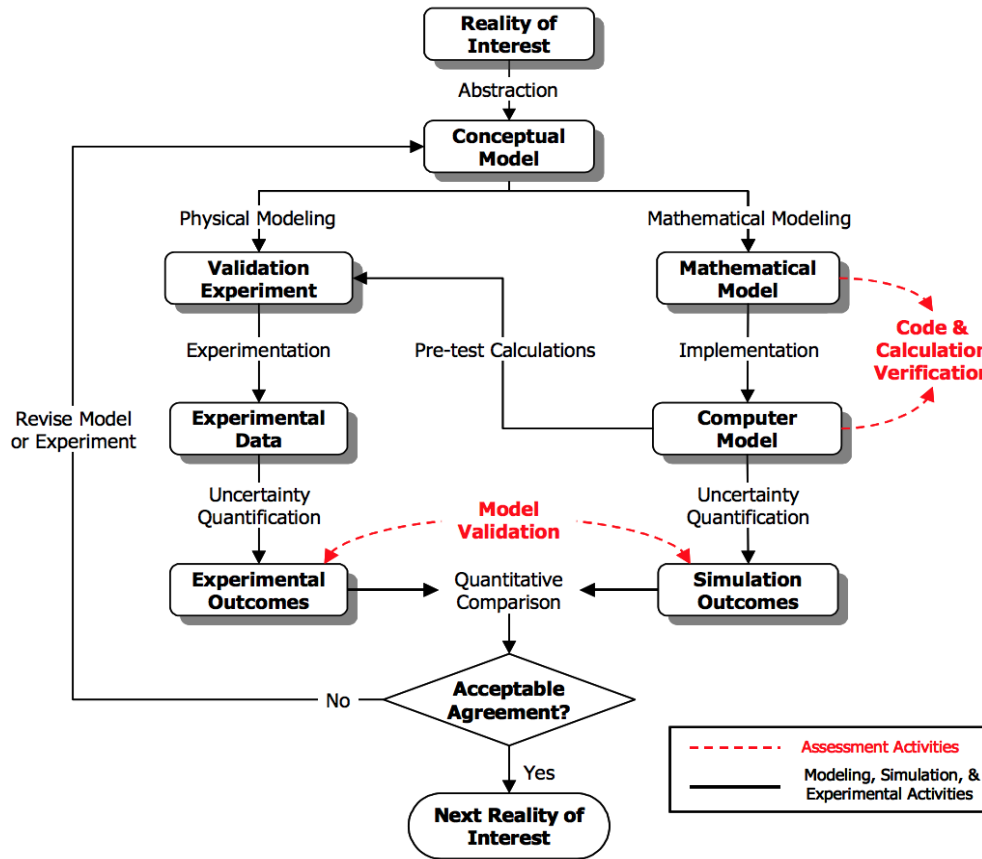


Figure 5.2 Model Development, Verification and Validation Process (Thacker Et Al 2004)

The objectives of V & V is to prove the (1) model for the physical system under investigated is correctly established, and (2) solving process of the computer model leads to acceptable results to original analysis problem. Verification and validation are correlated but distinctive since the activities for verification and validation are performed to find the answers of the aforementioned objectives, respectively. Verification is to prove if a physical object or system is represented appropriately, and validation is to tell if the solution from a virtual analysis is acceptable to original analysis problem. Verification is to make sure that the analytical or mathematical equations and the numerical procedure are determined and that defined procedure is verified comparing outcomes with each other. While validation is to make sure that the numerical results and animations are as expected and it can be validated by comparing with experimental data.

Table 5.1 Overview of Verification and Validation. (Sargent, 2011)

VERIFICATION	VALIDATION
To make sure it works	To make sure it does as it is supposed to do.
To get the math right.	To get the physics right.
To provide an accurate FE analysis.	To check the FEA against test.

The advantage of this study is the major process results such as analytical, numerical and experimental are performed, which supports to the verification and validation of the outcomes. The analytical model is developed by thesis Advisor Dr.Zhuming Bi. Furthermore, the equation is used for mathematical calculation, and the outcome results are correlated. Similarly, The Fort Wayne Metals has conducted all the experiments at their laboratory, and the outcome results are shared for the correlation with numerical results. The details of V & V of HHS tube models are in Figures 5.3, and 5.4, which show the material and boundary conditions considered for correlation of models with all aspects.

Table 5.2 Geometrical Data of HHS Tubes and Type of Analysis.

Sr.No	HHS tube Configuration	Number of Filars	Filar diameter (inch)	Inner diameter of the Tube (inch)	Mean Diameter of the Tube (inch)	Outer Diameter of the Tube (inch)	Pitch (inch)	Helical angle (Degree)
1	1x6x0.0075;0.050	6	0.0075	0.035	0.0425	0.05	0.0486	69.99
2	1x8x0.010;0.055	8	0.01	0.035	0.045	0.055	0.0986	55.1
3	1x12x0.005;0.28	12	0.005	0.018	0.023	0.028	0.107	34.03
4	1x16x0.005;0.045	16	0.005	0.035	0.04	0.045	0.1053	50.03
5	1x18x0.005;0.045	18	0.005	0.035	0.04	0.045	0.1309	43.82

Geometrical Dimensions		Material properties		
Inner Diameter:	0.018 inch	Density	0.0007409	lbs/in <sup>3</sup>
Outer Diameter:	0.028 inch	Youngs Modulus	1.45E+07	psi
Filar diameter:	0.005 inch	Poissons ration	0.3	
Filar count:	12			
Pitch distance:	0.107 inch			
Helical Angle:	33 degree			
Length of the HHS tube:	4 inch			

Plasticity	
Yield Stress(psi)	Plastic strain(%)
10342	0
12052	0.01183
14864	0.024109
19477	0.05451
25538	0.07951
32490	0.10241
40287	0.120452
71409	0.14133
98230	0.1585
134245	0.17847
155502	0.1923
169087	0.210354

Figure 5.3 Geometrical Dimensions and Material Data of HHS Tube 1x12x0.005;0.028

The boundary condition for an HHS tube is set as the fix at one end and the driving torque in clockwise direction at another end.

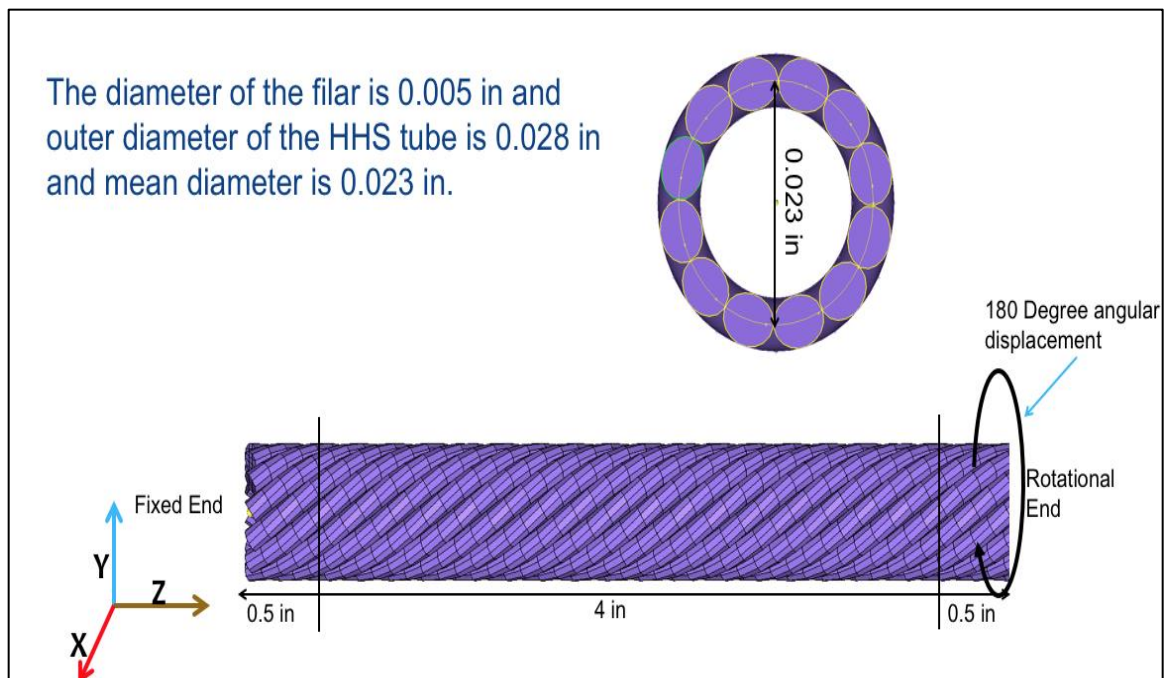


Figure 5.4 Load and Boundary Condition of HHS Tube

## 5.2 Verification of Simulation Model

As mentioned, the verification is to prove the simulation model is appropriately established. In this thesis, the verification process is performed by comparing the results from analytical model and simulation model.

### 5.2.1 Analytical Model

The analytical equation is derived by Dr. Zhuming Bi and with that equation the torque values are calculated in clockwise direction. Table 5.2 describes the configuration of HSS tubes 1x6x0.0075;0.050, 1x8x0.010;0.055, 1x12x0.005;0.028, 1x16x0.005;0.045 and 1x18x0.005;0.045 with the material properties shown in Figure 5.3. The boundary condition in Figure 5.4 is at one end fixed and angular displacement is put on another end.

The equation for the torque calculation under a given displacement is

$$T_{friction} = (1 + \sin^2\lambda + \min(\cos^2\lambda, \sin\lambda \cdot \cos\lambda)\mu) \left[ \frac{\theta_{rad} E d^4}{64 D N_b} N_w 2 \right] \quad \text{eq. (5.1)}$$

The varying parameter is the fixed angular displacements, and its values are set as the 180° clockwise rotation. The results from an analytical model are shown in Table 5.3.

Table 5.3 HHS Tube Models Analytical Results @ 180° Rotation.

Sr.No	HHS tube	Analytical Result (Torque, oz-in)
1	1x6x0.0075;0.050	0.15
2	1x8x0.010;0.055	1.24
3	1x12x0.005;0.028	2.28
4	1x16x0.005;0.045	0.17
5	1x18x0.005;0.045	3.9

### 5.2.2 Numerical Model

Figure 5.4 shows setup of virtual model in which the left side is fixed and an angular displacement is applied on the right side as the boundary condition. The element type is selected

as solid (C3D8I), and the elements and nodes details are illustrated in Table.5.4. Other simulation model settings are also illustrated in the table.

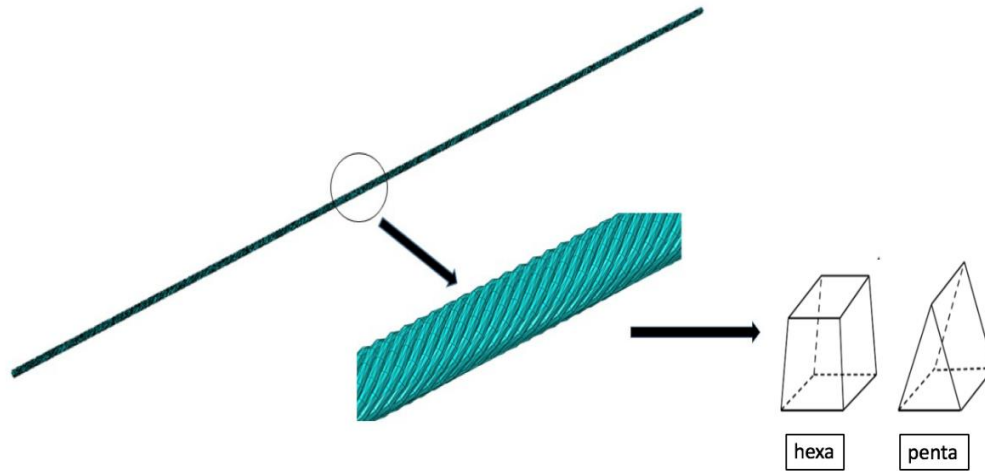


Figure 5.5 Hexa-Penta Mesh with C3d8I and C3d6 Element on Spiral Strand

Table 5.4 HHS Tube Models with Total Number of Elements and Nodes

Number	HHS tube Models	Total Number of Elements	Total Number of Nodes
1	1x6x0.0075;0.050	218162	309164
2	1x8x0.010;0.055	216672	307088
3	1x12x0.005;0.028	173952	232130
4	1x16x0.005;0.045	384576	545088
5	1x18x0.005;0.045	309744	439110

Table 5.5 HHS Tube Models Numerical Results @ 180° Rotation

Sr.No	HHS tube	Numerical Result (Torque, oz-in)
1	1x6x0.0075;0.050	0.132
2	1x8x0.010;0.055	1.43
3	1x12x0.005;0.028	1.738
4	1x16x0.005;0.045	0.125
5	1x18x0.005;0.045	3.743

### 5.2.3 Verification of Analytical and Numerical Results

The analytical and numerical graphs cannot be compared as the analytical is linearly static equation and whereas the simulation is completely non-linear. Another reason behind linear variation is that in the analytical calculation, the plastic data is not considered. Hence, the stiffness of wires is higher, and in turn, it makes the torque higher due to an increased resistance to deformation. The interest of the manufacturer is to know the torque values at 180 degree which can be calculated by the derived equation.

In the verification, the discrepancy of two results is defined as,

$$\varepsilon_{VF} = \frac{T_N - T_A}{T_A} \times 100\% \quad \text{eq. (5.2)}$$

where  $\varepsilon_{VF}$  is relative discrepancy for verification,  $T_N$  and  $T_A$  are the numerical and analytical torques under the given angular displacement respectively.

Table 5.6 Comparison of Numerical and Analytical Results with Relative Discrepancy Percentage

Sr.No	HHS tube	Numerical Result (Torque, oz-in)	Analytical Result (Torque, oz-in)	Relative Discrepancy (%)
1	1x6x0.0075;0.050	0.132	0.15	12.00
2	1x8x0.010;0.055	1.43	1.24	15.32
3	1x12x0.005;0.028	1.738	2.28	23.77
4	1x16x0.005;0.045	0.125	0.17	26.47
5	1x18x0.005;0.045	3.743	3.9	4.03



The results of the verification shown in table 5.5 The maximum discrepancy observed is 26.47 % for the 4th HHS tube model (1x16x0.005;0.045). It is known that analytical and numerical results converge, although numerical value seems a bit of higher for the 4th model (1x16x0.005;0.045). We still think it is acceptable since the torque values are very minimal in model 4 (1x16x0.005;0.045) and the actual value difference is 0.045 oz-in. More over the analytical model was derived based on linear equations and no nonlinearity used. The analytical equations has its own limitations which is one more factor. Overall the analytical results are predicting good range of result for initial approach.

### **5.3 Validation of Simulation or Numerical Model**

As mentioned, the validation is to prove the simulation model yields to an acceptable solution to an original physical system. The validation in this thesis is performed by comparing the results of the numerical models and experimental models. The simulation model has been explained in Section 5.2; in which the model set up is tried to mimic the experimental setup.

#### **5.3.1 Experimental Setup**

The experimental platform was set up by Fort Wayne Metals at their experimental lab in Fort Wayne, IN. For a quick overview, total 2 different experiments are performed to acquire data of material properties, i.e., tensile testing, torsional and testing clockwise. All tests are performed for 10 specimens and the generated data is averaged for further usage. With the tensile testing the acquired data was further proceeded to obtain the Young's modulus  $E$  as  $1.45\text{E}+07$  psi and the fracture strain ( $\epsilon_f$ ) as 0.211672, and the strain rate 0.0002 respectively. This data is utilized for all simulations. With the torsional test, the plot of angular displacement vs torque is achieved; it is further used for the correlation. The torsional test data is shown in Table 5.7.

Table 5.7 Experimental Results of HHS Tube @ 180° Rotation

Sr.No	HHS tube	Experimental Result (Torque, oz-in)
1	1x6x0.0075;0.050	0.1049
2	1x8x0.010;0.055	1.014
3	1x12x0.005;0.028	1.935
4	1x16x0.005;0.045	0.1035
5	1x18x0.005;0.045	4.247

### 5.3.2 Validation by Experiments

In validation, the discrepancy of two results is defined as,

$$\varepsilon_{VD} = \frac{T_E - T_N}{T_E} \times 100\% \quad \text{eq. (5.3)}$$

where  $\varepsilon_{VD}$  is relative discrepancy for validation,  $T_N$  and  $T_E$  are the Numerical and experimental torques under the given angular displacement, respective.

The result achieved from numerical and experimental method are compared for validation for HHS tube mentioned in Figure 5.6 to Figure 5.10 for four HHS tubes, respectively.

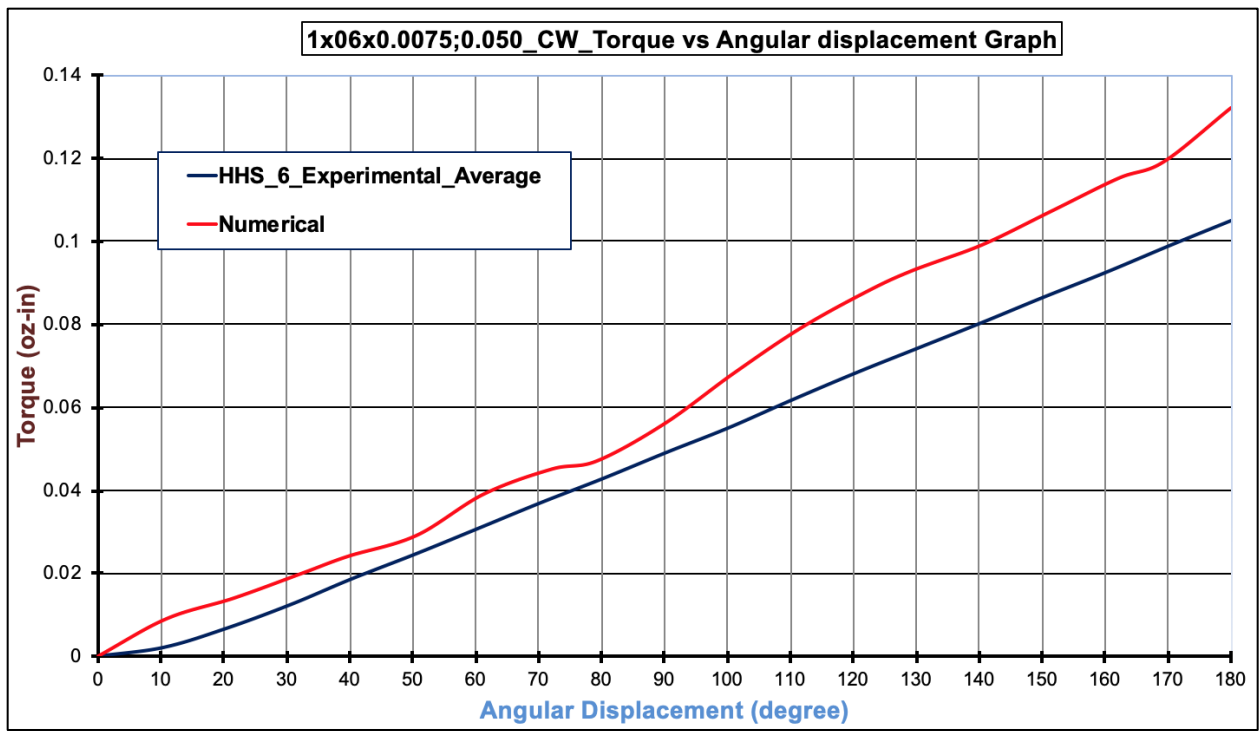


Figure 5.6 HHS Tube\_CW\_1x6x0.0075;0.050\_ Torque Comparison Results of Numerical and Experimental @ 180<sup>0</sup>.

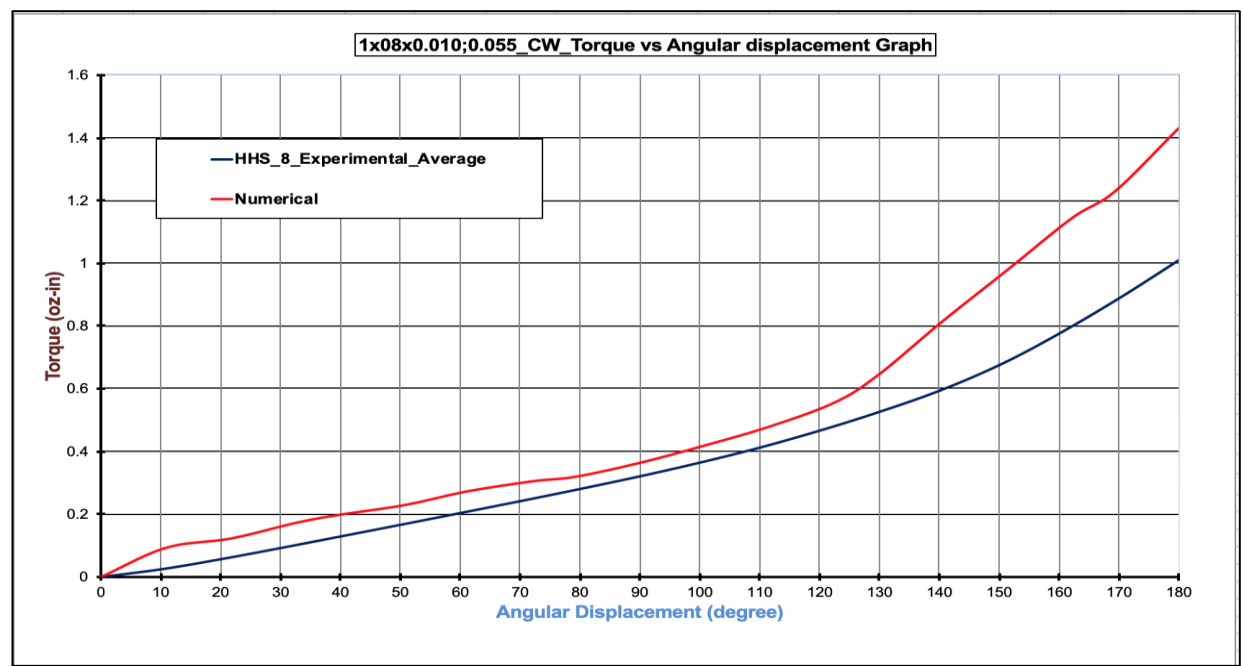


Figure 5.7 HHS Tube\_CW\_1x8x0.010;0.055\_ Angle Comparison Results of Numerical and Experimental @ 180<sup>0</sup>

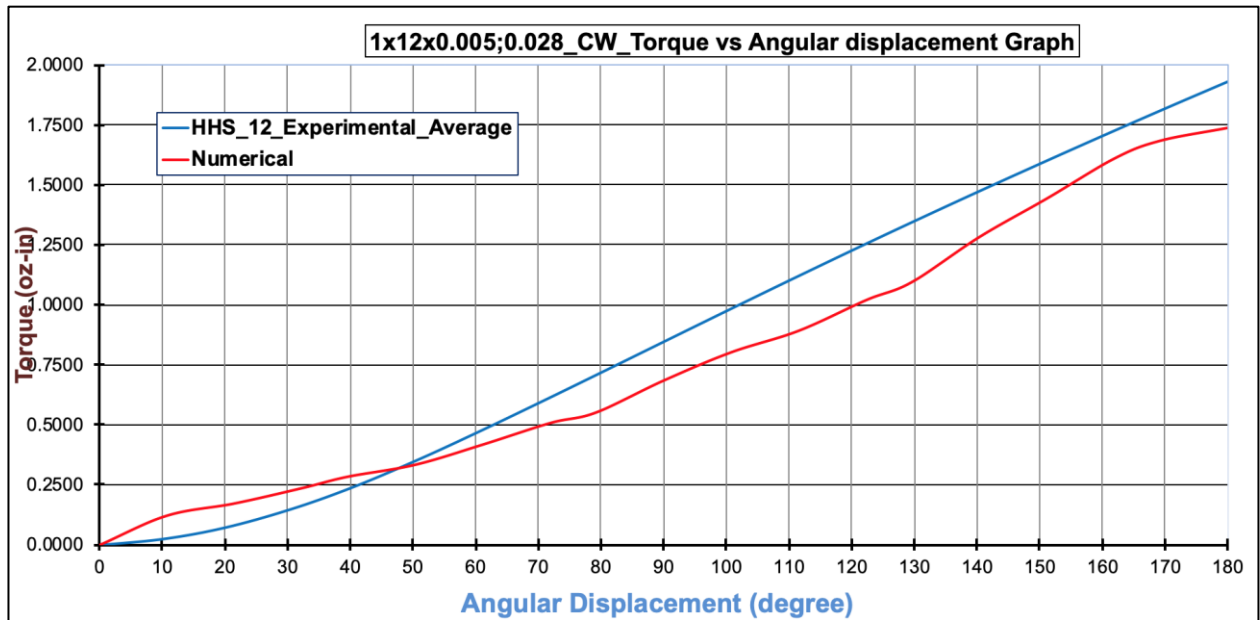


Figure 5.8 HHS Tube\_CW\_1x12x0.005;0.028\_ Torque Comparison Results of Numerical and Experimental @ 180°

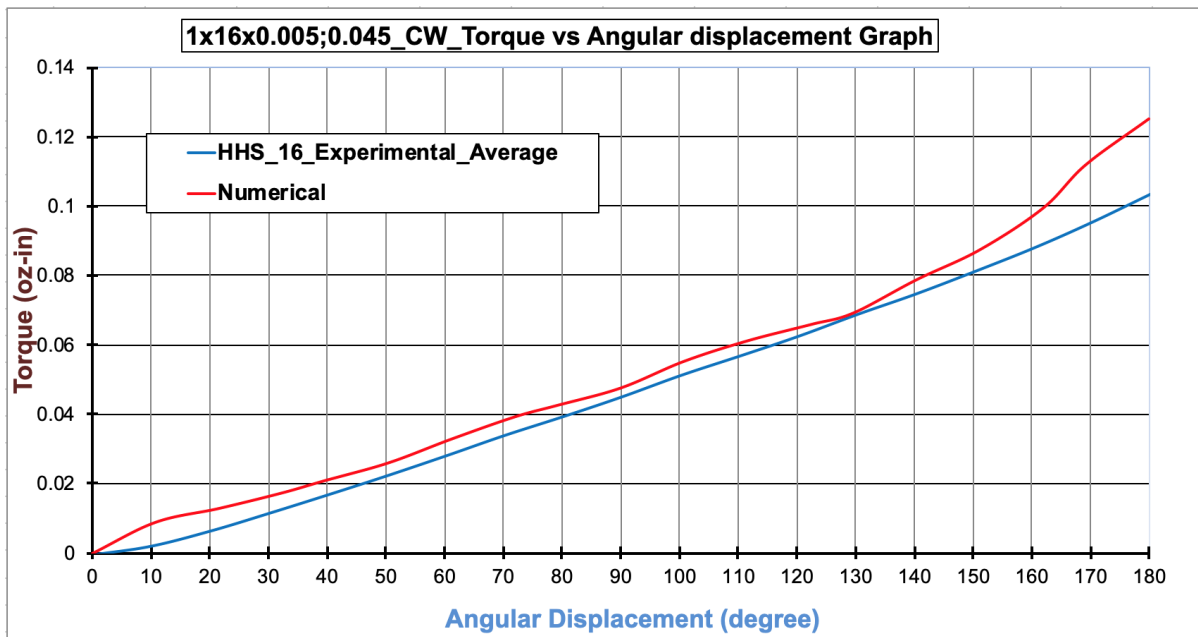


Figure 5.9 HHS Tube\_CW\_1x16x0.005;0.045\_ Torque Comparison Results of Numerical and Experimental @ 180°.

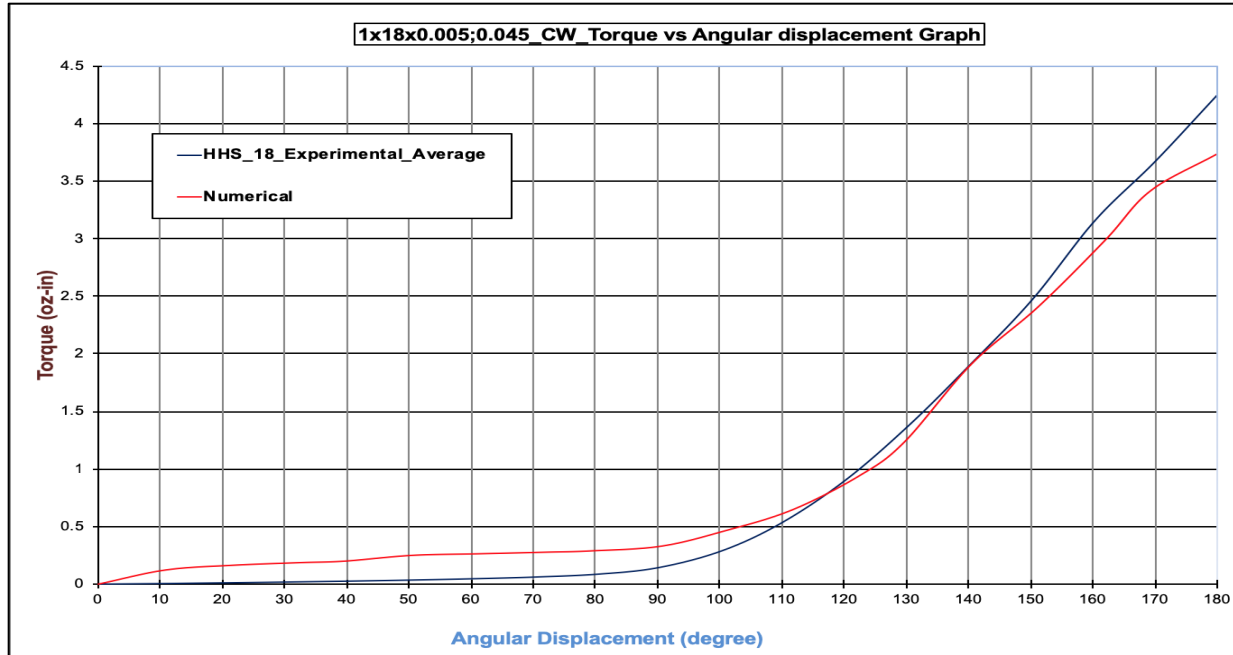


Figure 5.10 HHS Tube\_CW\_1x18x0.005; 0.045\_ Torque Comparison Results of Numerical and Analytical @ 180°.

Total five models are executed for this thesis as mentioned earlier. The overall results of the validation are shown in Table 5.8. It has been found that the maximum discrepancy is 41.03 % for the 2nd model (1x8x0.010;0.055). We still think it is acceptable since, on the other side, the discrepancy of all the other models are useful. The material graph is following the same path, and only the values are not precisely matching; additionally, the torque values are very minimal, and the difference in terms of numbers are considerably smaller. The cause for the variation of results especially for the 2nd model is the variety of the material properties, contact and the friction coefficient. Other than the comparison of experimental and numerical results, the animation behavior also is studied and accepted. This correlation is essential since a simplified analytical model often has some issues to represent real-time conditions, while in a numerical simulation model, most of the real-world situations can be represented. The numerical and experimental results are as expected and are accepted by the client FWM.

Table 5.8 Comparison Results Overall of Numerical and Experimental with Relative Discrepancy Percentage.

Sr.No	HHS tube	Numerical Result (Torque, oz-in)	Experimental Result (Torque, oz-in)	Relative Discrepancy (%)
1	1x6x0.0075;0.050	0.132	0.1049	<b>25.83</b>
2	1x8x0.010;0.055	1.43	1.014	<b>41.03</b>
3	1x12x0.005;0.028	1.738	1.935	<b>10.18</b>
4	1x16x0.005;0.045	0.125	0.1035	<b>20.77</b>
5	1x18x0.005;0.045	3.743	4.247	<b>11.87</b>

#### 5.4 Difficulties and Challenges V & V

Numerical simulation performed in Abaqus 6.14 with the explicit method. Due to the complex geometry, the mesh size is very small initially, and it is taking a lot of computing time to solve single simulation. As the torsional force causes the filars to come in contact during winding of wires, the response of torque is pretty much depending on that. Since the friction among the filars occurs to the contact of wires, the applied rotational load increases resistance, thereby increases the torque to overcome the resistant friction. The definition of the contact and the friction co-efficient value is always challenging and difficult to be estimated. The stress strain data of the material and elastic modulus does not seem precise. These values are averaged before they are used in an FEM model; however, these values play crucial in determining the torque subjected to the give displacement. The properties at wire contacts also affects the result from an analytical model since the analytical equation is linear and approximated. For a complex 3D geometry, the size of a system model has to be increased, thus makes impossible to solve analytically with hand calculations. The analytical equation used to calculate the torque is based on the approximation methods. In addition, the formulation does not account for nonlinear analysis. In our case, the plasticity nonlinear part plays a huge role in determining torque. The equations are based on a spiral spring which can be improved by adding additional parameters consideration.

#### 5.5 Summary of V & V

The purpose of comparison & Validation is to examine how big discrepancy of an analytical and numerical results developed based on experimental materials. The experimental test data is considered as benchmark and comparisons. The V & V are essential for decision

making as the results reported are obtained with all model with all perspectives. This model is considered for V & V as the experimental process executed by FWM, the entire procedure and data is precisely followed except for the consideration of uncertainties.

The torque vs angular rotation curves varies nonlinearly in both of the simulation and experimental methods; while it varies linearly in the analytical model since the analytical calculations follow the linear equilibrium methods. Hence, the maximum deviation lies between the results from analytical model and experiments than that of between the results of numerical model and experiments. As stated earlier, the analytical equations used here did not consider the nonlinear stress-strain which plays crucial role in obtaining results. The formula used for this project is the approximation of spiral spring equations.

Table 5.9 Overall HHS tube model torque results at 180°

Sr.No	HHS tube	Experimental Result (Torque, oz-in)	Numerical Result (Torque, oz-in)	Analytical Result (Torque, oz-in)
1	1x6x0.0075;0.050	0.1049	0.132	0.15
2	1x8x0.010;0.055	1.014	1.43	1.24
3	1x12x0.005;0.028	1.935	1.738	2.28
4	1x16x0.005;0.045	0.1035	0.125	0.17
5	1x18x0.005;0.045	4.247	3.743	3.9

The V & V procedure has concluded that empirical, analytical and simulation results data are shown good correlation as shown in table 5.9 and the animation are also realistic. Moreover, the fracture simulation the HHS tube breaks at the same location where the actual test does. Therefore, with the achieved results and comparison, it is concluded that numerical simulation is verified and validated as long as the material properties are defined appropriately.

## 6. CONCLUSION AND FUTURE WORKS

### 6.1 Summary of Thesis Work

This thesis is driven by request of research and development from a client company of HSS tubes (FWM). In many applications, Users of HSS tubes require the information about the capability of a tube to carry a torque without material failure; it is reflected by its measurement of carrying the torque applied at the adjacent end to the distal tip at a ratio of approximately 1:1, even when the tube is curved. The sizes of such an HHS tube is very small which ranges from 0.01 in to 0.1in in its diameter. Additionally, it is desirable to quantify examine other characteristics of tube under the maximum twisting load. Nowadays, the company needs numerous experiments to predict the torque responses; this practice involves in a high cost, long time, but the limited capabilities to deal with different operation conditions. A virtual analysis has its advantages since it avoids to prototype each design for an initial quotation; moreover, it can be analyzed quickly subjected to various loading conditions.

In the proposed thesis study, the main tasks and the corresponding outcomes are as follows.

- 1) **Background study.** The purpose was to clarify the analysis need of the products under investigation. The background study has found that very few works have been conducted on such cables; while many works have been put on conventional wires with normal sizes and focused on tensional loads. Those works helped to grasp some basic understanding of the ropes' responses subjected to various loading conditions. A comprehensive literature survey over 100 references has been conducted. The most relevant work was from Machida and Durelli (1973) on analytical models of ropes, and many other works were on the simulation of wires with normal sizes. As far as the medical wires with a size less than 0.1-in and the torsional loads are concerned, no work has been published so far; especially in using FEA to predict torsional response of helical hollow strands. It is concluded that the proposed research in this thesis has its great significance theoretically and practically.



- 2) **Development of analytical model.** The Analytical model is developed by Dr. Zhuming Bi thesis advisor; hence the analytical equation is used for only to calculate torque.
- 3) **Development of simulation model.** The procedure of FEA is presented in details and the commercial FEA tool Abaqus 6.14 is introduced to illustrate the implementation. Some important parameters related to an FEA model, such as mesh types, contacts, frictions and the types of analysis algorithms are discussed in details. The case studies are developed to show the feasibility of using a simulation approach to predict torsional capability of tubes. The parametric studies are developed to illustrate the flexibility of simulation approaches to deal with different design variables, configurations, and loading conditions of tube in virtual analysis.
- 4) **V & V.** To prove effectiveness of proposed simulation approach. Verification and validations are performed, respectively. In verification, the results from the analytical model are correlated to those results from the FEA models to verify the results from corresponding simulations. For validation, the experiments were designed and performed by Fort Wayne Metals, and the results from experiments are correlated to those results from the simulation. The comparison shown that results from the simulation models are acceptable and the FWM company was satisfied with the outcomes directly from simulations.

## 6.2 Conclusion

The thesis work led to encouraging results for the client company. It has been found that:

1. The characterization of HHS tube can be clearly defined as a virtual analysis problem; which corresponds an angular displacement to the torque applied to tube. In the defined virtual model, the main design variables are (a) number of filars and (b) the parameters for the shape and geometries of filars. To standardize the operation of characterization, the boundary condition for HHS tube is at one end fixed and angular displacement applied at other end in clockwise directions.

2. The literature survey has found the existing works were mainly on large strands and solid wire ropes with multiple layers. The methods in those works were applicable only to certain industry usage strands, especially for mining and bridges construction. The majority of works were confined to commonly used strands Independent wire rope core (IWRC) subjected to tensile, torsional and bending loadings. Therefore, the presented research is to characterize medical strands with a size range below 0.1 inch for their loading capabilities.
3. Numerical FEA models are developed to calculate torque required to generate specified angular deflection. The FEA model covers the same set of design variables as an analytical model. The proposed procedure and FEA model have been implemented in ABAQUS, and the nonlinearity of materials is considered in the simulation. In defining an FEA model, solid hexa-penta element is selected as a preferable element type (C3D8I) due to its robustness for a complex 3D geometry, the explicit algorithm is selected in solving stage, the step increment is increased rather than using quadratic elements to reduce computing time. Fracture failure was conducted using the presented model, and it led to the satisfactory result in predicting fracture failure in comparison with experimental tests. The scenario of fracture was visualized based on the stress distribution on outer edge of filars, and it generated excellent realistic results in visualization when the mesh size was finer. The proposed simulation model was proved as a fundamental tool to obtain acceptable results without intensive physical tests. However, obtaining good results from simulation needs high-capability computers since more and more computing power is required to get results sooner. In regards to the FEA model, it will be helpful to measure friction force engaged among wires of strand since the value of friction coefficient is critical to define the contact conditions in the model.
4. The parametric study is developed which was able to cover all of the possible design variables. A parametric study is able to reduce the computing time when the behaviors of tubes under the ranges of design variables are investigated, the trend of

the responses of a tube with respect to given parameters can be directly obtained. Note that the comparable results in a parametric study are numerically based.

5. To illustrate the applicability of using the simulation approach for torque prediction of new products, both of verification and validation were performed. The verification has found that the proposed model outcomes were in an acceptable range and the validation has found that the discrepancies of the results from the numerical models and experiments were within the range of normal values which were acceptable under the scenarios of numerous uncertainties in experimental setup and measurement.

In conclusion, this is the new effort in using FEA to characterize HHS tubes; the feasibility of the proposed method has been verified and validated, and it has proven its great potential to partially replace costly and lengthy experiments in characterizing medical HHS tubes subjected to torsional loads.

### **6.3 Future Works**

The results from the presented thesis shows the feasibility of using virtual analysis to replace physical tests in designing HHS tubes for new medical applications. However, the continuous effort is required to convert the presented method into a practical modelling tool as follows.

- 1) The future work is needed to refine the parameters and settings of FEA models by comparing simulation results with the experimental ones on as many specimen as possible. In addition, since no formulation has yet been developed for hollow tube, it is desirable to perform some experimental tests. The measured torques can be utilized to quantify some characterized constants suggested by Feyrer and Schiffner (1986); using the calibrated constants in an analytical model could eventually lead to better results to match results from experimental tests.
- 2) More comparative analysis should be done on varying cross sections and number of filars to correlate the results from analytical models and experiments. Moreover, the stiffness matrix formulation seems promising to increase the accuracy of computation since it use

more degrees of freedom to represent the displacements of each node. In addition, to obtain plasticity results which is nonlinear in nature, it would be interesting to solve for 1D elements using the stiffness matrix and mass matrix method for better accuracy. This can be extended to study the surface tension due to the contact forces; contact forces occur while winding the strand with 3D solid elements. Fracture analysis should be done with similar specimens to acquire sufficient data for averaging and comparing with simulation results. In the upcoming process, the virtual analysis will also involve in combining both torsional and axial loading on the strands. A funded research will pave the way to solve these complex problems; which can be applied for a wider scope of the applications in medical and other engineering industry in future.

- 3) Explore the possibility of creating some lookup tables to determine the torques using the data from the simulations; this will speed up the conceptual design of new HHS tubes since the lookup tables based on simulation will tell how various design variables will contribute to the torsional capability of HHS tubes.
- 4) More explorations on V & V aspect improve analytical model and FEA models. For example, conducting experiments to quantify frictions of wires in strands since it affects the predicted torque greatly. In this sense, new experiment needs to be designed to include new sensor and instrumentation in torsional tests to acquire friction coefficients for various HHS tubes under different operating conditions.

## REFERENCES

- 1) Adam and C. Sanchez (1999). Improvements in rod manufacturing technology to meet the increasing quality requirements of the wire industry. Proceedings of the 69th Annual Convention of the Wire Association International, Inc., Guilford, CT.
- 2) Avitzur, B. (1983). Handbook of Metal-Forming Processes. New York, John Wiley and Sons.
- 3) Benini Brian, Tension and Flex Fatigue Behavior Of Small Diameter Wires For Biomedical Applications.
- 4) Bert, C.W. And Stein, R.A. (1962), Stress Analysis of Wire Rope In Tension And Torsion (Determination Of Contact Forces) Part I & II Wire and Wire Products, May, V37, pp.621-624 and June pp. 769-770,772 & 816.
- 5) CALMONT Wire and Cable (2018), Medical Cable, <https://www.calmont.com/industries-served/medical/> , last accessed on April 24, 2018.
- 6) CALMONT Wire and Cable (2018), Custom Medical Cable, <https://www.calmont.com/2017/05/custom-cables-medical-devices/> , last accessed on April 24, 2018.
- 7) Cardou A and Jolicoeur. C (1996) "Semi continuous Mathematical Model For Bending Of Multi-Layered Wire Strands". Journal of Engineering Mechanics, 1996.
- 8) Castro, A. L. R. d., H. B. Campos, et al. (1996). "Influence of die semi-angle on mechanical properties of single and multiple pass drawn copper." Journal of Materials Processing Technology 60: 179-182.
- 9) Caughey T.K. and Irvine H.M. (1974), The Linear Theory of Free Vibrations of a Suspended Cable. Proceedings of The Royal Society, 1974.
- 10) Chi, M. (1971), "Analysis of Multi-Wire Strands in Tension and Combined Tension and Torsion, Report 71-9", Inst. of Ocean Sc. and Eng., Catholic Univ., Sept. 1971.
- 11) Chi, M. (1971), "Analysis of Operating Characteristics of Strands in Tension Allowing End-Rotation. Report 71-10", Inst. of Ocean Sc. and Eng., Catholic Univ., Sept. 1971.
- 12) Chi-Hui Chien and Costello, G.A. (1985), Effective Length of Fractured wire in Wire Rope ASCE, Vol. 111, No, 7, July, 1985. pp.953-961.
- 13) Chiang Y. J. (1996), "Characterizing simple-stranded wire cables under axial loading," Finite Elements in Analysis and Design, 24, pp. 49–66.

- 14) Cisna, A., Wehrle, J (2018). Helical Hollow Strand Tubing for Flexible and Easily Manipulated Medical Devices, <https://www.azom.com/article.aspx?ArticleID=13443>, last accessed on April 24, 2018.
- 15) Costello. G.A. (1990) Theory of Wire Rope. Springer-Verlag, 1990.
- 16) Costello G.A. (1983), "Stresses in Multilayered Cables", Journal of Energy Resources Technology, Asme, Sept- 1983, Vol-105, Pg:337-340.
- 17) Costello G.A. (1977) Large Deflections of Helical Spring Due to Bending, J. Applied Mechanics Trans, Proc Paper 12964, June, 1977 pp. 479-87.
- 18) Costello G.A. and LeClair R.A. (1988), Axial Bending and Torsional Loading of a Strand With friction Journal Of Offshore Mechanics And Arctic Engineering Vol. 110 Feb. 1988 PP 38-42.
- 19) Costello, G.A. And Sinha S.K. (1977) "Torsional Stiffness of Twisted Wire Cables", J. Of Then Engineering Mechanics Division, Vol.103, No.EM4, Aug, 1977 pp. 767-70.
- 20) Costello, G.A. And Sinha, S.K. (1977) "Static Behavior of Wire Rope", Journal of The Engineering Mechanics Division December, 1977 pp.1011-1023.
- 21) Costello, G.A. and Phillips, S.W. (1973) Contact Stresses in Twisted Wire Cables, Proc. ASME JL Eng. Mech. Div. 1973 Vol.99, pp.331-341.
- 22) Costello, G.A. And Phillips, J.W. (1974) A More Exact Theory for Twisted Cables, Proc. ASCE, J. ENG. Mech. DIV. 1974 Vol. 100 pp. 1096-9.
- 23) Costello, G.A. And Phillips, J.W. (1976), Effective Modulus of Twisted Wire Cables, Journal of The Engineering Mechanics Division, February, 1976 pp. 171-181.
- 24) Costello, G.A. and Phillips, J.W. (1979), "General Axial Response of Stranded Wire Helical Spring", Int. J. Linear Mechanics Vol 14, pp.247-257.
- 25) Costello, G.A. and Phillips, J.W. (1985), Analysis of Wire Ropes with Internal Wire rope Cores Transactions of the ASME, Vol.52, Sept, 1985, pp. 510-516.
- 26) Costello G.A, Phillips J.W. and Miller R.E. (1980), Contact Stresses in a Straight Coss-Lay Wire Rope Proc. 1st ann. Wire Rope Symp, Denver, March 1980 pp. 177-199.
- 27) Costello, G.A. And Miller, R.E. (1979), "Lay Effect of Wire Rope" Engineering Mechanics Division Vol.105 No. EM4 August, 1979 pp. 597-607.
- 28) Costello, G.A. And Miller, R.E. (1980), "Static Response of Reduced Rotation Rope J, of The Engineering Mechanics Division Vol.106, No.EM4, August 1980 pp. 623-631.

- 29) Costello, G.A. And Butson G.J. (1982), Simplified Bending Theory for Wire Rope  
ASCE J. ENG. MECH. DIV April, 1982 Vol.108, No.2, pp.219-227.
- 30) Cress H.A. (1955), MSc Thesis "A Theoretical Investigation of Contact Stresses In A 6  
x 7 Wire Rope" The Ohio State University 1955.
- 31) Dieter, G. E. (1986). Mechanical Metallurgy. New York, McGraw-Hill Book Company.
- 32) Emergo Group, Inc. (2009). Implementing a Medical Device Post-Market Surveillance  
Program. Retrieved August 18, 2009, from 69.  
<http://www.emergogroup.com/articles/implementing-post-market-surveillance>.
- 33) Exponent. (n.d.). Medical Device Regulatory Compliance and Recall (Overview).  
Retrieved September 15, 2009, from  
[http://www.exponent.com/medical\\_device\\_product\\_recall\\_support/](http://www.exponent.com/medical_device_product_recall_support/).
- 34) Feyrer K. (2007), Wire Ropes, Tension, Endurance, Reliability. Springer-Verlag, 2007.
- 35) Fort Wayne Metal (2018). HHS® tube, or Helical Hollow  
Strand, <https://fwmetals.com/products/hhs-tube/>, last accessed on April 24, 2018.
- 36) Gibson, P.T. Cress, H.A. Kaufman, W.J. Gallant, W.E (1970) Torsional Properties of  
Wire Rope, March 1, 1970 pp.1-11.
- 37) Hall, H.M. (1951), Stresses in Small Wire Ropes Wire, March 1951, pp.228, & 258.
- 38) Hansom O.P. (1949), Mechanics of Locked coil Steel Wire Ropes, PhD Thesis  
University of Birmingham.
- 39) Hruska F.H. (1951), Calculation of Stresses in Wire Ropes Wire September 1951  
pp.766–801.
- 40) Hruska F.H. (1953), Tangential Forces in Wire Ropes. Wire and Wire Products, May  
1953 vol.28, pp. 455-460.
- 41) Hruska, F.H. (1951), “Geometrie im Drahtseil Draht” 4 1953 Nr.5
- 42) Hruska, F.H. (1952), Radial Force in Wire Ropes Wire, May 1952 vol 27 pp. 459-463.
- 43) Hobbs R.E. and Raoof. M (1988) “Analysis of Multilayered Structural Strands”. Journal  
of Engineering Mechanics, 1988.
- 44) Huang, N.C. (1978) Finite Extension Of An Elastic Strand With A Central Core, ASME  
Jnl Of App. mechs, vol 45, No4, 1978, PP852-858

- 45) Irvine H. M., and Caughey T. K. (1974), "The linear theory of free vibrations of a suspended cable," *Proceedings of the Royal Society of London*, 341, pp. 299–315.
- 46) Karamchetty S.D.S.R. and Sr. Engineer, Math Tech Inc, Washington Dc and W.Y. Yuen (1979), The University of Newcastle, N.S.W, Australia "Contact Problem in Wire Ropes", *Journal of Mechanical Design* Vol-01/October 1979, Pg:702-710.
- 47) Kirchhoff J.F. (1859), *Math (Crelle)*, BD 56, 1859.
- 48) K. Kumar, J.E. Cochran, J.A. Cutchins (1997), "Contact Stresses in Cables Due to Tension and Torsion", *Journal Of Applied Mechanics*, Vol-64, Dec-1997, Pg:935-939.
- 49) Knapp, R.H. (1979), Derivation of A New Stiffness Matrix for Helically Armoured Cables Considering Tension and Torsion, *Intl J. For Numerical Methods in Engineering*, vol14,1979, PP515-529.
- 50) Knapp, R.H. (1988), Helical Wire Stresses in Bent Cables. *Journal of Offshore Mechanics and Arctic Engineering*. Feb., 1988 Vol. 110 PP 55-58.
- 51) Knapp, R.H. (1975), Non-linear Analysis of a Helically Armoured Cable with Non-Uniform Mechanical Properties In Tension, IEEE Paper No 75CH0, (95-1,) OEC, Proc IEEE Conference On Engineering In the Ocean, Environmental And Marine Tech Sec,11th Annual Meeting, San Diego, Ca1,1975, PP155-164.
- 52) Laura, P. A. and Casarella, M. J. (1968), - A Survey of Publications on Mechanical Cables and Cable Systems, Report 68-1, Thesis No. 893, Institute of Ocean Sc. in Eng., Catholic Univ., Dec. 1968.
- 53) Leissa A.W. (1959), Contact Stresses in Wire Ropes Wire and Wire Products, Vol. 34 March, 1959 pp. 307-314, pp 372-373.
- 54) MacFarlane M, Rosen J, Hannaford B, Pellegrini C, and Sinanan M (1999), "Force Feedback Grasper Helps Restore Sense of Touch in Minimally Invasive Surgery," *Journal of Gastrointestinal Surgery*, vol. 3, no. 3, pp. 278–285, May-June 1999.
- 55) Machida S and Durelli Aj. (1973), Response of A Strand to Axial and Torsional Displacements. *J. Mech. Eng. sci* 1973; 15:241–51.
- 56) Mazzella Companies, 2018 WireRope\_Catalog, [https://www.mazzellacompanies.com/portals/0/pdfs/MazzellaCatalog13\\_WireRope\\_LR.pdf](https://www.mazzellacompanies.com/portals/0/pdfs/MazzellaCatalog13_WireRope_LR.pdf), last accessed April 24, 2018.
- 57) Mcconnell K G and Zemek Wp. (1982), A Model to Predict the Coupled Axial Torsion Properties Of Acsr Electrical Conductors. *J. exp. Mech* 1982; 22:237–44.



- 58) Moorthy, Sathikh S Mbk, and Krishnan M. A (1996), Symmetric Linear Elastic Model for Helical Wire Strands Under Axisymmetric Loads. *J Strain Anal Eng Des* 1996;31 (September (5)):389–99.
- 59) Naohiko Miyata, Tomihisa Kato, Kenji Miyata, Kazumi Matsuo, Ryuji Kusuda, Yoshinobu Nakagoshi, Tadakazu Kato. Asahi Intec Co (Nagoya, Japan, 2005) (2005). Wire Stranded Medical Hollow Tube and Medical guide wire. Patent No: 6881194 B2 (April 19 2005).
- 60) Newman William (M. D.) (1881), Surgical cases, mainly from the wards of the Stamford, Rutland & General Infirmary, London. 1881 page-123- 145.
- 61) Parsons, M. G. and Casarella, M. J. (1969), "A Survey of Studies on the Configuration of Cable Systems under Hydrodynamic Loading. Report 69-1, Thesis No. 893, Institute of Ocean Sc. and Eng., Catholic Univ., May 1969.
- 62) PHI Learning private limited, New Delhi.
- 63) Phillips J.W. and Fotch P.D. (1983), Preliminary Analysis of Filler-Wire Hoisting Rope Proc. 18th Midwestern Mechanics Conf., May 16-18 1983 PP397-340.
- 64) R. D. Thomson and J. W. Hancock, (April 1984), Ductile failure by void nucleation, growth and coalescence.
- 65) Robert G. Sargent (2008), Verification and Validation of Simulation Models, Proceedings of the 2008 Winter Simulation Conference.
- 66) Rosen J, MacFarlane M, Richards C, Hannaford B, Sinanan M (1999). Surgeon-tool force/torque signatures--evaluation of surgical skills in minimally invasive surgery. (1999) 62:290-6.
- 67) Reensnyder, H.S. (1972) The Mechanical Behavior and Fatigue Resistance of Steel Wire Strand And Rope Internal Report, Bethlehem Steel Corporation, June 1972.
- 68) Sayenga,D. (1980) The Birth And Evolution Of The American Wire Rope Industry, Proc. of the First Annual Wire Rope Symposium, Denver, Colorado. Published by Engineering Extension service, Washington state University, Pullman, Washington, USA, March 1980, PP275-335.
- 69) Sayenga D (1999), History of Wire Rope.
- 70) Seely, F.B. (1967) And Smith Advanced Mechanics Of Materials.
- 71) Stanley James C, Veith Frank, Wakefield Thomas W (2014), "Current Therapy in Vascular and Endovascular Surgery E-Book" Elsevier Health Sciences, Mar 28, 2014.

- 72) Starossek U. (1991), "Dynamic stiffness matrix of sagging cable," *Journal of Engineering Mechanics*, 117(12), pp. 2815–2829.
- 73) Starossek U. (1994), "Cable dynamics- A review," *Structural Engineering International*, (3), pp. 171–176.
- 74) Starkey, W.L. & Cress H.A. (1959), *An Analysis of Critical Stresses and Mode of Failure Of A Wire Rope. I, Of Engineering for Industry*, Nov, 1959 pp.307-311.
- 75) Timoskenko S. (1956), *Strength of Materials Part II* 3rd Ed.D. Van Nostrand Company, Inc. New York Mar., 1956 PP 295-298.
- 76) Triantafyllou M. S. (1984), "Linear dynamics of cables and chains," *The Shock and Vibration Digest*, 16(3), pp. 9–17.
- 77) Triantafyllou M. S. (1987), "Dynamics of cables and chains," *The Shock and Vibration Digest*, 19(12), pp. 3–5.
- 78) Tobushi H, Hachisuka T, Hashimoto T, Yamada S (1998), "Cyclic Deformation and Fatigue of a TiNi Shape-memory Alloy Wire Subjected to Rotating-Bending", *Journal of Engineering Materials and Technology-Transactions of the ASME*, 120(1):6470, 1998.
- 79) Ulbrich Inc. (2018), Wire datasheet. <https://www.ulbrich.com/resources/wire-datasheets/>, Last accessed on 5<sup>th</sup> May 2018.
- 80) Utting W.S. and N. Jones (1987), "The Response of Wire Rope Strands to Axial Tensile Loads –Part I", *Experimental Results And Theoretical Predictions*, *Int. J. Mech. Sci.* 29 (9) (1987)605–619.
- 81) Utting W.S. and N. Jones (1987), "The Response of Wire Rope Strands to Axial Tensile Loads –Part II", *Comparison of Experimental and Theoretical Predictions*, *Int. J. Mech. Sci.* 29 (9) (1987) 621–636.
- 82) Utting W.S. and N. Jones (1988), *Axial-Torsional Interactions and Wire Deformation In 19-Wire Spiral Strand*, *J. Strain Anal. Eng. Des.* 23 (2) (1988) 79–86.
- 83) Velinsky S. A. (1985), "General nonlinear theory for complex wire ropes," *International Journal of Mechanical Sciences*, 27, pp. 497–507.
- 84) Velinsky S. A. (1989), "On the design of wire rope," *Journal of Mechanisms, Transmissions, and Automation*, 111(9), pp. 382–388.
- 85) Velinsky S.A. (1981), *PhD Thesis Analysis of Wire Ropes with Complex Cross Section* University of Illinois At Urbana-Champaign 1981.

- 86) Velinsky S.A, Anderson G.L. and Costello G.A. (1984), Wire Rope with Complex Cross Section, J, Eng. Mech. Div. Mar.,1984, Vol.110 No.3, PP 380-91.
- 87) Velinsky S.A. (1985), Analysis of Fibe-Core Wire Rope Transactions of the ASME, vol.107, Sep.,1985, pp.388-389.
- 88) Velinsky S.A. (1989), "On the Design of Wire Rope", Journal Of Mechanism, Transmission & Automation In Design, Sept-1989, Vol-111, Pg:382-388.
- 89) Velinsky, S.A. (1985), General Nonlinear Theory for Complex Wire Rope, Int, J. Mech. Sci. Vol 27, No. 7/8 PP 497-507, 1985.
- 90) Velinsky S.A. & Schmidt J.D. (1988), A Simplified Treatise on The Effect of Wear In Cables Journal Of Offshore Mechanics And Arctic Engineering vol. 110 Feb. 1988 PP-32-37.

## APPENDIX A. ANALYTICAL CALCULATION

Below equations are developed by Thesis Advisor Dr.Zhuming Bi and are used to calculate the Analytical calculations.

$$T_{no\ friction} = \frac{\theta_{rad} E d^4}{64 D N_b} N_w 2$$

$$T_{bonded} = 2T_{no\ friction} = 2\left[\frac{\theta_{rad} E d^4}{64 D N_b} N_w 2\right]$$

$$T_{friction} = (1 + \sin^2 \lambda + \min(\cos^2 \lambda, \sin \lambda \cdot \cos \lambda) \mu) \left[\frac{\theta_{rad} E d^4}{64 D N_b} N_w 2\right]$$

Where,

p: pitch of the filar

D: Mean diameter of the HHS tube

d: diameter of the filar

T: applied torque

$\theta_{rad}$  = the twist angle in radian(Angular displacement)

$N_w$  = number of filars in HHS tube

$N_b$  = number of coils or turns

E = young's modulus of elasticity

I = moment of inertia

$\mu$  : friction coefficient

$\lambda$  : is the pitch twist angle ( $\tan^{-1} \frac{\pi d}{p}$ )

## APPENDIX B. LETTER OF SUPPORT

PHN 260.747.4154 9609 Ardmore Avenue  
FAX 260.747.0398 Fort Wayne, IN 46809

[fwmetals.com](http://fwmetals.com)



**FORT WAYNE METALS**

Turning knowledge into solutions.

August 8, 2018

Zuhming Bi, Ph.D., P. Eng.  
Department of Civil and Mechanical Engineering  
Purdue University Fort Wayne  
2101 E. Coliseum Blvd, Fort Wayne, IN 46805

Re: DilipKumar Devpalli Master of Science Thesis Support

Dilip has worked with the engineering team at Fort Wayne Metals to develop a computational model for one of our significant products, Helical Hollow Strand Tube, HHS®. This is a complex product which we needed to increase our understanding of the product's performance. In particular, we need to be able to predict several performance criteria without having to run multiple empirical models for customers. Dilip has confirmed that his predictive model has good correlation for torsional deflection with empirical testing.

Dilip's numerical model will accelerate the product development cycle for our customers. We appreciate the effort that Dilip provided in the creation of this model. We support the conferment of his Master of Science degree for this project.

Lawrence Kay  
Director Engineering  
Fort Wayne Metals Research Products Corp.